THE DEVELOPMENT OF HEPARIN-BASED MATERIALS FOR TISSUE ENGINEERING APPLICATIONS TO TREAT ROTATOR CUFF TENDON INJURIES

A Dissertation
Presented to
The Academic Faculty

by

Song P. Seto

In Partial Fulfillment
Of the Requirements for the Degree
Doctor of Philosophy in the
Program of Bioengineering

Georgia Institute of Technology
May 2014

Copyright © 2014 by Song P. Seto

THE DEVELOPMENT OF HEPARIN-BASED MATERIALS FOR TISSUE ENGINEERING APPLICATIONS TO TREAT ROTATOR CUFF TENDON INJURIES

Approved by:

Dr. Johnna S. Temenoff, Advisor
Department of Biomedical Engineering
Georgia Institute of Technology

Dr. Manu O. Platt
Department of Biomedical Engineering
Georgia Institute of Technology

Dr. Robert E. Guldberg
School of Mechanical Engineering
Georgia Institute of Technology

Dr. Athanassios Sambanis
School of Chemical Engineering
Georgia Institute of Technology

Dr. Alexandra Peister
Department of Biology
Morehouse College

Date Approved: March 25, 2014

Dedicated to my loving family.

ACKNOWLEDGEMENTS

In retrospect, the past six years seems to have flown by (really). I thought I knew what to expect, but experiencing a Ph.D. program has been a personal journey that I am glad I didn't give up on. My stubbornness though could not have carried me through without the help of many individuals who I have met here and who have supported me from the beginning. I would like to acknowledge the people who have directly contributed to my research and to the completion of this thesis.

First, I wish to thank my thesis committee members: Dr. Robert Guldberg, Dr. Alexandra Peister, Dr. Manu Platt, and Dr. Athanassios Sambanis. Their expertise in their respective fields continually gave me technical details to mull over, and collectively, they kept me on track to finishing my thesis. Dr. Guldberg has the ability to ask questions that range from the largest scope to the smallest technical detail, and his expertise in animal studies have been helpful in my research. I am thankful for Dr. Peister's encouragement and support, as well as her attention to detail to the cell culture work of my thesis. I have enjoyed collaborating with Dr. Platt, for his dedication to teaching his students as well as for his enthusiasm for research that have sprouted numerous new ideas. I can rely on Dr. Sambanis to ask challenging questions that make me realize that there is still so much to learn.

There are many researchers who have helped me along the way, out of their own volition and kindness. Everyone in the Platt lab has been welcoming and generous with time and materials. I would like to especially thank Dr. Jerald Dumas and Catera Wilder for their insight on cathepsins, zymography, and Western blotting. Candace Fleischer and

Dr. Josh Morris in Dr. Christine Payne's lab were incredibly accommodating in training me in circular dichroism measurements and in the pursuit of decent spectra. Dr. Bernard Kippelen and his lab in ECE generously allowed me to use their circular polarized microscope and assisted me when I waged battles with that imaging software. Dr. Brani Vidakovic gave valuable statistical consultation throughout the years, although he may be disappointed that we never incorporated Bayesian statistics into our work. Current and former Gleason lab members, Alex Caulk, Dr. Anastassia Pokutta-Paskaleva, and Dr. Roy Wang were kind enough to introduce me to the practical aspects of second harmonic generation imaging; we will put it to good use. Dr. Spero Karas, Dr. Timothy Ghattas, Kyle Webb and others at Emory have been extremely helpful in securing an IRB and subsequent tissue samples, while going out of their way to be supportive.

Particular recognition goes to past members of the lab that directly contributed to my research. A big thank you goes to the former post doc in the lab, Yongzhi Qiu, who was essential in setting up the animal studies and teaching me all the techniques I needed to go forward. I am grateful for his help and patience even long after his physical presence in the lab. My undergrads have made me believe that Georgia Tech students are some of the best around, and I am sure they will all be successful. Kyle Pate, Ryan Adams, Meredith Fay, and Kevin Ang Li have all been instrumental in my research projects. Additionally Maria Elena Casas, as a graduate rotation student, was incredibly helpful in automating an image analysis technique that would have taken way too long to finish on my own.

I wish to thank those in the Department of Biomedical Engineering and Institute for Bioengineering and Biotechnology for their support and in ensuring operations

proceeded smoothly. Shannon Sullivan, Penelope Pollard, and Kristen Laquidara have been kind in making sure my tuition waivers and reimbursements were in order, even if I wasn't so timely with submitting forms. Sally Gerrish is always generous with her time and I am grateful for her work in connecting graduate students with alumni. I am thankful that Dewayne Roberson makes everything in the building run smoothly, although I'm sure our lab has an outrageous fictitious invoice for all the times we've inconvenienced him. I knew I was going to be taken care of in the BioE program when I met Chris Ruffin; his smile and gentle demeanor belied all the work that he did to keep the program running. Laura Paige is his capable successor and she has endured my double-checking of everything to ensure that I will graduate. The great events and overall kindness from James Godard, Colly Mitchell, Floyd Wood, Megan McDevitt, Alyceson Andrews, and Karen Ethier have made my experience here very enriching; I hope everyone I work with in the future is as capable and positive as this crew. I am incredibly thankful for all the core facilities that I had access to, and the capable Steve Woodard, Aqua Asberry, and Andrew Shaw, and Dr. Laura O'Farrell for ensuring that they were functional. I relied heavily on the expertise of Aqua and Andrew for many phases of my project. The PRL staff also deserves a big thank you for being friendly and efficient, such that *in vivo* work was a little less painful.

My experience at Georgia Tech has been enriched through the programs I've been able to take part in. I count myself lucky to have worked with Franklin Bost as a teaching assistant for sophomore and senior design. I feel that I learned just as much as the undergraduate students and feel honored to have assisted with their design concepts. Similarly, I enjoyed working with Mark McJunkin in sophomore design; his enthusiasm

for product design is infectious and made me appreciate the creative aspect of medical device design. My experience in the Graduate Leadership Program allowed me to befriend some of the most ambitious yet down-to-earth people in the department and I am grateful to have been included in the inaugural group. Being a part of the CD4 Fellowship allowed me to take see all the drug delivery, design, and development research taking place on campus as well as in Puerto Rico. All these experiences were great opportunities to supplement my education and each has given me something to carry forward into my career.

I have been lucky to meet many students within the biomedical and bioengineering programs, and want to acknowledge everyone who has helped me in this journey, no matter how small. I can't begin to thank everyone properly, but I extend my sincerest thank you to each person who helped me get to this point. I am fortunate to have befriended people who have made my experience here in Atlanta very enjoyable.

I need to extend gratitude to my advisor, Dr. Johnna Temenoff, who welcomed me into her lab in the summer of 2008 and introduced me to the field of hydrogels. She has provided motivation and challenges throughout my time at Georgia Tech, and as a result, I have become a stronger researcher. There were many times when I got mired in details and failed experiments, and she was essential in reminding me of the bigger picture such that I could move on. I am grateful for the opportunities she has given me and for the trust she has in me. Over the years, I have come to see Johnna as both a colleague and friend. I will always remember the amazing meals she treated us to, how excited everyone was at Harry Potter World, and the time when she humored us by skipping at Epcot. I am incredibly thankful for her mentorship.

Some of my fondest memories of grad school are with the Temenoff Lab, and I am lucky to have made some wonderful friends from the people I work with. I joined the lab when the lab was composed of the nicest "bros" around. Derek Doroski was the stalwart of the lab; he put in place many of the procedures of the lab that we take for granted. He is incredibly diligent and committed to work and family, but he is also great at making people laugh with his quick-wit and ability to compose song lyrics to popular tunes. Peter Yang has the ability to make me laugh over the dumbest things and I value him as a friend who really tried to get to know me when I joined the lab. He was always willing to help me with computer issues and questions I had in the lab, and even now he continues to be someone that I can turn to for advice. Jeremy Lim is also another person who I turned to for advice in grad school and he has become a great friend over the years. I've always admired his intelligence and commitment to his work, and I have grown to value how easy it is to fall into conversations with him. I likely know fewer of Taymour Hammoudi's stories now than when he was in grad school (he should put them in some sort of collection), but the ones I know are probably imprinted in my brain after hearing them so often. Aside from his storytelling, I greatly admire him as a scientist and appreciate that he was always nosy in a good way. Jen Lei's easy-going personality makes her great to work with and I've enjoyed our friendship outside of lab. Her commitment to fitness constantly encourages me to not be so lazy, yet I still think she's in over her head with all those hot yoga passes. I have had the pleasure of getting to know Torri Rinker outside of the lab and admire her dedication and passion for all her pursuits. Her encouragement and friendship was invaluable in the past year. Not only am I grateful to Melissa Goude for being a great caretaker of Lennon, I appreciate her kindness and

empathy in asking about my family. I feel as if I still have a lot to learn of her, but know that her creativity and work ethic will take her far. Tobias has been a terrific resource in the lab and was essential in helping me with the desulfation of heparin. He has also become a great friend who I can always rely on to learn about something new and to challenge me to think differently.

I wouldn't be here without the love and support from my family. I am indebted to my parents, who have worked so hard for my future, such that I could never call myself hardworking in comparison to them. They have shown me by example the concepts of sacrifice and persistence, and I can only begin to honor them. I have to thank my brother, Jong, for giving me the inspiration to pursue bioengineering in college. I feel as if I am always trying to keep up with him, partly out of sibling rivalry and partly because he makes me want to do my best. My sisters, Song Yee and Helen, complete my personality and have been my personal cheerleaders since I went off to college. Song Yee's drive to succeed and her confidence are qualities I admire and hope rubs off on me. I am always surprised at how much Helen has matured, and in her young age she has reminded me repeatedly how important relationships to other people are. My family now includes Masa, my partner in life, who I am grateful to have met and who has given me the love and respect that makes my life even fuller. He has supported me in some of my most challenging endeavors and I love him for exactly the way he is. Thank you for everything.

TABLE OF CONTENTS

LIST OF TABLES

LIST OF FIGURES

LIST OF ABBREVIATIONS

^{1}H NMR	proton nuclear magnetic resonance
ALP	alkaline phosphatase
ANOVA	analysis of variance
APMAm	N-(3-aminopropyl)methacrylamide
APS	ammonium persulfate
BM-MSCs	bone marrow-derived mesenchymal stem cells
BMP	bone morphogenetic protein
BSA	bovine serum albumin
CD	circular dichroism
D2959	Irgacure 2959
ddH_2O	distilled, deionized water
dH_2O	distilled water
DMEM	Dulbecco's Modified Eagle Medium
DMMB	dimethylmethylene blue
DMSO	dimethyl sulfoxide
dsDNA	double stranded deoxyribonucleic acid
DSF	differential scanning fluorimetry
ECM	extracellular matrix
EDC	N-(3-dimethylaminopropyl)-N'-ethylcarbodiimide

EDTA	ethylenediaminetetraacetic acid
ELISA	enzyme-linked immunosorbent assay
FBS	fetal bovine serum
FGF	fibroblast growth factor
FITC	fluorescein isothiocyanate
GAG	glycosaminoglycan
GPC	gel permeation chromatography
Hep	heparin
Hep^{-}	completely desulfated heparin
Hep^{-N}	N-desulfated heparin
Hep^{-N-6O}	6O,N-desulfated heparin
HS	heparan sulfate
IGF	insulin-like growth factor
MAm	methacrylamide
MMP	matrix metalloproteinase
M_n	number average molecular mass
MSC	mesenchymal stem cell
M_w	weight average molecular mass
MWCO	molecular weight cut off
NMP	1-methyl-2-pyrrolidinone
O.D.	optical density
OB	osteoblast

OCT	optimum cutting temperature
OPF	oligo(poly(ethylene glycol) fumarate)
PBS	phosphate buffered saline
PDGF	platelet-derived growth factor
PEG	poly(ethylene glycol)
PEG-DA	poly(ethylene glycol)-diacrylate
PEO	poly(ethylene oxide)
pI	isoelectric point
PI	polydispersity index
PTFE	polytetrafluoroethylene
RFU	relative fluorescence unit
RGD	arginine-glycine-aspartic acid
s.d.	standard deviation
SLRP	small leucine-rich proteoglycans
Sulfo-NHS	N-hydroxysulfosuccinimide
TEMED	tetramethylethylenediamine
TGF	transforming growth factor
TIMP	tissue inhibitor of metalloproteinase
UV	ultraviolet light
W_d	lyophilized weight
W_s	swelled weight

SUMMARY

Surgical repair of torn rotator cuff tendons have a high rate of failure and does not address the underlying pathophysiology. Tissue engineering strategies, employing the use of multipotent progenitor cells or growth factors, represent potential therapies to improve the outcome of rotator cuff surgery. The use of glycosaminoglycan-based biomaterials in these therapies may enhance the effectiveness of cell and growth factor delivery techniques. Furthermore, understanding the cellular and molecular mediators in tendon overuse can help elucidate the causes of tendon degeneration. Thus the overall goals of this dissertation were to 1) develop heparin-based biomaterials to enhance cell pre-culture and maintain growth factor bioactivity and 2) characterize the histological and enzymatic changes in a supraspinatus tendon overuse model.

To investigate the use of heparin in enhancing dynamic signaling, mesenchymal stem cells (MSCs) were encapsulated in heparin-containing hydrogels and evaluated for differentiation markers when cocultured with a small population of differentiated cells. To probe the effect of sulfation of heparin on the interactions with protein, selectively desulfated heparin species were synthesized and evaluated for their ability to bind and protect proteins. Finally, to develop a tendon overuse model that can become a test bed for testing future targeted therapeutics, an animal model was evaluated for tissue damage and protease activity. Together these studies represent a multi-pronged approach to understanding how tendon tissues become degenerative and for developing technologies to improve the biological fixation of tendon to bone in order to reduce the need for revision surgeries.

CHAPTER 1

INTRODUCTION

1.1 Motivation

Rotator cuff disease is a complex shoulder condition that can range from acute tendon tears to chronic tendinopathy. The supraspinatus tendon, which participates in arm abduction, is commonly afflicted due to highly repetitive work and can result in shoulder pain and dysfunction [1]. Due to the relative avascularity and low celluarity of tendon tissue, intrinsic healing may not be adequate and surgical intervention may be necessary [2]. Over 200,000 Americans per year require shoulder surgery to repair the rotator cuff, with the volume of repairs likely increasing as the current population ages [3]. While surgery can alleviate symptomatic shoulder dysfunction, revision surgeries can be as high as 57% and do not address the underlying pathophysiology [4]. Commonly cited causes for revision surgeries include tendons pulling out of sutures and poor tendon-bone integration, particularly with degenerative tendon [5-8].

Recapitulation of the natural interface between tendon and bone would improve tissue integration after tendon reattachment surgery [7]. This interface of tendon to uncalcified fibrocartilage to calcified fibrocartilage before inserting to bone allows for stress dissipation at intact tendon attachment sites [9]. Tissue engineering approaches have investigated the development of phasic tissues by graded material, ligand, or cell incorporation [10-12]. However, after tendon reattachment, it is important to quickly stabilize the tendon-bone interface, minimize the amount of granular tissue that forms between tendon and bone, and accelerate the early stages of healing in order to populate

the interface with desired cells. Tissue engineering strategies frequently employ the use of multipotent progenitor cells to either rebuild the tissue environment or secrete paracrine factors that elicit endogenous cell responses. Mesenchymal stem cells (MSCs) are multipotent progenitor cells found in the adult bone marrow, that are capable of differentiating into bone, cartilage, and fibrous tissues [13]. Delivery of MSCs to transected tendons have shown acceleration of early healing responses [14]. These cells can be sensitive to paracrine signals, as MSCs cocultured with differentiated cell types can become differentiated and lead a more established *in vivo* phenotype [15, 16].

Delivery of bioactive factors, such as bone morphogenetic protein (BMP)-2 is another avenue to improve integration of tendon to bone [17, 18]. BMP-2 has the ability to induce cell migration of osteoblasts and mesenchymal progenitor cells and encourage mesenchymal stem cell differentiation into an osteochondral or osteogenic lineage [19-24]. These cell types are available during a typical rotator cuff surgical procedure, particularly if the tendon is reattached at a bony trough [25, 26]. BMP-2 is currently approved by the FDA for use in spinal fusion, however, use of supraphysiologic doses and a collagen carrier that has weak affinity for BMP-2 increases cost of treatment and places patients at risk of side-effects due to off-site effects [18, 27-29]. A suitable delivery system that can reduce the high dosage of BMP-2 by limiting burst release and protecting the bioactivity of BMP-2 is desired.

Finally, understanding what cellular and molecular mediators are involved in tendon overuse can help elucidate the causes for degenerative tendon. While past injury models include tendon transection and collagenase injection, mechanical overuse of tendon is more physiologically relevant and may provide insight into the mechanisms of

chronic tendinopathy. Additionally, use of an animal model that can yield repeatable results will be essential in becoming a test bed for testing targeted therapeutics, including growth factor delivery systems and cellular therapies. A multi-pronged approach to understanding how tendon tissue become degenerative and developing technologies to improve the biological fixation of tendon to bone will help develop therapies that prevent shoulder dysfunction and the need for revision treatments.

1.2 Research Objectives

The objective of this research was to understand protein interactions with heparin and heparin derivatives as a tissue engineering approach to eventually treat tendon overuse injuries. This was achieved by 2 parallel focus areas: 1) to understand the effects of heparin in crosslinked and soluble forms and 2) to evaluate an inbred rat tendon overuse model. Heparin is a highly sulfated, linear glycosaminoglycan (GAG) with important clinical roles such as an anti-coagulant, and in biologic roles such as in stabilizing growth factor-receptor complexes [30, 31]. Its high sulfation level and various biological roles render it an attractive biomaterial for affinity delivery systems.

A heparin-containing hydrogel system was developed to encapsulate MSCs in order to evaluate the effect on osteogenic marker expression during coculture with monolayers of osteoblasts. Heparin was chemically modified to allow covalent attachment within a synthetic hydrogel network. Upon finding that diffusion within heparin-containing hydrogels could be reduced by higher sulfation level, modulation of overall negative charge and level of protein interaction was achieved by chemically desulfating heparin. The high negative charge density of heparin is known to bind

positively-charged proteins electrostatically as well as bind specific proteins with heparin-binding sites. The role of heparin sulfation on maintaining BMP-2 bioactivity was explored by heat treating BMP-2 with and without heparin derivatives and assessing the growth factor bioactivity. While improving tendon-bone integration is a motivation in developing effective tissue engineered constructs that can address a clinical need, it is also important to evaluate an injury model in order to prevent tendon rupture. A shoulder overuse protocol was adapted for an inbred strain of rat to determine histological and enzymatic events that occur in overused tendon. This overuse model is physiologically relevant and can elucidate cellular changes that precede chronic tendinopathy and tendon rupture. The **central hypotheses** of this research are that 1) engineered heparin-based materials can enhance signaling to MSCs from sequestered factors and can preserve protein bioactivity even after chemical desulfation and 2) a tendon overuse model in an inbred strain of rat will show tissue damage by overuse that is accompanied by increased activity of proteases. These hypotheses were explored through the following three specific aims:

Hypothesis I: MSCs encapsulated in hydrogels containing increasing amounts of covalently-crosslinked heparin will produce higher levels of osteogenic markers when co-cultured with monolayers of osteoblasts.

Specific Aim I: Determine the ability of heparin-containing hydrogels to amplify alkaline phosphatase activity (ALP) and mineralization of a large population of MSCs with a small population of osteoblasts.

Coculture systems have been utilized to enhance proliferation of cells of interest and differentiate stem cells with a population of differentiated cells [32, 33]. Heparin-containing materials have been shown to sequester and protect proteins from the environment, and may be beneficial in a coculture setting by maintaining active soluble signals within the hydrogel [34]. Coculture systems with MSCs have previously been studied with various differentiated cell types from orthopaedic tissues and the following study uses osteoblasts as a model differentiated cell type to study the effects of the heparin-containng hydrogels [35, 36]. Other differentiated cells found at the insertion site of tendon such as chondrocytes and tenocytes may be adopted for use in this system.

Heparin was functionalized to allow covalent incorporation into PEG-based hydrogels. MSCs were encapsulated in hydrogels of increasing heparin content and then cocultured with monolayers of osteoblasts or MSCs in the absence of dexamethasone. Acellular hydrogels were cocultured in parallel to determine cell-mediated effects. Alkaline phosphatase (ALP) activity, calcium accumulation, and von Kossa staining evaluated the effect of coculture and heparin on MSCs within the hydrogels. To examine the interaction of positively-charged proteins with heparin-containing hydrogels, solutions of fluorescently-tagged model proteins were incubated with acellular hydrogels to examine the distribution of protein within the hydrogel after 24 hours.

Hypothesis II: The ability of heparin to protect BMP-2 against thermal stress will decrease as the sulfation level of heparin derivatives decrease, due to loss of negative charge density.

Specific Aim II: Chemically desulfate heparin and determine BMP-2 bioactivity after heat treatment when complexed with heparin and desulfated derivatives of heparin.

Heparin is used as an anti-coagulant therapy, and in order to reduce off-site effects, inactivation of the anti-coagulation feature of heparin while maintaining its protective abilities is necessary. This has been explored by chemically removing sulfates from heparin [37]. Much research has gone into characterizing the interaction of fibroblast growth factor (FGF)-1 and -2 with heparin, in which heparin can protect FGF-1 and -2 from denaturing environments in a heparin sulfation-dependent manner [38]. Less is known about how BMP-2, a heparin-binding protein with a flexible heparin-binding domain, can be protected by heparin molecules. Furthermore, since the high negative charge density of heparin can affect diffusion of charged molecules within a hydrogel, heparin desulfation would provide a library of less charged materials for future applications.

Selectively desulfated heparin derivatives were prepared and characterized by change in chain length, proton nuclear magnetic resonance and overall sulfation level. *E. coli*-derived BMP-2 was heat-treated for a range of times, either alone or incubated with heparin derivatives. The BMP-2 was subsequently administered to the myogenic C2C12 cell line to test for growth factor bioactivity by measuring ALP activity. Interactions between the heparin derivatives and a model positively-charged protein, histone, was qualitatively evaluated by differential scanning fluorimetry.

Hypothesis III: Longer periods of downhill treadmill running causes tissue damage to the insertion region of the supraspinatus tendon in rats, concomitant with an increase in cathepsins, a potent class of collagenases and elastases.

Specific Aim III: Establish an overuse protocol in an inbred strain of rat and evaluate changes to tissue organization and expression of active cathepsins.

A physiologic model of tendinopathy may provide molecular clues as to what causes tissue degradation. An overuse model for the supraspinatus tendon can recapitulate the repetitive sliding of the insertion region of the tendon beneath the bony acromion. Upon tissue injury, a multitude of proteases may become activated, including cysteine cathepsins, which are proteases involved in degradation and remodeling of the extracellular matrix, but have been found to be misregulated in diseases such as osteoporosis and osteoarthritis [39, 40]. Furthermore, cathepsins may form complexes with different types of GAGs and it has been shown that the collagenolytic activity of cathepsin K can become inhibited upon binding to heparin, the biomaterial of interest in this thesis [41].

An established decline running protocol was used for an inbred Dahl Salt Resistant strain of rat for up to 8 weeks [42]. Tendons were evaluated histologically by semi-quantitative histological scoring and circular polarized light microscopy. Gelatin zymography was performed at the insertion and midsubstance regions of tendon to measure cathepsin activity.

1.3 Significance and Scientific Contribution

The studies in this dissertation provide significant insights into the role of naturally-derived, sulfated materials in protein and cell interactions. The established growth factor binding ability of heparin was used as an opportunity to develop covalently crosslinked heparin-containing hydrogels in order to make coculture systems more efficient by sequestering factors around MSCs. The development of a heparin-containing hydrogel platform for cell encapsulation that can improve pre-treatment of a large population of MSCs with a smaller population of differentiated cells is an important strategy if the availability of differentiated cells is a limitation. By using osteoblasts as a model differentiated cell type, heparin hydrogels were shown to influence MSC-mediated expression of osteogenic markers. However, culture with bulk heparin-containing hydrogels revealed that geometry and overall heparin content can affect the distribution of positively-charged proteins within the hydrogel. This study was important in establishing how protein interactions with heparin-containing hydrogels can affect protein presentation to encapsulated MSCs and highlights the value of being able to tune the amount of heparin and overall sulfation within hydrogels.

Development of heparin biomaterials without its anti-coagulant feature is important for future *in vivo* work as well as allow us to probe the importance of sulfation level and chain conformation in protein interactions. While heparin can act as a cofactor in growth factor signaling with FGF-1 and -2 and their receptors, less has been gleaned about the interaction of growth factor and heparin complexes that do not affect signaling, but still protect growth factors from denaturation. We have shown that even relatively small perturbations of sulfation level can drastically affect growth factor protection by

heparin. However, with increasing amounts of thermal stress, heparin derivatives with intermediate sulfation can maintain BMP-2 bioactivity better than BMP-2 alone, indicating that overall sulfation remains a factor in growth factor protection. These studies suggest that there is a balance between preserving the protective effects of heparin and selective desulfation. As such, these studies on soluble complexes of heparin and growth factor can help establish design criteria for sulfated glycosaminoglycan-containing hydrogels.

Adaptation of a tendon overuse model with an inbred strain of rat will allow the exploration of cell-based and material-based therapies in the future. The animal model and tissue analysis technique used resulted in a fundamental study on a new class of enzymes within overused tendon. Cathepsin activity may represent a novel mechanism for tissue degeneration upon mechanical overuse of tendon and may be a potential target for therapies. Cathepsins can form complexes with heparin, and in the case of cathepsin K, the complex may have an inhibitory effect on the protease. This feature will be important to explore with heparin-based biomaterials. Overall, this animal model provides a framework for studying the gamut of degeneration leading to rupture, and provides an opportunity to develop a test bed for targeted growth factor and cellular therapeutics to advance understanding of chronic tendinopathy.

By understanding the progression of tendinopathy in an animal model, appropriate heparin-derived cell-based and material-based therapeutics can be developed to slow down the progression of disease or supplement current procedures to treat ruptured tendons.

CHAPTER 2

BACKGROUND AND LITERATURE REVIEW

2.1 Tendon

2.1.1 Tendon Function and Structure

Tendons are fibrous connective tissues that transmit forces from muscle to bone to create and stabilize joint movement. Historically characterized as a passive tissue that transmits the tensile forces of muscles, tendon has a rather complex role as a stress buffer between muscle and bone that can also withstand compression and shear as it passes around bony or fibrous structures [43, 44]. Their mechanical utility allows muscles to be placed away from the joint and aids in efficient energy expenditure [43, 45]. Tendons vary in geometry, from ribbons to rounded cords, and can be surrounded by differing structures such as synovial sheaths or bursae to reduce friction [46].

2.1.1.1 Hierarchical Structure

The hierarchical structure of tendon extends from the secreted collagen molecule to organized tendon tissue. On the smallest scale, 3 polypeptide collagen chains wrap themselves into a helix to form water-soluble tropocollagen [2, 47]. Sets of tropocollagen molecules self-assemble and crosslink together to form microfibrils, which can be further organized into fibers. Collagen fibers are interspersed with tenocytes and can appear to have a crimped waveform when the tendon is not loaded in tension. Collagen fibers are then organized into tube-like fascicles. Finally, tertiary fiber bundles of fascicles and the tendon itself are surrounded by contiguous connective

tissues (endotenon and epitenon) that separate subunits and also serve to bring in blood vessels and nerves [44, 46].

2.1.2 Tendon Composition

Tendon tissues are densely organized tissues composed primarily of collagen, proteoglycans and elastin, with collagen comprising up to 70-80% of the dry weight of tissue [48]. Of the collagens, ~60% of the dry weight is due to type I collagen, up to 10% is type III collagen, and type IV, V, and VI are present in smaller amounts [48, 49]. The high tensile strength of tendon is primarily due to the parallel arrangement and intermolecular crosslinking of type I collagen. Increased type III collagen expression has been found in areas of small diameter fibrils, suggesting that it may play a role in tissue remodeling [50].

Elastic fibers, which are responsible for the extensibility of other tissues, make up at most 2% of the dry mass of tendon, yet its presence is not uniform across all tendons [2]. It has been identified across the entire flexor digitorim profundus tendon and is more consistently found near the insertion regions of tendons [51]. Elastic fibers are composed of the elastin, fibrillins, and microfibril-associated glycoprotein [52].

Proteoglycans make up approximately 1-2% of the dry weight of tendon yet may aid in withstanding tensile and compressive stresses [2, 53]. Decorin, a small leucine-rich proteoglycan (SLRP), can bind collagen directly through its core protein or glycosaminoglycans (GAGs) to regulate fibrillogenesis and control cell proliferation [54-56]. Other SLRPs such as biglycan, fibromodulin, and lumican are present in smaller amounts and can also regulate type I collagen organization and fibril diameter [56]. Large, or modular proteoglycans, such as aggrecan and versican are negatively-

charged molecules that can resist compressive forces through their charge-to-charge repulsion, and have been found in higher quantities in compressed zones [2, 56, 57].

The predominate cell type in tendon is the tenocyte, which organize longitudinally in-between collagen fibers and extend long cell processes into the extracellular matrix (ECM). This specialized fibroblasts is responsible for secreting ECM molecules as well as collagen turnover. During development, metabolically active tenocytes, tenoblasts, appear rounder, more numerous, and exhibit large endoplasmic reticulum-to-cytoplasm ratio, indicative of high protein synthesis. As the tissue matures, tenocytes become flatter, fewer in number, and appear to enter a quiescent state [58, 59]. Despite being sparsely populated with tenocytes, tendon can still respond to mechanical stimuli through the complex network of gap junctions between cells [60]. The characterization of resident tendon cells has been to date insufficient, but recent identification of tendon stem/progenitor cells may aid the process [61].

2.1.3 Tendinopathy

Tendons are highly adaptable, coupling remodeling with increased training load, frequency, or duration of loading [62]. However, tendon, for reasons not entirely clear, can procure localized damage even while undergoing loadings within physiological limits [50]. Since tendons are not very cellularized or vascularized, repair is often impaired [47, 63]. Tendinopathy has been adopted as a general term for tendon disorders characterized mainly by a combination of pain, swelling, and impaired performance [64, 65].

Overuse tendon disorders, or tendinopathies, are increasingly common diagnoses for sports and occupational injuries. Tendinopathy can account for approximately 50%

of all sports injuries [66]. Musculoskeletal disorders account for 30% of all work-related injuries that require time away from work, a measure of severity of injury, with tendon disorders requiring a higher median number of days away from work than the average of all disorders. Additionally, the highest number of days away from work was highest for injuries of the shoulder [67]. Rotator cuff injury is one of the most prevalent orthopaedic injuries to the upper extremities, causing pain, weakness, and limited motion of the shoulder joint. Once injured, shoulder tendinopathy can become chronic [68]. It has been estimated that costs for work-related upper extremity disability carries a direct cost of $6.1 billion/year, but this figure is likely higher when indirect costs to employers such as loss of productivity, quality, and replacement costs are factored in [69, 70].

Although the complete etiology of tendinopathy remains to be determined, numerous studies have shown that overuse, inappropriate loading, and the internal status of surrounding tissues are all factors in tendon disorders [62, 71]. Overuse activity alone was demonstrated to cause significant increases in cross-sectional area and decrease in maximum stress by four weeks compared to controls in the supraspinatus tendon of rats [42, 72]. Histological measures from overuse research show tendons with increased cellularity, collagen fiber disorganization, and rounded cell morphology, characteristics used to describe tendinopathic tendon [42, 73]. Tendinopathy at the insertion site, the enthesis, is one of the most common forms of tendinopathy that affects the supraspinatus, common wrist extensor, quadriceps and patellar tendons [74]. The enthesis can exhibit a zonal architecture consisting of tendon, uncalcified fibrocartilage, and calcified fibrocartilage before insertion into bone [75, 76]. This complex structure may reflect the unique loads experienced by the region between tendon and bone [9].

2.1.4 Supraspinatus Tendon

2.1.4.1 Anatomy

The glenohumeral joint consists of the humeral head positioned within the glenoid fossa of the scapula and stabilized by the rotator cuff capsule. The rotator cuff capsule contains ligaments and tendons, which include the supraspinatus, infraspinatus, teres minor, and subscapularis tendons, which work antagonistically to stabilize movement [77]. On the anterior side, the subscapularis inserts onto the humeral neck and lesser tuberosity. The supraspinatus attaches to the superior face of the greater tuberosity, followed by insertion of the infraspinatus on the posterior side. Finally, the teres minor tendon inserts to the greater tuberosity, inferior to the infraspinatus tendon. These tendons interdigitate with their neighboring tendons, leading to the possibility of load sharing [77].

The supraspinatus muscle works in concert with the deltoid muscle to allow arm abduction, which causes the supraspinatus tendon to pass under the coracoacromial arch, which consists of the coracoacromial ligament spanning between the bony acromion and coracoid process [78]. The geometry of the supraspinatus tendon differs across the tendon. The anterior portion of the supraspinatus tendon, which is characterized by a cord-like appearance, is approximately twice as long as the posterior region, which is wider and flatter [79, 80]. The insertion (lateral) region where tendon inserts into bone shows a zonal transition from tendon tissue to fibrocartilage tissue and is commonly termed the “critical zone” for the preponderance of tears that occur in that region [81].

2.1.4.2 Factors in Supraspinatus Tendinopathy

In addition to acute injuries, chronic degeneration of tissue can cause tears within the supraspinatus tendon. While there is no consensus as to which factors ultimately cause tendon degeneration, it is likely a combination of causes that make tendons susceptible to injury. Overuse of the rotator cuff is commonly accepted as one factor for injury, with many athletes who require overhead actions exhibiting chronic tendinopathy [82, 83]. Other causative factors have been grouped into intrinsic and extrinsic factors. Intrinsic factors include any changes within the tendon tissue that may alter the state of the tissue. This may include changes to vascularity within the tissue and to the compositional state of the ECM [84]. These factors may relate to the overall status of the patient such as age, activity level, and overall health. It has been shown that while collagen content in healthy supraspinatus tendon does not change with age, collagen remodeling may naturally increase after a certain age, possibly as a secondary response to a change within the tendon [85].

The extrinsic factors to tendon degeneration are based on structures outside the tendon that may cause damage to the tissue, primarily through impingement. Impingement can be caused by the coracoacromial arch, which lies superior of the supraspinatus tendon. Certain geometries of the acromion were correlated with higher incidences of tendon tears [86-88]. When the anterior portion of the acromion was more hooked, rather than flat, the supraspinatus tendon was more likely to become compressed, resulting in primary impingement. Impingement by a lateral extension of the acromion, by the coracoacromial ligament, or by the posterosuperior glenoid labrum has also been suggested as causative factors [89-91]. Secondary impingement can occur when preceded by an event that produces joint instability. Commonly seen in athletes,

imbalance in trained muscles can cause increased humeral head translation outside the glenoid fossa, leading to tendon impingement [92, 93].

2.1.4.3 Location of Supraspinatus Tendon Tears

While most tears have been observed to occur at the insertion region, there is less agreement on whether more tears occur in the anterior versus posterior region [80, 94]. More conclusive data has shown that the articular side of the tendon can experience greater forces when the abduction angle is ~60%, as this side may undergo compression from the humeral head [81, 95]. However, with higher angles of abduction, the bursal side may experience greater strain [95]. This mismatch in strain between the articular and bursal faces of tendon may cause intratendinous shear and lead to microtears, particularly on the articular surface [81]. While tears are a clear result of overuse, biochemical changes within the tissue prior to any tears can be informative on the pathophysiology of tendionopathy.

2.1.4.4 Tissue-level Changes in Tendinopathy

Histopathological characteristics of tendinopathy can vary widely, but it is accepted that overuse tendinopathy can proceed without an observable inflammatory response [96]. Instead, collagen fiber separation and disorganization, increase in non-collagenous extracellular matrix, and increase number of cells are observed in overuse tendinopathy [96-98]. The pathogenesis of tendinopathy has been explored by elucidating cellular responses to mechanical loads. In a study of the supraspinatus tendon that underwent compression, transcription profiling revealed increased expression of cartilage-associated genes such as procollagen type 2 alpha1 (*Col2a1*), aggrecan (*Agc1*), and sex determining region Y-box 9 (*Sox9*) [99]. Increase in decorin,

versican and aggregan gene expression was followed by an increase in total sulfated GAG content after rotator cuff overuse in a rat [100]. These findings suggest that the overused tendon shifted toward a cartilaginous phenotype, possibly as a result of the tendon repeatedly passing through the acromial arch. The exact mediators that cause collagen disorganization have not been fully defined in supraspinatus tendon overuse, but change in cell status and release of messenger molecules have been purported to contribute to tendon degeneration. Stress-activated programmed cell death may cause a loss of tissue maintenance and release of nitric oxide, a molecule that can modulate matrix metalloproteinases have been described after tendon overuse [101, 102].

2.1.4.5 Treatment Limitations

After tendon injury, tendon may not recover its original mechanical strength and may predispose the remaining tendon to injury [63, 79]. Conservative treatments may not address the functional recovery of the supraspinatus tendon, and in cases of tendon rupture, surgery may be needed to reattach the tendon. When possible, the tendon is reattached to the greater tuberosity through anchoring and suturing [103]. While treating recalcitrant pain and tendon tears, reinjury rates have been as high as 57% and do not address the underlying pathophysiology that can lead to tendon ruptures and re-tears [4]. Even as commercial ECM materials become available for rotator cuff repair with the hopes of stimulating intrinsic healing potential, a clearer understanding of how overuse injuries proceed will help develop better treatments [104].

2.2 Review of Current Work in Understanding Tendon Injury

Different animal models and tendon injury mechanisms exist, and the results inform different aspects of tendon injury. An acute tear, commonly performed by tendon transection, recruits an inflammatory response and has been useful in identifying cell types and biomolecules that participate in tendon healing. These studies may inform the types of signaling that should be recapitulated in studying regenerative strategies for tendon-to-bone repair [105]. On the other hand, mechanical overuse models, if they resemble the anatomy and function of human tendons, can be better models for elucidating mechanisms in chronic tendon injuries that are clinically relevant.

2.2.1 Intrinsic Growth Factor Response to Acute Tendon Injury

The intrinsic healing capacity of tendons has been studied in order to develop regenerative treatment options. When tendon was transected and allowed to heal, an upregulation of growth factors from different cell types were identified. In a healing rabbit rotator cuff, fibroblast-secreted FGF-2 was active through the proliferation and remodeling stages and may stimulate the proliferation of resident tendon cells [106, 107]. Platelet-derived growth factor (PDGF), insulin-like growth factor (IGF), transforming growth factor-β (TGF-β), and bone morphogenetic protein (BMP)-12 were similarly found during tendon healing [106, 108]. These factors can have overlapping roles in cell proliferation, matrix synthesis, and chemotaxis of cells. Thus these growth factors have been used to accelerate and improve tendon healing. Direct injection of FGF-2 was shown to increase cell proliferation and expression of type III collagen 7 days after injection into a rat patellar tendon [109]. PDGF, a potent mitogen that is stored in α granules and secreted by a variety of cells, was able to stimulate collagen and non-

collagen protein synthesis in tendon explants and improved the mechanical properties of healing tissue [110, 111].

2.2.2 Chronic Tendon Injury Model

Chronic tendon injuries in animals can be induced through overuse exercises and have been informative in describing modes of tendon injury that consider anatomical and functional relevance to human tendon injuries. The rat was selected as an appropriate model to replicate shoulder overuse due to similar soft tissue and bony anatomy around the supraspinatus tendon [112]. With overhead movement caused by downhill running, the supraspinatus tendon shows an excursion beneath the acromion similar to human supraspinatus tendon [105]. This animal model has shown evidence of pro-inflammatory markers such as elevation of cyclooxygenase-2 and five-lipoxygenase activating protein gene expression [113]. However, inflammatory cells are not typically seen in this overuse model, indicating that inflammatory mediators may be induced in the tissue by other cytokines [42, 113]. Overuse may also cause early expression of IGF-1 and increased expression of nitric oxide synthase, but their roles in tendinopathy have not been determined [102, 114]. The tendon changes in this overuse model has been shown to be repeatable, with increases in cartilaginous features, most likely due to repetitive compression as the supraspinatus tendon slides beneath the acromion [99, 115].

2.3 Proteolytic Degradation of Collagen

2.3.1 Matrix Metalloproteinases

Human matrix metalloproteinases are a family of at 23 zinc-dependent endopeptidases, capable of cleaving a host of extracellular proteins. Most MMPs display

a similar overall structure consisting of a propeptide region, a zinc-containing catalytic domain, a linker peptide, and a hemopexin domain [116]. The MMP family can be categorized by their typical substrates: 1) collagenases (MMP-1, MMP-8, MMP-13), 2) gelatinases (MMP-2, MMP-9), 3) stromelysins (MMP-3, MMP-10), 4) matrilysins, and 5) membrane type MMPs [117]. While baseline MMP activity is low, they can be readily induced by inflammatory cytokines, growth factors, cell-cell, and cell-matrix interactions [118]. They are secreted as latent enzymes and can be activated by other enzymes at physiological pH [119]. The collagenases are able to degrade interstitial collagens of type I, II, and III into characteristic ¾ and ¼ fragments, by unwinding the collagen helix and cleaving α chains in succession [120]. Gelatinases can degrade the smaller collagen fragments released during activity of the collagenases, as well as directly cleaving collagen types IV, V, and XI. While MMP-2 is a gelatinase, it can also directly cleave type I, II, and III collagen, although it is much less active than MMP-1 [121]. The stromelysin MMP-3 is known to play an important function in activating pro-MMPs and can be crucial in initiation collagen degradation [122]. MMP activity is tightly monitored by reversibly binding 1:1 to tissue inhibitors of metalloproteinases (TIMPs).

Due to the importance of MMPs in tissue maintenance and remodeling, as well as their presence in various diseases, they have also been studied in degenerative tendon. Macroscopically normal supraspinatus tendons have demonstrated relatively high levels of MMP-1, MMP-2, and MMP-3, suggesting that this tendon undergoes high turnover and remodeling compared to the biceps brachii tendon, which rarely experiences pathology [123]. However, ruptured supraspinatus tendons showed increased activity of

MMP-1 and decreased activity of MMP-2 and -3, resulting in significant amounts of denatured collagen and less overall collagen that may weaken the overall mechanical properties of the tendon [123, 124]. Decreased expression of MMP-3 has been correlated to increased expression of proteoglycans in chronic tendinopathy, suggesting that decreases in certain MMPs may also prove to be a pathological feature [125]. Additionally, an imbalance between MMPs and TIMPs, which has been shown with torn rotator cuff tendons, may signal a disruption in tissue homeostasis [126].

2.3.2 Cysteine Cathepsins

Cysteine cathepsins are mostly monomeric papain-related proteinases with currently 11 members. These proteinases have a wide range of functions, from bone remodeling to wound healing to antigen processing [127-129]. They are optimally active at acidic pH and are usually located within lysosomal compartments [130]. Cathepsins generally share the same overall structure of two domains separated by a "V"-shaped catalytic region. On one side of the catalytic domain, α helices dominate, while on the other side, a β barrel motif exists [131]. In the catalytic region, a conserved cysteine residue on one side coordinates with a histidine residue on the opposite side at the β barrel region to cleave a substrate [132]. Cathepsins are translated with a propeptide region that can be enzymatically cleaved by other proteases such as cathepsin D or pepsin, or removed autocatalytically at acidic pH [132, 133]. Since high concentrations of cathepsins can exist within lysosomes, they are tightly regulated by a reversible, tight-binding superfamily of inhibitors. The cystatin superfamily of cathepsin inhibitors consists of 3 families: 1) stefins, 2) cystatins, and 3) kininogens [134]. Stefins

lack a signal peptide and primarily act intracellularly, while cystatins and the larger kininogens can act extracellularly [132].

Cathepsin L is potent in degrading elastin and collagen type I, more efficiently than cathepsin B [135, 136]. Cathepsin L can cleave collagen at the telopeptide regions, causing loss of crosslinks and instigating depolymerization. Cathepsin K was originally detected in osteoclasts and ovaries, but its expression has subsequently been detected in epithelia and other cells [137]. Cathepsin K is able to cleave collagen I and II through the triple helix near the N-terminal region, rather than the well-defined collagenase-sensitive site, as well as the telopeptide regions [138]. This is in contrast to collagenases which can typically only cleave at one or the other [139].

2.4 Cocultures of MSCs with Differentiated Cell Types1[1]

Paracrine and autocrine signaling can affect gene expression, protein production, proliferation, and apoptosis in the tissue microenvironment – significant issues in forming physiologically viable tissues, from development to remodeling to regeneration [35]. The concept of cocultures, studies involving at least two different cell types to understand the potential cellular crosstalk effects, attempt to address the paradigm of tissues as modular systems that cannot be treated in isolation. With this perspective, crosstalk between cells affects the metabolism and fate of neighboring cells. Coculture systems have the potential to expand the available number of cells for clinical applications by using signals from a small pool of primary cells to induce differentiation in a large population of stem cells [36].

[1] Portions of this section were adapted from Seto SP, Temenoff JS. Coculture Systems for Mesenchymal Stem Cells. In: Fisher JP, Mikos AG, Bronzino JD, Peterson DR, eds. *Tissue Engineering: Principle and Practices*. Boca Raton, FL: CRC Press; 2012:21.1-21.6.

2.4.1 MSC Cocultures with Chondrocytes

Recent results with chondrocytes cultured in 3D environments have shown that cocultured MSCs express osteogenic phenotypes. Articular chondrocytes encapsulated in alginate beads and suspended over a monolayer of bone marrow-derived MSCs (BM-MSCs) remained viable in the system for up to 21 days. Alkaline phosphatase (ALP) expression, an indicator of mineralization, was elevated in MSCs with exposure to chondrocytes. In fact, the longer the time in coculture, the more accelerated the calcium deposition and phenotypic change from spindle-shaped to osteoblast-like cuboidal-shaped [140]. An osseous phenotype could form by day 28 when both MSCs and articular chondrocytes were encapsulated in alginate and cultured in the presence of dexamethasone and ascorbic acid, suggesting that one of the cell types was maturing or differentiating [141]. By utilizing cells from two different species of animals to allow specific gene probing, the cartilaginous phenotype of the coculture was shown to originate from the chondrocytes, but higher glycosaminoglycan (GAG) production and type II collagen production was seen with a greater number of MSCs in the coculture system [141]. Several additional studies have utilized encapsulated MSCs cocultured with chondrocytes cultured in 3D, and have shown increased expression of chondrocyte markers such as type II collagen and aggrecan, but did not report the presence of hypertrophic markers [142-144].

MSCs are presumed to be more sensitive to contact-dependent signals than more differentiated cells, which may make them amenable to direct coculture [145]. ALP activity was measured in cocultures that varied the relative number of cells to 1:1 and 1:2 MSC to chondrocyte pellet co-cultures. Both groups suppressed ALP activity, but

the 1:2 group exhibited a significantly lower ALP activity than controls [146]. Furthermore, these MSC-chondrocyte cell pellets fully inhibited mineralization when implanted subcutaneously into immunodeficient mice, suggesting that certain cocultures can inhibit chondrocyte hypertrophy [146]. Conversely, the MSC-only pellet produced a calcified cartilaginous tissue when implanted and exhibited the presence of collagen type X and elevated ALP levels. When rabbit MSCs were cultured with chondrocytes in hydrogels at ratios of 1:1 and 3:1, higher type II collagen and aggrecan expression was observed for the 1:1 group compared to the 3:1 group [144]. Taken together, the relative amount of chondrocytes in the co-culture system may affect the levels of chondrogenic expression observed as well as the degree of chondrocyte hypertrophy. Stem cell contact with articular chondrocytes in a 3D environment may help prevent hypertrophy [147].

2.4.2 MSC Cocultures with Osteoblasts

Studies with conditioned media from osteoblasts have indicated that osteogenic genes and phenotype can be induced in stem cells, but some of these studies utilized dexamethasone, a potent glucocorticoid, which can mask signaling between cells [148, 149]. Results from these conditioned media experiments contradict another study in which mature osteoblasts were only slightly osteogenic toward C3H10T1/2 stem cells, indicating that media type can affect the phenotype observed [150]. Furthermore, the use of conditioned media is not representative of the dynamic signaling that can occur between two cell types over time.

Two-way signaling between osteoblasts and MSCs may produce a differentiation niche similar to that seen in the natural microenvironment [151]. Murine osteoblasts cocultured with MSCs in a transwell system showed no change in proliferation or gene

expression over 3 weeks in dexamethasone-free medium. The cocultured MSCs, however, showed increased expression of runx2, osterix, osteopontin, and bone sialoprotein at 3 weeks compared to MSC-only controls [152]. Similarly, human MSCs cocultured with human osteoblasts exhibited upregulation in bone sialoprotein-2, lipoprotein receptor, ALP, and osteocalcin by day 14 when cocultured with twice the amount of osteoblasts than MSCs [151]. The results indicate that soluble factors from osteoblasts can induce MSCs into a more osteogenic phenotype by upregulating both early and late bone markers over time.

Cell-to-cell contact between MSCs and osteoblasts can enhance communication between cells. Gap junctions, transmembrane channels between neighboring cells that allow communication through the cytoplasm, are present between osteoblasts, osteoclasts, and osteocytes [153]. Connexin 43 is the most abundant gap junction in bone and beyond allowing cells to respond to external stimuli, has been shown to be required for osteoblast differentiation and function [153-155]. Human osteoblasts were shown to couple to bone marrow stromal cells and allow Luciferase dye transfer, a phenomenon that was inhibited by the application of octanol, an inhibitor of gap junction communication [156].

The exact mechanisms that link cell contact or soluble signaling to gene expression remain elusive, but depend on the types of signals, downstream effects, and cell contact proteins involved. The Wnt pathway was identified to play an inductive role in MSC differentiation in studies comparing indirect and direct co-culture without osteogenic factors [152, 157]. The increased secretion of Wnt by osteoblasts was observed with a concomitant increase in β-catenin and TCF/LEF1 levels, downstream

effectors of Wnt, in MSCs cultured indirectly with osteoblasts. However, the upregulation of bone-related markers in indirect co-culture were reversed when osteoblasts were cultured in direct contact with MSCs in a ratio 1:4 in a mixed monolayer [152]. Direct cell culture offset the stimulatory effect of osteoblasts by crosstalk between cadherin-β-catenin pathway and the Wnt pathway. In this study, it is suggested that soluble factors can induce osteogenesis in MSCs while cell contact can reduce osteogenic differentiation potential.

2.5 Bone Morphogenetic Protein-2 (BMP-2)

2.5.1 *In Vivo* Roles of BMP-2

BMPs are part of the transforming growth factor-β superfamily and play vital roles in skeletal development [158]. Bone morphogenetic proteins (BMPs) were first identified as a component of decellularized and demineralized bone matrix that had bone-forming capabilities [159, 160]. They were subsequently shown to be sufficient in inducing cartilage and heterotopic bone *in vitro* and *in vivo* [24, 161, 162]. BMP-2, -4, and -7 are disulfide-linked dimers that have been found to have many roles in bone and cartilage development as well as postnatal fracture healing [163]. In developing limbs, BMP-2 is expressed in the mesenchyme surrounding early cartilage condensation and may play roles in cell recruitment and differentiation of cells into chondrocytes [164]. Additionally, BMP-2 can accelerate the transition of proliferating chondrocytes to hypertrophy [165]. In the early stage of endochondral ossification in bone fracture healing, many cells increase expression of BMPs in the callus, suggesting that BMPs participate in differentiating cells in the callus [165]. Specifically, they have been shown

to be a potent factor in mesenchymal stem cell differentiation into osteochondrogenic or osteoblastic precursor cells [21, 23, 24].

2.5.2 BMP-2 Structure

Bone morphogenetic protein-2 (BMP-2) is structurally very similar to BMP-4. BMP-2 exists as a homodimer with each subunit of approximately 114 residues stabilized by 3 intrachain disulfide bonds that form a cysteine knot [160, 166]. The overall structure of each subunit is composed of predominately β-sheets in addition to 4 α-helices [166, 167]. While the monomer differs from many other globular proteins because it lacks a substantial hydrophobic core, 2 hydrophobic cores are formed upon dimer formation between the α3 of one subunit and the β-strands of the other subunit, forming a single disulfide bond. While it has been observed that BMP-2 appears to be relatively stable since it is retrieved by harsh chemical treatments [160], the solubility of the non-glycosylated form is unusual because it prefers an acidic environment and its solvent-accessible hydrophobic residues tend to make BMP-2 aggregate [168].

2.5.3 Signaling Pathway

BMPs can signal through binding serine/threonine kinase receptors, composed of type I and II subtypes [169]. After heterotetrameric clustering of these receptors, signal transduction proceeds through Smad 1/5/8, whereby the phosphorylated Smad molecule associates with Smad 4 and ultimately translocates to the nucleus to activate transcription factors such as Runx2 [170]. BMP in the extracellular space can be inhibited by noggin or chordin by directly interfering with the receptor binding epitope [171].

2.5.4 Clinical Use of BMP-2

The current approved delivery system for BMP-2 is via an absorbable collagen sponge and has been used in spinal fusion as the Medtronic Infuse® Bone Graft. This product, introduced in 2002, has been approved for spinal fusion, open tibial fractures, and sinus augmentation [172, 173]. However, BMP-2 has low affinity to collagen and has been shown to have a short half-life in solution [28, 174]. Possibly to counter this, delivery vehicles are often loaded with supraphysiological doses of BMP-2 [29], which increases overall costs and has been shown to have adverse effects, such as bone resorption [27, 29, 172, 175].

2.5.5 BMPs in Tendon-to-Bone Integration

BMP-2 and BMP-7 have been detected during patellar tendon healing, suggesting that these molecules take part in intrinsic healing [176]. Resident tendon stem/progenitor cell populations, although just a small fraction of tendon cells, can be induced to form osteotendinous junctions with treated with BMP-2 [61]. When BMP-2 was used to calcify tendon prior to fixation in a bone tunnel, better integration and higher ultimate failure loads were observed [17]. BMP-2, in a low dose, may accelerate the healing response between tendon and bone causing the tendon to fail away from the repair site by as early as 4 weeks [18].

2.5.6 Heparin-Binding Region of BMP-2

When the N-terminal of BMP-2 was proteolytically cleaved, some unspecific binding and variability in biological activity was reduced, indicating that this region may take part in diverse binding, dependent on cell type and environment [169]. It has been since shown that this sequence preceding the first cysteine knot at the N-terminal is

heparin binding [168]. Unlike some other TGF-β factors, this region is not covalently attached to the protein core by disulfide bonds [177], making this region relatively flexible. The crystal structure determination of BMP-2 has often characterized this region as a disordered area with primarily basic residues [168, 177]. This disorder has been implied to be advantageous in binding the heterogeneous structures of glycosaminoglycans such as heparin or the structurally similar heparan sulfate [177, 178].

2.6 Heparin

2.6.1 Structure and Biosynthesis

Heparin is a linear, helical glycosaminoglycan (GAG) polymer composed of repeating units of uronic acid and glucosamine residues [30, 179]. It has the highest negative charge density of known biomolecules due to numerous carboxyl and sulfate groups. Heterogeneous in weight, heparin ranges from 3-30kDa (average 15kDa) [180]. A disaccharide unit on average contains 2.7 sulfate groups, often substituted on the 6O- and N- position on glucosamine; and the 2O- position on iduronic acid [30, 181]. The uronic acid residues are primarily composed of L-iduronic acid and exhibit conformational flexibility that may aid in specific protein interactions [182, 183]. Furthermore, the N- position on glucosamine can be left unsubstituted, acetylated, or sulfated, thereby increasing heterogeneity in sulfation [184].

Heparin, and the structurally similar heparan sulfate proteoglycan, has many functions that include regulating cell adhesion and protease storage [185, 186]. Biosynthesis of heparin and heparan sulfate begin similarly with non-sulfated GAG

molecules attached to a protein core. In post-processing steps, sulfotransferases couple sulfates to the pyranose subunits and a sequence of proteases ultimately release heparin from peptides [187, 188]. Unlike heparan sulfate, which can be found widely distributed on cell surfaces, heparin is primarily found in mast cells and some hematopoietic cells [189].

2.6.2 Heparin-Protein Interactions

2.6.2.1 Antithrombin III

Heparin can have very specific interactions with proteins, such as that described with the glycoprotein antithrombin III. Antithrombin III was found to bind with heparin at high affinity at a 1:1 stoichiometry and accelerate its inhibition of thrombin and factor Xa [190]. It was found that a very specific sequence of heparin, a pentasaccharide sequence with a relatively rare 3-O sulfate on glucosamine, was the smallest and most necessary fragment for activity [191-194]. This sequence also required a conformational change of iduronic acid into a skew boat form, further supporting that a change in geometry of heparin was needed to induce a corresponding change in antithrombin [193].

2.6.2.2 Fibroblast Growth Factors

The most researched protein-heparin interactions after antithrombin-heparin are likely those with fibroblast growth factor (FGF)-1 and -2. Although they have similarities, FGF-1 exhibits lower affinity for heparan sulfate than FGF-2 [195]. Heparin-binding amino acid sequences have been identified for these growth factors and it has been determined that variations in heparin sulfation can affect binding and signaling [196-198]. Only the N- and 2-O sulfation of heparin was necessary to bind FGF-2, but stimulation of FGFR1 required the presence of 6-O sulfation on heparin

[199]. In contrast, 6-O sulfation was necessary for the biological activity of FGF-1 [200, 201]. While FGF-1 and FGF-2 are structurally similar, their interaction with heparin differs. Heparin behaves more as a co-factor for FGF-2 signaling, in which it helps dimerize FGF-2:FGFR1 units [31]. In the case of FGF-1, multiple FGF-1 molecules complex with heparin in solution and subsequently bind to receptors that are induced to dimerize [202]. In both cases, while there may be some controversy on to the minimal binding sequence, heparin is necessary in promoting FGF signaling when surface heparan sulfates are absent [31, 203, 204].

Binding to heparin can protect FGF-1 and -2 from denaturation due to heat and proteolysis, likely by forming specific interactions that prevent protein unfolding or access to proteases [205-207]. It was shown that a 5-molar excess of heparin could protect FGF-1 from 1% trifluoroacetic acid treatment or heat treatment at 65°C for 5 minutes, while only an almost stoichiometric 1:1 amount of heparin was needed to protect FGF-2 from the same treatments [205]. Furthermore, heparin was able to protect FGF-2 from 2% trypsin cleavage for up to 8 hours, while FGF-2 without heparin was degraded by 3 hours [208].

There are other heparin-binding proteins such as BMP-2 and heparin-binding epidermal growth factor-like factor with identified heparin-binding domains [168, 209]. Both these growth factors contain heparin-binding domains near the N-terminal, but neither growth factors require heparin for growth factor-induced signaling such as in the case with FGF-1 and -2. Rather, exogenous heparin can maintain BMP-2 concentrations in cell culture medium by preventing BMP-2 inhibition by noggin [174]. While endogenous cell-surface heparan sulfate molecules sequester BMP-2 and mediate BMP-

2 internalization, heparin may play a role in keeping BMP-2 away from the cell surface and limiting BMP-2 endocytosis [22, 210].

2.6.3 Heparin and Heparan Sulfate Mediation of Stem Cell Differentiation

2.6.3.1 Changes in expression of heparan sulfate during stem cell differentiation

Heparan sulfate has a critical role in binding and activating growth factors for cell signaling in tissue development. More recently, there has been evidence of the evolving presence and structure of proteoglycans themselves in stem cell biology. Murine embryonic stem cells exhibited enhanced heparan sulfate (HS) synthesis following a transition into embryoid bodies or endodermal cells [211]. Also, HS shifted from an unusually low sulfated variant in embryonic stem cells to a more highly sulfated form in progenitor cells [211, 212]. This change was accompanied by the relatively early activity of N-sulfotransferases, followed by 6O, 3O-sulfotransferases [212]. This research suggests that the presence of certain proteoglycans such as HS may signal cell exit from a pluripotency state to a more differentiated cell type.

2.6.3.2 HS and Heparin in osteogenic differentiation

Exogenous addition of HS has been shown to increase the expression of osteoblast markers in osteogenic environments. Local administration of bone derived HS to a rat femoral fracture caused an increase in callus size alongside increased expression of Runx2, ALP and FGF-1, suggesting that HS could enhance osteogenesis in endogenous cells [213]. When HS proteoglycans from differentiated osteoblasts were administered to pre-confluent, preosteoblast MC3T3-E1 cells, Runx2, ALP, and osteopontin expression was enhanced [214]. Additionally, the source of HS had an effect on cultures, as soluble and surface-derived HS upregulated different FGF receptors,

likely in response to the different core proteins from the different sources. Endogenous liberation of HS by heparinase treatment can also cause an increase in osteogenic gene expression, in addition to an increase in BMP signaling through the Smad pathway [215]. This suggests that HS may enhance the changes in growth factor presentation that can cause shifts in cell membrane receptors [216, 217].

While heparin lacks the core protein of HS, the presence of heparin has been shown to enhance osteogenic differentiation of MSCs without the addition of growth factors as well [218]. In contrast to the above results, some studies have shown that heparin can inhibit osteoblastic differentiation or decrease the number of bone nodules formed, but these studies were conducted with soluble heparin in which medium was replenished regularly [219, 220]. Frequent replenishment may deplete the concentration of growth factors that remain bioactive while bound to heparin in solution.

2.7 Heparin-Containing Delivery Systems

2.7.1 Physical Incorporation of Heparin

Heparin can be incorporated into delivery systems in a variety of methods. One avenue is to use heparin in its native form without chemical modification. This has the benefit of retaining biological activity of heparin, which was shown to decrease with higher degrees of chemical modification [34]. Polyelectrolyte multilayer coatings are produced by layer-by-layer deposition of alternating cationic and anionic polyelectrolytes. By adjusting fabrication techniques, layer thicknesses and capacity for growth factor storage can be tuned [221, 222]. Heparin layered with cationic chitosan on tissue culture polystyrene had to ability to store and delivery FGF-2 to induce cell

proliferation better than soluble delivery of FGF-2 [223]. The ability for heparin to interact with growth factors and retain its bioactivity motivates the use of heparin. With this concept, complexes between heparin and positively-charged proteins directly can be formed. When the complex is strongly hydrated, a soluble complex can form, and with decreasing amounts of hydration where the net charge approaches 0, a coacervate can form as a liquid-liquid phase transition [224]. A coacervate of heparin, FGF-2, and a polycation to neutralize remaining charges had the properties of remaining injectable, reducing burst release, and preserving FGF-2 bioactivity [225, 226]. The complexity of the unmodified heparin delivery system can increase as more features are required. To combine an enzymatically degradable hydrogel with affinity features, a fibrin-based delivery system was developed with covalent attachment of a heparin-binding peptide that electrostatically immobilized heparin [227]. When this system was used to deliver TGF-β in a tendon defect, accelerated healing at early timepoints was observed, with improved tendon properties by 28 days [228].

2.7.2 Covalent Crosslinking of Heparin into Hydrogels

Chemical modification of heparin to allow covalent attachment to delivery systems, particularly hydrogels, has been investigated for protein delivery and cell encapsulation where release of soluble heparin is not desired. Covalent crosslinking of polymers can occur with radical initiation or Michael-type additions between constituents with reactive side groups [229, 230]. Heparin, with its numerous carboxyl and hydroxyl groups, is amenable to chemical substitutions such as thiols, methacrylates and malemides [231-233]. Since side groups such as carboxyls can be important in growth factor binding, a balance needs to be achieved where enough chemical

modification allows robust hydrogel formation while also retaining bioactivity [231, 234]. It has been shown that increasing the amount of methacrylation from 6% to 22% on heparin can significantly reduce the amount of BMP-2 binding, although the level of affinity needed may depend on the application [34]. The addition of small quantities (up to 1% w/w) of heparin into a delivery system was shown to attenuate burst release and prolong the time of growth factor release [233]. By introduction of cell-adhesive peptides such as RGD, cell encapsulation was also achieved within heparin-containing hydrogels, allowing more complex delivery systems [34, 235].

CHAPTER 3

DIFFERENTIATION OF MESENCHYMAL STEM CELLS IN HEPARIN-CONTAINING HYDROGELS VIA COCULTURE WITH OSTEOBLASTS[2]

3.1 Introduction

Tissue engineering approaches, using combinations of cells, scaffolds, and bioactive factors, have been explored for the restoration of orthopaedic tissues such as bone, ligaments, and cartilage [236-238]. An attractive cell source for cell therapies is mesenchymal stem cells (MSCs), multipotent cells with significant proliferative and regenerative capacity *in vitro* [239]. In addition to their expansion potential, MSCs have been differentiated toward osteogenic, chondrogenic and myogenic lineages, enabling their use in reconstructing orthopaedic tissues [240]. Direct delivery of MSCs into tissue defects has shown some salutary effects [241], but the *in vivo* therapeutic efficacy can be improved by priming MSCs toward the desired cell lineages prior to implantation [242]. In prior work, pre-treatment of MSCs in differentiation media for as little as 4 days showed enhanced MSC-mediated chondrogenic and osteogenic extracellular matrix production when implanted *in vivo* [243, 244]. While treatment with specified media formulations has shown to be effective in "pre-differentiating" cells prior to transplantation in some cases, recapitulating the native differentiation environment where multiple morphogens are presented temporally to MSCs remains desirable,

[2] Portions of this chapter were adapted from Seto SP, Casas ME, Temenoff JS. Differentiation of mesenchymal stem cells in heparin-containing hydrogels via coculture with osteoblasts. Cell Tissue Res. 2012;347:589-601.

especially for cells with less characterized differentiation pathways such as intervertebral disc cells [245].

Coculture systems have been utilized previously to enhance proliferation of cells of interest and differentiate stem cells with a population of differentiated cells [32, 246]. Certain cell types, such as intervertebral disc-derived cells, as well as osteoblasts, have limited expansion capabilities *ex vivo* [36, 243] so the ability to regulate a large population by culturing with a small pool of primary cells would be useful in a variety of cell-based therapies. In this study, we have chosen to examine osteogenic differentiation of human MSCs cocultured with human osteoblasts as a proof-of-concept experiment, but the approach described could be easily transferred to other cell types of interest for specific applications.

Heparin, a highly-sulfated linear glycosaminoglycan (GAG), (and the structurally similar heparan sulfate) has been implicated in many biological processes such as tissue morphogenesis, wound repair, establishment of morphogen gradients, and regulating the availability of growth factors to cells [217, 247]. In addition, there is evidence that complexation with heparin protects growth factors from enzymatic degradation and may catalyze growth factor presentation to cells, inducing such responses as proliferation and MSC differentiation [247-250]. These functions have prompted investigations of the use of heparin as a drug delivery system and cell carrier. Heparin has been immobilized in different scaffolds including poly(ethylene glycol)-based materials [235, 251, 252]. Recently, heparin has also been integrated in cell-adhesive and enzyme-sensitive hydrogels to enable cell-mediated degradation of heparin-containing carrier materials [253, 254]. The presence of heparin was

demonstrated to attenuate burst release of bone morphogenetic protein-2 (BMP-2) and basic fibroblast growth factor, both signals associated with osteogenesis [251, 255], from PEG-based hydrogels.

While much previous work with heparin-based biomaterials has focused on their use as a growth factor release vehicle and/or suitability for cell encapsulation, few studies have been conducted investigating heparin-containing biomaterials' role in sequestration of multiple soluble factors from the culture environment. In response, we have designed synthetic, poly(ethylene glycol)-based hydrogels with varying degrees of incorporated heparin to examine if the amount of heparin present influences osteogenic differentiation of embedded MSCs when cocultured with osteoblasts. For many orthopaedic applications, hydrogels are advantageous as they provide a 3D culture environment that is more representative of native tissues while providing a high degree of control over the properties surrounding encapsulated cells [256]. In these experiments, MSCs were encapsulated in hydrogels composed of oligo(poly(ethylene glycol) fumarate) (OPF)/poly(ethylene glycol)-diacrylate (PEG-DA)/heparin methacrylamide (heparin MAm), subsequently placed in a transwell insert, and cocultured with a monolayer of osteoblasts. We hypothesized that MSCs cultured in hydrogels with higher amounts of heparin would produce higher levels of osteogenic markers over time when compared to hydrogels without heparin. Additionally, we hypothesized that coculture of encapsulated MSCs with osteoblasts would promote the osteogenic phenotype when compared to encapsulated MSCs cocultured with a monolayer of MSCs. In particular, alkaline phosphatase activity, calcium accumulation, and histology were evaluated for up to 21 days. Furthermore, in order to better understand possible mechanisms behind

the results observed, the hydrogels were also characterized for their ability to differentially sequester charged model proteins from solution.

3.2 Materials and Methods

3.2.1 Polymer Synthesis

Oligo(poly(ethylene glycol) fumarate) (OPF; Mn = 23,900 ± 200 Da, polydisperity index (PI) = 4.1 ± 0.1) and poly(ethylene glycol)-diacrylate (PEG-DA; Mn = 3,800 ± 20 Da, PI = 1.1 ± 0.0) were synthesized, purified, and stored as previously described [257, 258]. OPF and PEG-DA were analyzed by gel permeation chromatography (GPC, Shimadzu GPC and Waters column) to determine molecular weight and the polydisperity index. For cell encapsulation studies, the arginine-glycine-aspartic acid (RGD) adhesion peptide (Peprotech, Rocky Hill, NJ) was conjugated to a 3400 Da MW acrylated-PEG-succinimidyl valerate spacer (Laysan Bio, Arab, AL) according to previous protocols [259].

In order to allow heparin crosslinking, heparin was modified using N-(3-dimethylpropyl)-N'-ethylcarbodiimide (EDC) / N-hydroxysulfosuccinimide (sulfo-NHS) chemistry modified from a previous protocol [260]. N-(3-aminopropyl) methacrylamide (APMAm; Polysciences, Warrington, PA) was conjugated to high molecular weight heparin sodium salt from porcine intestinal mucosa (17-19kDa, Sigma-Aldrich, St. Louis, MO) to form heparin methacrylamide (MAm). In a solution of 0.005 mmol EDC (Sigma-Aldrich) and 0.005 mmol sulfo-NHS (Sigma-Aldrich) in dH_2O, 1.61 mg/mL heparin sodium salt (~0.00125 mmol GAG by mer MW) was combined with 0.005 mmol APMAm. The reaction mixture was incubated at room

temperature for 2 h with stirring at pH 5-6. Another round of the above amounts of APMAm and EDC were added, and the reaction was allowed to proceed for another 2 h. After a total reaction time of 4 h, the mixture was dialyzed against 10 mM NaCl for 1 day, followed by dH_2O for 2 days and then lyophilized (Labconco, Kansas City, MO) for 4 days. All polymers were stored at -20°C until use. Structures of polymers used are shown in Figure 3.1.

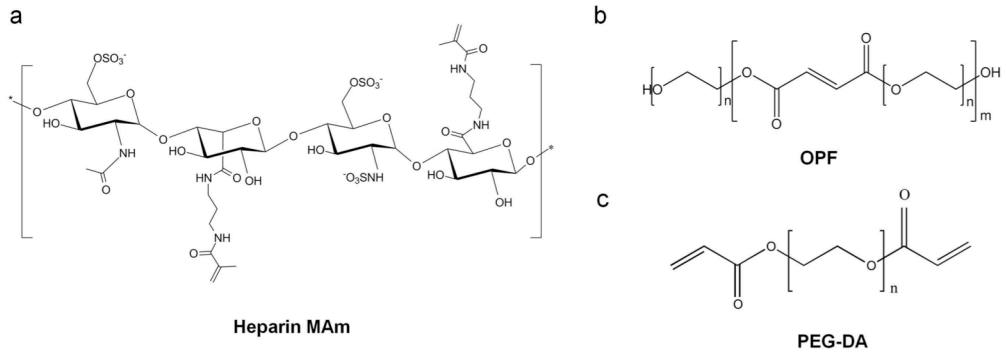

Figure 3.1 Polymers utilized in these experiments. (a) Chemical structure of heparin methacrylamide (MAm). (b) Chemical structure of oligo(poly(ethylene glycol) fumarate (OPF). (c) Chemical structure of poly(ethylene glycol)-diacrylate (PEG-DA).

3.2.2 Heparin-Containing Hydrogel Fabrication

OPF and PEG-DA were used as a mixture of 50:50 by weight in all hydrogels. Heparin MAm was incorporated in amounts of 0%, 1%, and 10% weight of total dry weight of polymer and subsequently dissolved in PBS (Invitrogen, Carlsbad, CA) with 0.05% w/w Darocur 2959 (D2959, CIBA Chemicals, Tarrytown, NY) for an initial water content of 90% (w/w). Macromer solutions were dispensed in 40 μL amounts into PTFE (Teflon) wells and crosslinked under 365 nm UV light (UVP, Upland, CA) at an

approximate intensity of 10 mW/cm^2 for 15 minutes. Resulting hydrogel disks were 6 mm in diameter and ~1 mm thick.

3.2.3 Hydrogel Characterization and Heparin Release

Hydrogel discs containing 0%, 1%, and 10% heparin MAm were fabricated as described above and were allowed to swell for 24 h in PBS at 37°C. The swollen hydrogel discs were weighed and subsequently lyophilized for 24 h. The dry weights were measured and the fold swelling ratio of swollen to dry weights (W_s/W_d) were calculated.

To image hydrogels with sulfated GAGs, hydrogels were stained at 2 time points. After fabrication, hydrogels were allowed to swell in a solution of 1,9-dimethylmethylene blue (DMMB; Sigma-Aldrich) for 5 hours with hourly replacement of DMMB, rinsed in PBS, and imaged with a digital camera. A second set of hydrogels was allowed to soak in PBS for 4 days, with daily replacement of PBS, and thereafter stained in a solution of DMMB for 1.5 hours.

To evaluate the ability of heparin MAm to remain covalently crosslinked in hydrogels, a heparin MAm release study was conducted. Hydrogels were fabricated as detailed above and placed in 1 mL of PBS. On days 1, 2, 3, and 4 the entire volume of supernatant was removed and replaced with fresh PBS. Supernatant volumes were recorded and amount of heparin MAm in the supernatant was determined by comparison to standards incubated with DMMB and read on a plate reader at 520 nm.

3.2.4 Human Mesenchymal Stem Cell (MSC) Culture

Cryopreserved human MSCs were obtained from Texas A&M Health Science Center College of Medicine Institute for Regenerative Medicine at Scott & White and

were harvested and characterized as described elsewhere [261]. Thawed cells were expanded in growth media consisting of alpha-minimum essential medium (α-MEM, Mediatech, Manassas, VA) containing 16.3% fetal bovine serum (FBS, HyClone, Logan, UT), 1% antibiotic-antimycotic solution (A/A, Mediatech), and 1% 200 mM L-glutamine (Mediatech). Cells were cryopreserved at passage 3. For encapsulation, MSCs were thawed, expanded until 80% confluent, and trypsinized with 0.05% trypsin/EDTA (Mediatech). Cells were encapsulated at passage 4 at a density of $10x10^6$ cells/mL.

3.2.5 Human MSC Encapsulation and Viability Staining

Heparin methacrylamide (MAm) was incorporated in amounts of 0%, 1%, and 10% (w/w) in OPF/PEG-DA hydrogels containing 1μmol/g of the RGD peptide sequence. Polymers and peptide were dissolved to a final concentration of 10% w/w in cell suspension and PBS containing 0.05% w/w D2959. The macromer and cell solution was dispensed in 40 μL aliquots and crosslinked for 15 min under UV exposure in Teflon molds.

For viability studies, hydrogels were maintained in cell medium containing αMEM, 10% FBS, 1% A/A, and 1% 200 mM L-glutamine. Medium was exchanged every 3 days. At days 1 and 21, hydrogels were rinsed for 30 min in sterile PBS and subsequently incubated in LIVE/DEAD staining solution (Invitrogen) for 45 min at 37°C. Hydrogels were rinsed of excess stain and imaged with a confocal microscope (LSM 510; Carl Zeiss, Germany) at 3 points on each gel. Three hydrogels for each formulation were imaged and z-stacks were collected at 10 μm intervals. Images located within the interior of each stack were compared.

3.2.6 Osteoblast Cell Culture and Coculture with MSC-laden Hydrogels

3.2.6.1 Monolayer cell culture

Human osteoblasts (Lonza, Walkersville, MD) were expanded for 9 doublings in osteoblast growth medium (Lonza) supplemented with osteoblast growth medium SingleQuots (Lonza). Osteoblasts were trypsinized and stored frozen in medium, 10% FBS, and 10% dimethyl sulfoxide (DMSO; Sigma-Aldrich) until use. Upon thawing, cells were seeded into 12-well plates at a density of 10,000 cells/cm^2 and allowed to proliferate for 4 days in growth medium consisting of low glucose DMEM (Mediatech), 10% FBS (HyClone), 1% amphotericin B (Mediatech), and 0.1% gentamicin (Mediatech). After 4 days in growth medium, osteoblasts were incubated for 3 days in osteogenic medium (10% FBS, 1% amphotericin, 0.1% gentamicin, 50 μM L-ascorbic 2-phosphate sesquimagnesium (Sigma-Aldrich), 10 mM β-glycerolphosphate (Alfa Aesar, Ward Hill, MA), and 100 nM dexamethasone (Alfa Aesar)) in order to preserve the cell phenotype prior to switching the cells to the coculture medium.

For coculture with MSC monolayers, passage 4 MSCs were plated at 20,000 cells/well in 12-well plates 2 days prior to start of the coculture study to allow cells to attach and equilibrate from thawing.

3.2.6.2 MSC Encapsulation

MSCs were encapsulated in 0%, 1% and 10% heparin MAm hydrogels as detailed above. Acellular hydrogels were also fabricated and served as blank controls. Blanks and cell-laden hydrogels were placed in 0.4 μm pore transwells (Corning, Lowell, MA) and placed over wells of osteoblasts or MSCs. Coculture system medium consisted of 10% FBS, 10 mM β-glycerolphosphate, 50 μM L-ascorbic acid 2-phosphate sesquimagnesium, 1% amphotericin B and 0.1% gentamicin in low glucose DMEM.

Medium was exchanged every 3 days. At day 11, in order to prevent over-confluence of cells, MSC and osteoblast monolayers were replaced with cells pre-cultured in the same conditions as the original plates. On days 1, 14, and 21, hydrogels (n=3 per culture condition) were retrieved, rinsed of medium, crushed with a pellet grinder, suspended in 750 µl ddH_20 and underwent 3 freeze-thaw cycles to lyse cells for assays to quantify DNA content, alkaline phosphatase activity, and calcium concentration. Also on day 21, hydrogels (n=2 per culture condition) were collected for histology.

3.2.7 Biochemical Assays for DNA Content, ALP Activity, and Calcium Accumulation

DNA content was quantitatively analyzed over time by the Quant-iT PicoGreen dsDNA Assay kit (Invitrogen) per manufacturer's instructions. Fluorescent output was read with a plate reader (SpectraMax M2e; Molecular Devices, Sunnyvale, CA).

For the ALP assay, in a 96 well plate, 50 µL aliquots of the cell lysates were incubated with 100 µl of 20 mM p-nitrophenol phosphate substrate solution (Sigma-Aldrich) and 50 µL alkaline buffer at 37°C for 60 min. A standard solution was made with a serial dilution of p-nitrophenol in ddH_2O (Sigma-Aldrich) and similarly incubated with the substrate solution and alkaline buffer. The absorbance at 405 nm was read on a plate reader and the ALP activity was determined using the standard curve.

Calcium concentration was determined by reaction of calcium in the samples with Arsenazo III (Genzyme Diagnostics, Cambridge, MA), producing a blue-purple complex. Homogenized samples were incubated overnight in an equal volume of 1 N acetic acid at 37°C. In a 96 well plate, 25 µL aliquots of samples were incubated at room temperature with 275 µL of Arsenazo reagent for 10 min. Standard solutions were made

by serial dilution of calcium chloride in acetic acid. The absorbance of each well was read at 650 nm. Acellular hydrogels were fabricated and cocultured with monolayers of osteoblasts or MSCs, similar to cell-laden hydrogels. In all biochemical assays, values from acellular hydrogels were subtracted from data values obtained from cell-laden hydrogels. Three samples were analyzed for each sample type at each time point.

3.2.8 Histological Evaluation of Mineralization

At day 21 of the coculture experiment, hydrogels were fixed in 10% neutral buffered formalin for 2 hours and stored in 20% sucrose solution overnight at 4°C. Samples were embedded in a 50:50 ratio of optimum cutting temperature (Sakura Finetek, Torrance, CA) compound:20% sucrose by volume, placed in a vacuum chamber for 4 h to increase penetration of embedding material into samples, and flash frozen in liquid nitrogen. Histological sections of 10 μm thick slices were obtained from a cryostat (HM 560 Cryo-Star; Microm, Germany) and stained with von Kossa stain. Briefly, sections were incubated in a 5% solution of silver nitrate (Sigma-Aldrich) in ddH_20 for 15 min under a UV lamp. Slides were washed with ddH_20 and unreacted silver nitrate was removed by incubating sections with 5% sodium thiosulfate for 3 min. Sections were counterstained with eosin. Slides were examined by light microscopy (Eclipse TE2000-U, Nikon, Melville, NY).

3.2.9 Cell Density on Hydrogel Surfaces

On days 1 and 21 of coculture, hydrogels were rinsed with PBS and placed in solutions of 0.01 ng/mL Hoechst 33258 stain (Invitrogen) in PBS for 2 h in an incubator. Hydrogels were imaged from the surface down to 200 μm below the surface by collecting z-stacks at an interval of 10 μm on a confocal microscope (Zeiss 510 NLO

META). Z-stacks were projected into a 2-dimensional image and analyzed for cell number by counting nuclei in ImageJ (NIH, Bethesda, MD).

3.2.10 Model Protein Absorption into Heparin-containing Hydrogels

To examine the electrostatic interaction between charged proteins with heparin-containing hydrogels, negatively-charged casein (MW=19-24 kDa; Sigma-Aldrich) and positively-charged histone from calf thymus (MW=11-21 kDa; Sigma-Aldrich) at pH 7.4 were conjugated to fluorescein isothiocyanate (FITC, Acros Organics). 100 mg of protein was dissolved in 25 mL of bicarbonate buffer solution at pH 8.3. A total of 1.25 mL of a 2 mg/mL FITC solution in DMSO was slowly dropped into the protein solution and 70.2 mg of ammonium chloride (Sigma-Aldrich) was added to the reaction. The reaction was allowed to proceed for 8 h at 4°C protected from light. The conjugated protein solutions were then dialyzed against ddH_20 for 4 days.

Hydrogels containing 0%, 1%, and 10% wt. heparin were fabricated and allowed to swell in PBS overnight. Hydrogels were then placed into 24-well plates with 1 mL of FITC-conjugated protein solution for 1 day. For confocal imaging, each hydrogel was taken directly from the protein solution and placed in the cell chamber containing PBS for immediate imaging. Three spots per hydrogel and 3 gels per condition were imaged. All microscope settings (master gain=670, digital gain=1.0, digital offset=-1.68, pinhole=94 μm, and laser=488 nm, 3%) were maintained across all samples. The average fluorescence value for each layer of the stack was computed and compiled in MATLAB (Mathworks, Natick, MA). In order to average the 3 stacks from each hydrogel, a MATLAB algorithm was created to align the maximum fluorescence value of each stack. The relative fluorescence value was then averaged from the 3 stacks at

each depth through the hydrogel, resulting in an average curve for each hydrogel. The average fluorescence values over the 3 hydrogels for each condition were computed similarly. Statistical analysis was performed on predetermined depths and limited to less than half of the hydrogel thickness, as the ability to collect data past a depth of 600μm was attenuated when z-stacks were collected.

3.2.11 Statistical Analysis

Results are displayed as mean ± standard deviation. ALP activity and calcium data were transformed with the Box-Cox transformation for analysis. Data were analyzed by one-way, two-way, and/or three-way analysis of variance to identify groups with significant differences and interactions. Tukey's *post hoc* with the significance level set at $p<0.05$ indicated significant differences between individual samples. Statistical analysis was performed with Systat Software (Chicago, IL).

3.3 RESULTS

3.3.1 Hydrogel Characterization and Heparin Release

Hydrogels formed robust gels after 15 min of UV exposure and the addition of up to 10% wt. heparin did not statistically affect the swelling ratio of the hydrogels (Figure 3.2a). There was a slightly deeper staining observed in the 10% wt. heparin MAm hydrogels versus the 1% heparin formulations when hydrogels were allowed to swell in DMMB for 5 hours after fabrication. The 0% wt. heparin hydrogels did not exhibit staining characteristic of GAG incorporation. Additionally, after 4 days in PBS (replenished daily), the 10% wt. heparin hydrogels were obviously stained a deep purple, confirming that greater amounts of sulfated heparin were present within this formulation

after removal of any uncrosslinked fractions (Figure 3.2a, bottom row). In addition, the staining also appeared to suggest that sulfated heparin was distributed relatively uniformly throughout the hydrogels and clear differences existed between hydrogel types even after 4 days of soaking in PBS. Release of uncrosslinked heparin MAm from the hydrogels occurred in a burst release at 1 day, with little additional release thereafter (Figure 3.2b). By day 4, the cumulative percent released from 1% and 10% wt. heparin MAm hydrogels were not significantly different.

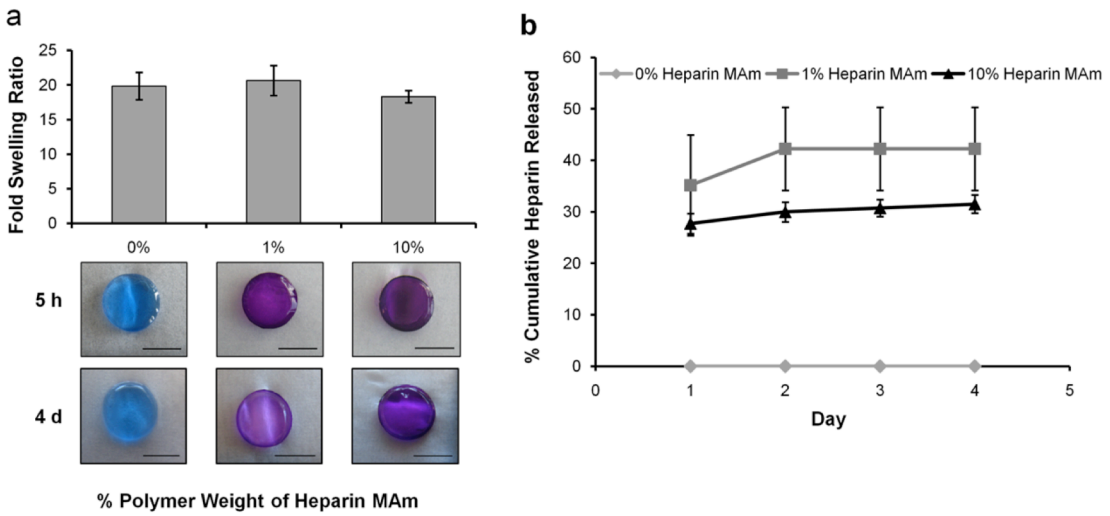

Figure 3.2 Heparin MAm can be covalently integrated within hydrogels without affecting the swelling ratio and with minimal release of heparin MAm from hydrogels over time. (a) Fold swelling of 1% and 10% wt. heparin MAm/wt. polymer hydrogels were not significantly different than fold swelling of hydrogels without heparin MAm ($p>0.05$, n=4±S.D.). DMMB staining of hydrogels at 5 hours and 4 days after fabrication showed more intense staining with incorporation of increasing amounts of heparin MAm. *Scale bar*=5 mm. (b) The cumulative release of uncrosslinked heparin MAm at day 4 was not significantly different between the 1% than 10% wt. heparin MAm hydrogels.

LIVE/DEAD staining revealed that MSCs encapsulated in 0%, 1%, and 10% wt. heparin MAm hydrogels were predominately viable throughout the hydrogel thickness and viability was comparable between day 1 and day 21 (Figure 3.3).

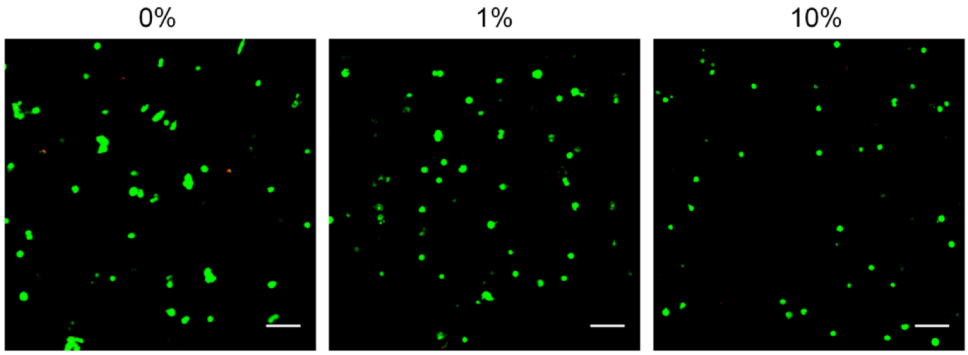

Figure 3.3 Human mesenchymal stem cells (hMSCs) remain viable in heparin MAm-functionalized hydrogels for 21 days. Live cells are stained green and non-viable cells are stained red. *Scale bar*=100μm

3.3.2 Biochemical Assays for DNA Content, ALP Activity, and Calcium Accumulation

DNA retrieved from hydrogels on day 21 showed that the DNA level from 0% wt. heparin MAm hydrogels cocultured with MSCs was significantly lower than the DNA content of 10% wt. heparin MAm hydrogels also cocultured with MSCs (Figure 3.4). In comparison between coculture types, 10% wt. heparin MAm hydrogels cocultured with MSCs had a higher DNA content than 10% wt. heparin MAm hydrogels cocultured with osteoblasts. Within the osteoblast coculture group, all hydrogels had statistically different DNA content from each other. In all samples, there was a significant decrease in DNA content by day 21 either from day 1 or day 14 (data not shown).

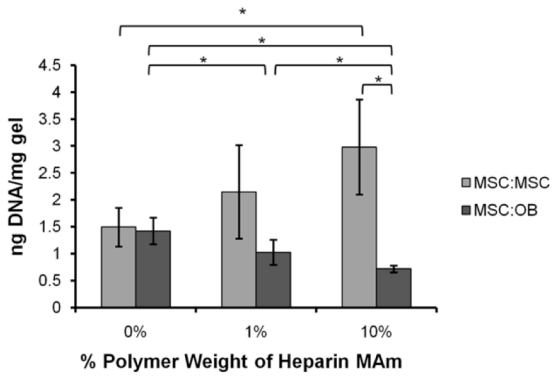

Figure 3.4 DNA content from cocultured hydrogels on day 21 show no significant differences between MSC and osteoblast cocultures in 0% and 1% wt. heparin hydrogels. There is a significant decrease in DNA quantified in 10% wt. heparin MAm hydrogels cocultured with osteoblasts compared to all other hydrogels cocultured with osteoblasts. * designates a significant difference ($p<0.05$, n=3±S.D.) between indicated samples.

When in coculture with osteoblasts, the MSCs encapsulated in 0%, 1%, and 10% wt. heparin MAm hydrogels exhibited significantly higher ALP activity on day 1 than samples cocultured with MSCs (Figure 3.5a). This trend continued until day 21, with all samples cocultured with osteoblasts exhibiting higher ALP activity than the same hydrogel type cocultured with MSCs at the same time point. While the MSCs encapsulated in the 1% wt. heparin MAm hydrogels did not exhibit any change in ALP activity over time, the cells in the 0% wt. heparin MAm hydrogels showed either no change (when cocultured with MSCs) or a decrease (when cocultured with osteoblasts) between day 1 and 21. With MSCs encapsulated in 10% wt. heparin MAm hydrogels, ALP activity increased over time when cocultured with osteoblasts resulting in a 5-fold increase from day 1 to day 21. This sample exhibited the highest ALP activity compared to all samples on day 21. Conversely, ALP activity decreased with time for MSCs in 10% wt. heparin MAm samples cocultured with MSCs.

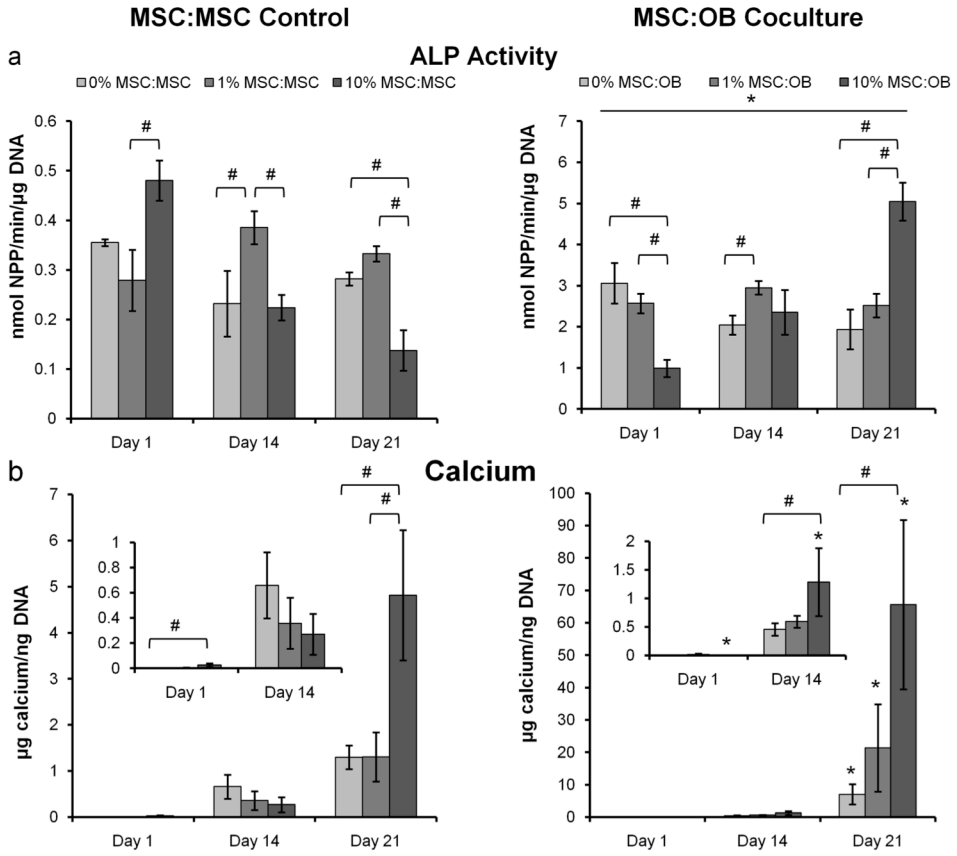

Figure 3.5 10% heparin MAm hydrogels with encapsulated MSCs and cocultured with osteoblasts show marked alkaline phosphatase (ALP) activity and calcium accumulation by day 21 compared to other hydrogel formulations. (a) Higher ALP activity was observed for hydrogels cocultured with osteoblasts compared to coculture with MSCs. Hydrogels containing 10% wt. heparin MAm showed significantly higher ALP activity than other hydrogel types by day 21 ($p<0.05$, $n=3\pm$S.D.). Note different scales for y-axes. (b) Calcium accumulation increased over time for each hydrogel type, with 10% MSC:OB showing the highest calcium concentration by day 21 compared to all other samples besides 1% MSC:OB ($p<0.05$, $n=3\pm$S.D.). Note different scales for y-axes. * indicates significant difference from MSC:MSC coculture at the same day and hydrogel type; # designates significant difference between indicated samples.

Little to no calcium accumulation was observed in all samples on day 1 of coculture, but by day 21, the 1% and 10% wt. heparin MAm cell-laden hydrogels accumulated significantly more calcium when cocultured with osteoblasts compared to MSC coculture controls (Figure 3.5b). By day 21, the 10% wt. heparin MAm samples cocultured with osteoblasts showed an over 50-fold increase in calcium content from

day 14 and was significantly higher than the MSC coculture controls on the same day. Encapsulated MSCs cocultured with MSCs did not exhibit any large differences in calcium accumulation between hydrogel types until day 21, when calcium accumulation was greatest in the 10% wt. heparin MAm hydrogels (Figure 3.5b). Differences between osteoblast and MSC cocultures were not observed for 0% and 1% wt. heparin MAm samples until day 21, when samples cocultured with osteoblasts showed marked increase over samples cocultured with MSCs. MSCs in 10% wt. heparin MAm hydrogels initially showed slightly higher calcium amount in samples cocultured with MSCs, but by day 14, samples cocultured with osteoblasts showed significantly higher calcium accumulation.

3.3.3 Histological Evaluation of Mineralization

Histological evaluation of hydrogels after 21 days of coculture by von Kossa staining shows cell-associated mineral accumulation in all samples, regardless of coculture conditions (Figure 3.6). Mineral accumulation also occurred on the edges of 1% and 10% wt. heparin MAm hydrogels cocultured with osteoblasts, with more intense mineral staining in the 10% wt. heparin MAm samples (Figure 3.6e). Mineral deposition was also observed for the 10% wt. heparin MAm hydrogels cocultured with MSCs, although to a lesser extent (Figure 3.6f).

3.3.4 Cell Density on Hydrogel Surfaces

There were no significant differences in cell density on all cocultured hydrogels on day 1. Counting cells on the surface of hydrogels cocultured with MSCs and osteoblasts at day 21 revealed that the cell density on 10% wt. heparin MAm samples was not significantly different between coculture types. Additionally, the cell density on 10% wt. heparin MAm hydrogels was lower than on 0% wt. heparin hydrogels and not

significantly different than the number of cells on the surface of 1% wt. heparin hydrogels (data not shown).

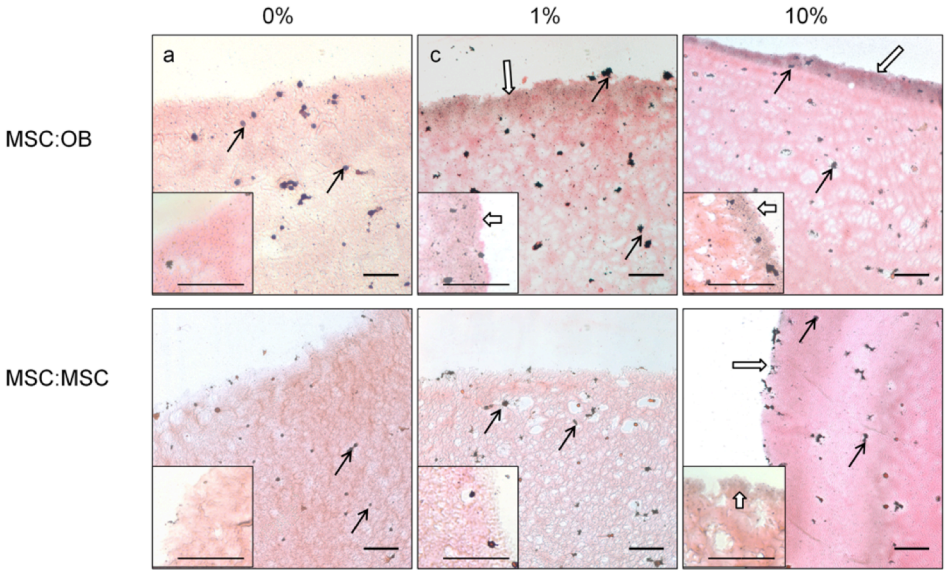

Figure 3.6 Mineralization occurs pericellularly, with additional surface mineralization on the 10% heparin hydrogels. Histological sections showing mineralization (stained black) of 0% (a-b), 1% (c-d), and 10% (e-f) wt. heparin MAm hydrogels cocultured with osteoblasts (a, c, e) and MSCs (b, d, f) on day 21. All samples exhibited cells with mineralization within the interior of the hydrogels (black arrows). The 1% and 10% wt. heparin MAm samples cocultured with osteoblasts exhibited mineralization on the periphery of the hydrogels (c,e, white arrow). The 10% wt. heparin MAm samples cocultured with MSCs showed peripheral staining to a lesser degree (f). Insets show magnification of representative edges of the hydrogels. *Scale bar*=100µm

3.3.5 Model Protein Absorption into Heparin-containing Hydrogels

In this study, model proteins, casein and histone, were chosen for their respective negative and positive overall charge at pH 7.4. Confocal images showed that casein and histone have different profiles within the hydrogels and across the varying amounts of heparin MAm. Casein was distributed relatively uniformly throughout the hydrogel thickness in all hydrogel formulations (Figure 3.7a-c). Histone displayed a more uniform distribution in the 0% wt. heparin MAm samples, but appeared more localized to the

surface of the hydrogels in 1% and 10% wt. heparin MAm samples (Figure 3.7d-f). The protein intensity in the 0% wt. heparin MAm hydrogels was similar across depth of the hydrogel for both casein and histone (Figure 3.7g). However, with 1% and 10% wt. heparin MAm, the histone fluorescence decreased with increasing depth into the hydrogel, with a more precipitous decrease in intensity with depth in the 10% wt. heparin MAm hydrogels (Figure 3.7h, i). In 10% wt. heparin MAm hydrogels, the same fluorescence intensity was collected for both casein and histone within the first 100 μm

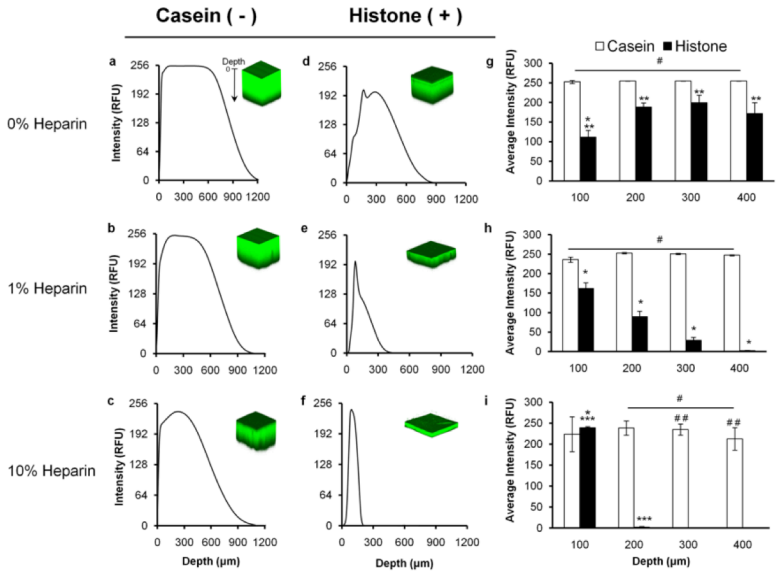

Figure 3.7 Negatively and postively-charged proteins have different absorption profiles into 0%, 1%, and 10% wt. heparin MAm hydrogels. FITC-casein was absorbed into the entire thickness of the hydrogels across all heparin amounts (a-c). FITC-histone was absorbed into the entire thickness of the 0% wt. heparin MAm samples (d), but only penetrated a small fraction of the 1% and 10% wt. heparin MAm samples (e,f). Column graphs show average intensity of labeled proteins at specified depths across 0%, 1%, and 10% wt. heparin MAm hydrogels (g-i). # indicates that the casein intensity is significantly higher than the histone intensity at the same depth and heparin content; ## indicates that the intensity is lower than the casein intensity at the corresponding depth in the 0% wt. heparin MAm hydrogels; * indicates difference from all other histone intensity measurements in the same hydrogel type; ** indicates difference in histone intensity from the other hydrogel types at the same depth; *** indicates that the histone intensity is different than the histone intensity at the same depth in the 1% wt. heparin MAm hydrogels.

of the hydrogel, but the average histone intensity dropped close to 0 with increasing depth. Alternatively, casein intensity remained relatively uniform throughout the analyzed depth.

3.4 DISCUSSION

Coculture systems may help achieve certain phenotypes or level of differentiation prior to transplantation for stem cell-based therapies [151, 262]. Here, MSCs were cocultured with osteoblasts as a proof-of-concept study in order to better understand the role of the biomaterial environment in priming stem cells in coculture with native, differentiated cells. In the present study, cells remained viable in all hydrogel formulations through 21 days of culture (Figures. 3.3 and 3.4), but the interaction of heparin-containing biomaterials and osteoblast-mediated paracrine signaling significantly promoted the differentiation of MSCs toward the osteogenic lineage.

In these experiments, cells were encapsulated within hydrolytically degradable hydrogels that show little degradation over the study period [263], which may prevent cell proliferation and induce a rounded cell morphology. However, these materials were chosen because previous research has shown similar materials to have the appropriate mesh size (Å to nm) to allow diffusion of nutrients for cell encapsulation [264, 265], while preventing potential confounding factors for this study, such as cell spreading. The high viability and number of cells (Figure 3.3) observed in all samples is in concurrence with previous studies of encapsulated cells [251, 266-269]. There were no differences in the DNA content of hydrogels between coculture type within the 0% and 1% wt. heparin

hydrogel formulations on day 21 (Figure 4.4), indicating that DNA content was not a factor in the differences observed in the bioassays. Although less DNA was observed in the 10% wt. heparin MAm hydrogels cocultured with osteoblasts compared to other hydrogel types (Figure 4.4), this may be attributed to the increased mineralization in these hydrogels, which can hinder DNA diffusion out of the gel for subsequent quantification [263].

The absence of significant differences in fold swelling up to 10% dry wt. heparin MAm suggests similar mesh sizes between hydrogel types [270], which implies that there are relatively minor differences in mechanical properties and transport through the network between these formulations [271]. Non-crosslinked heparin MAm in hydrogels is primarily released by day 1, which precludes any long-term effects of soluble heparin in the system. Therefore, the biological results observed from these experiments can be primarily attributed to increasing amounts of heparin incorporated into the hydrogels. Increasing amounts of heparin in hydrogels have been shown to reduce release of positively-charged growth factors (Supplementary figure A.1), and may play a role in sequestering soluble factors from the coculture environment.

In this study, a 3D hydrogel environment was investigated as a means to expose a relatively large number of MSCs to a much small number of cells in monolayer. For these experiments, the number of MSCs originally encapsulated was approximately 5 times greater than the osteoblasts used in each cocultured sample. Past studies have shown increased osteogenic markers such as ALP activity by day 14, but use of twice the number of osteoblasts compared to MSCs may have accelerated the differentiation in that coculture study [151]. The results in this study suggest that a smaller pool of

differentiated cells can successfully be used to prime a larger population of MSCs, which could be important when *ex vivo* expansion of a differentiated cell type is limited. Results demonstrate an increase in ALP activity, particularly in the 10% wt. heparin MAm hydrogels cocultured with osteoblasts, which suggests that MSCs differentiated toward the osteogenic lineage. ALP is one marker for osteoblastic differentiation and indicates the capacity for cells to produce a mineralized matrix [140, 151]. In this study, the elevated ALP activity observed in samples cocultured with osteoblasts suggests that heparin interacted with osteoblast-secreted factors to mediate MSC-directed ALP production not seen in acellular controls. In a prior study, increased bone-related gene expression as well as increased calcium staining by alizarin red in MSCs by 3 weeks have been shown in cocultures involving monolayers of MSCs and osteoblasts [152]. In the present study, an increase of ALP activity by day 21 for the coculture with osteoblasts is comparable in timescale.

It has been found that ALP production is stimulated by BMP-2 administration and regulated through the canonical Wnt pathway [272]. The presence of members of the BMP family is likely in our coculture system since it has been established that osteoblasts can secrete BMP-2, BMP-4, and BMP-7, which are known to induce osteogenesis in MSCs [273, 274]. Furthermore, previous research has shown that specific BMP interaction with heparin results in the augmentation of the biological activity of BMPs, as reflected in the production of mineralized tissue or induction of osteoblastic differentiation of MSCs [34, 249, 275], which makes these hydrogel formulations particularly suited to enhancing pro-osteogenic signaling from nearby cells.

Calcium deposition, a late marker that indicates the capacity for cell-mediated matrix mineralization [276], on day 14 was greatest in the 10% wt. heparin MAm samples cocultured with osteoblasts, but by day 21 all samples cocultured with osteoblasts exhibited greater calcium accumulation over their MSC cocultured counterparts (Figure 3.5). Calcium accumulation was higher in samples cocultured with osteoblasts even after subtraction of calcium values from acellular controls, suggesting that the increase in calcium is at least partially cell-mediated by MSCs or the crosstalk between MSCs and osteoblasts.

Mineralization, as evidenced by von Kossa staining was evident around cells throughout all samples with more intense staining on the edges of 1% and 10% wt. heparin MAm hydrogels cocultured with osteoblasts (Figure 3.6). Previously, MSCs have been shown to differentiate and mineralize in PEG-based hydrogels in the presence of osteogenic medium, including the glucocorticoid dexamethasone [277]. In order to unmask the signaling that can occur between MSCs and osteoblasts, dexamethasone was not used in our coculture system, but increases in ALP activity and mineralization were still observed in the hydrogels. The coculture medium did include β-glycerolphosphate, a source of phosphate, which has been shown to be necessary to initiate mineralization [278] yet does not greatly increase the expression of bone proteins such as bone sialoprotein and osteocalcin in a manner like dexamethosone [279]. Mineralization was not observed on the surface of 0% wt. heparin MAm hydrogels and were not as heavily mineralized in MSC controls at higher heparin amounts, indicating that the presence of heparin may affect the level of mineralization observed, but cell mediation of mineralization is also necessary, as evident in this study. Similarly, there was no

significant difference between cell density on the 10% wt. heparin MAm hydrogels cocultured with MSCs or osteoblasts at either day 1 or 21 of culture, indicating that the extra mineral observed on the surface of samples cocultured with osteoblasts was not due to additional cells on the surface.

Although the mechanism is unknown, previous research has shown evidence that heparin can prevent mineralization in differentiating cells [219, 280], in contrast to the results presented here. These prior studies utilized soluble or adsorbed heparin, which may be removed upon media changes, along with any biomolecules that may have complexed with them. The level of soluble heparin concentration has been shown to have a biphasic effect on mineralization [281], but it is not known how mineralization is affected by covalently bound heparin as used in this study. Benoit et al. showed that osteogenic differentiation of MSCs was possible in heparin-functionalized PEG hydrogels, possibly due to integrin engagement or BMP binding [251]. Additionally, the interaction between heparin and extracellular proteins, such as collagen and fibronectin, may improve mineralization in heparin-containing materials [282, 283].

Heparin has been shown to have increasing affinity for positively-charged proteins with increasing chain length and sulfation [284]. In this experiment, high molecular weight heparin was used and the DMMB assay revealed that sulfated molecules were retained in the hydrogels, suggesting that high affinity may exist between secreted soluble factors and heparin in the coculture system. Although it was expected that electrostatic interactions between protein and heparin could occur uniformly throughout the entire hydrogel thickness, it was observed that the presence of heparin reduced diffusion of positively-charged molecules, such as the model protein

histone, into the hydrogel, particularly in the 10% wt. heparin MAm formulation (Figure 3.7). This phenomenon was not observed when hydrogels were allowed to absorb the similarly sized, negatively-charged protein casein. Molecular transport is often limited by molecular size, but there is emerging research on the filtering effects of charged extracellular matrix (ECM) molecules that may act as an electrostatic bandpass [285]. An *in vivo* study has shown that the presence of heparan sulfate in the ECM can decrease the effective diffusion coefficient of polyanion-binding lactoferrin through tissues by ~60% [286], indicating that the effective charge of heparin can affect the diffusion of charged molecules in our system. These studies correlate well with our observations of positively-charged histone sequestration primarily to the surface of heparin-containing hydrogels.

For future design of biomaterials to "capture" soluble signals from the medium or another nearby cell type, results from our studies suggest that surface, rather than bulk, biomaterial modification methods may be all that is required at high amounts of heparin. Additionally, the overall heparin amount incorporation can be reduced to allow more uniform transport of soluble factors in hydrogels of thickness on the order of 1 mm or greater. Results from our study between charged proteins and heparin-containing hydrogels also have implications in creating new biomaterials to exclusively "capture" and localize positively-charged proteins for future studies in growth factor presentation to cells or in creating soluble factor gradients.

While further work is required to elucidate the particular factors that bind to the heparin hydrogels and the effect of soluble factor transport through heparin-containing hydrogels on uniform priming and extent of differentiation of cells, our results are

encouraging for the use of GAG-based biomaterials to tune the responsiveness of cells in coculture and holds promise as a means of priming a large population of stem cells with only a small biopsy. Prior research has shown that pre-culture can instruct *in vivo* differentiation and improve clinical outcome, and our studies represent a potent method to prime MSCs, especially when control over the extent of differentiation is desired [241, 242, 244, 287]. As such, the ability to prime a large population of cells by employing GAG-based biomaterials and in conjunction with a smaller pool of differentiated cells is an attractive method that could greatly increase the feasibility of using autologous cells for orthopaedic tissue engineering and regenerative medicine.

3.5 Conclusions

Overall, these studies capitalize on the ability of heparin to bind charged soluble factors for a novel approach to priming stem cells. MSCs encapsulated in higher amounts of heparin exhibited elevated levels of osteogenic markers when cocultured with osteoblasts in the absence of dexamethasone. Increase in ALP activity, calcium accumulation, and surface mineralization over 21 days was most drastic in 10% wt. heparin MAm hydrogels cocultured with osteoblasts, suggesting that the biomaterial composition can modulate differentiation of MSCs exposed to paracrine signals from nearby osteoblasts. In the future, these proof-of-concept studies will be instructive in developing a framework for a biomaterial-based stem cell priming system with various other differentiated cell types. As demonstrated here, the ability to promote paracrine signaling between cells in the expansion phase via biomaterial carrier design has

exciting implications in the field of regenerative medicine, particularly for cases when treatments are limited by the availability of differentiated, autologous cells.

CHAPTER 4

PRESERVATION OF BMP-2 BIOACTIVITY BY SOLUBLE HEPARIN DEPENDS ON SULFATION LEVEL

4.1 Introduction

Bone morphogenetic proteins (BMPs), members of the transforming growth factor (TGF)-β superfamily, were first identified as a component of decellularized and demineralized bone matrix that had bone-forming capabilities [159, 160]. They were subsequently shown to be sufficient in inducing cartilage and heterotopic bone *in vitro* and *in vivo* [161, 162]. In developing limbs, BMP-2 is expressed in the mesenchyme surrounding early cartilage condensation and may play roles in cell recruitment and differentiation of cells into chondrocytes [164]. Additionally, BMP-2 can accelerate the transition of proliferating chondrocytes to hypertrophy [288].

Participation in bone and cartilage formation has made BMP-2 attractive for tissue regeneration applications. It is currently available as a therapeutic protein and an absorbable collagen sponge has been approved as its carrier for spinal fusion, open tibial fractures, and sinus augmentation [172, 173]. However, BMP-2 has low affinity toward collagen, leading to diffusion out of the scaffold and into off-site areas [28]. Additionally, BMP-2 has been shown to have a short half-life, suggesting a lower potency for the overall therapeutic *in vivo* [174]. To counter this, delivery vehicles are often loaded with supraphysiological doses of BMP-2, which increases overall costs and has been shown to cause adverse effects [29, 172, 175]. An ideal therapeutic would limit

diffusion out of the scaffold to prevent offsite side-effects and prevent loss of BMP-2 bioactivity to improve clinical efficacy and lower costs.

Heparin, a highly sulfated glycosaminoglycan (GAG), can bind many growth factors, either electrostatically or through carbohydrate specific sequences. This feature makes it an attractive biomaterial to reduce burst release. However, heparin is used clinically as an anti-coagulant [289], which may limit its use *in vivo* unless the anti-coagulant aspect is ablated. Although it was shown that selective desulfation of heparin can significantly reduce the anti-coagulant activity of heparin [290, 291], heparin desulfation may impact the interactions between heparin and proteins. The specific heparin binding to fibroblast growth factor (FGF) -1 and -2 has been studied extensively and was shown to protect FGF from acidic, enzymatic and high temperature conditions [205, 208, 292]. It was found that N- and 2-O sulfation on heparin aided binding of heparin to FGF-2, but the 6-O sulfate group was needed to stimulate the FGF receptor for FGF-induced cell signaling [199]. Removal of these specific sulfation patterns reduced FGF-induced signaling. In contrast to these studies, how the role of sulfation level and sulfate arrangement on heparin affects the bioactivity of bone morphogenetic protein (BMP)-2 has not been as well established, despite the use of BMP-2 in clinical applications.

To date, the protective effects of desulfated heparin derivatives on BMP-2 when exposed to denaturing environments have not been elucidated. Unlike FGF-2, which requires heparin for signaling, BMP-2 has a heparin-binding domain removed from the active site of the protein [168]. And unlike other TGF-β factors, this heparin-binding region is not covalently attached to the protein core by disulfide bonds, making this

region relatively flexible [177]. This flexibility has been implied to be advantageous in binding the heterogeneous structures of heparin or the structurally similar heparan sulfate [177, 178]. Understanding the interactions between desulfated heparin derivatives and BMP-2 can help develop safe and effective delivery systems.

Bacterial expressed recombinant proteins commonly exhibit a lack of glycosylation compared to mammalian expressed proteins. Glycosylation can confer benefits in terms of improved solubility and pharmacokinetics, but the glycosylation of recombinant proteins expressed in eukaryotic cells remain difficult to control and reproduce [293]. While protein expression from *E. coli* systems lack the glycosylation machinery, it has the benefit of being procedurally simple, rapid, cost efficient, and well-characterized [294, 295]. In addition, these non-glycosylated proteins are suitable for studies that probe how the protein backbone may be affected by external factors, without the confounding effects of glycans.

The objective of Specific Aim II was to evaluate how the level of sulfation on heparin affects the stability of BMP-2 when exposed to thermal stress. Three desulfated derivatives were evaluated: N-desulfated (Hep^{-N}), 6-O,N-desulfated ($Hep^{-N,-6O}$), and completely desulfated heparin (Hep^{-}). The hypothesis of this study was that soluble complexes formed between heparin and BMP-2 can protect BMP-2 against thermal denaturation, and that this protection varies with the sulfation level on the heparin molecule. Using an established cell-based bioactivity assay, the bioactivity of non-glycosylated BMP-2 was evaluated following exposure to high temperature over 15 minutes in order to probe the effect of co-delivery of heparin derivatives. Interactions with desulfated heparin derivatives were further probed by measuring the thermal

stability of a positively-charged model protein, histone, when heated over 31-81°C in differential scanning fluorimetry.

4.2 Materials and Methods

4.2.1 Heparin Modifications and Characterization

4.2.1.1 Heparin Desulfation to Hep^{-N} and $Hep^{-N,-6O}$

Heparin sodium salt from intestinal mucosa (Sigma-Aldrich) was desalted by passing a ~10mg/mL solution of heparin in ddH_2O through an ion exchange column. Dowex 50WX4 resin (mesh size 100-200, Sigma-Aldrich) was dispersed in ddH_2O and poured into a preparative column (460mm effective length, 10mm internal diameter, Ace Glass) with a sealed fritted disc (70-100μm) and glass stopcock at the outlet. The resin was washed with ddH_2O until the supernatant ran clear. The heparin solution was added slowly to the resin and collected in a 500mL round bottom flask. After all the heparin solution was poured through, the column was washed with an additional 2 lengths of water. Adding pyridine in 2mL increments, the pH of the desalted heparin was increased to ~6. Excess water and pyridine was evaporated on rotary evaporator (Buchi). The solution of heparin pyridine was then dialyzed for 3 days, flash frozen in liquid nitrogen, and lyophilized to a powder.

For Hep^{-N} production, heparin pyridinium salt was dissolved at 1mg/mL in a 90% DMSO/10% ddH_2O solution [290, 296]. The mixture was stirred in a round bottom flask at 50°C for 2h using a water bath. The solution was then cooled on ice and precipitated by an equal volume of 95% ethanol (VWR) saturated with sodium acetate (VWR). The precipitate was centrifuged and supernatant decanted. The precipitate was

washed once more with ethanol prior to mixing with dH_2O. The solution was dialyzed for 3 days with daily exchanges of dH_2O and then lyophilized.

For $Hep^{-N,-6O}$ synthesis, a solution of 10mg/mL of heparin pyridine was made in 90% N-methylpyrrolidone (NMP, Acros Organics)/10% ddH2O [301]. The solution was mixed in a round bottom flask and heated to 90°C on a heating mantle for 48h. The solution was then cooled on ice and precipitated with 95% ethanol saturated with sodium acetate. The precipitate was stirred for an additional 2h on ice and then centrifuged to remove excess ethanol and H2O from heparin. The resulting powder was dissolved in H2O and dialyzed for 3 days prior to lyophilization.

4.2.1.2 Heparin Desulfation to Hep^-

Nonselective desulfation was carried out with a protocol adapted from Kantor and Schubert [297]. Heparin sodium salt was stirred at 5.0mg/mL in methanol (VWR) containing 0.5% v/v acetyl chloride (Acros Organics). The dispersion was centrifuged and acidic methanol was replaced on days 1, 3, and 6 to produce a methyl ester of heparin. The product was then dissolved in 20mL dH_2O per gram of heparin before precipitation in an excess of 95% ethanol while on ice. The methyl ester of heparin was centrifuged and washed in ethanol twice. In the last wash, the methyl ester was precipitated with ethyl ether (Fisher) and vacuum dried at <5mmHg.

The methyl ester of desulfated heparin was demethylated at 25mg/mL in 0.1M potassium hydroxide (KOH) for 24h to produce Hep^-. The Hep- product was then neutralized in 4mL of 100mg/mL potassium acetate (Fisher) in 10% v/v acetic acid (VWR) per gram of starting product, and precipitated in an excess of ethanol on ice. Hep^- was washed in ethanol and ethyl ether, vacuum dried, and stored at -20°C until use.

4.2.1.3 Material Characterization

Removal of sulfate groups in all desulfation protocols was confirmed by dimethylmethylene blue (DMMB) assay for sulfated GAGs [298]. The absorbance of DMMB at 520nm was measured for increasing concentrations of heparin derivatives. The absorbance values for 4.5μg/mL heparin derivatives were normalized to the absorbance value of native heparin at the same concentration to compute relative sulfation levels.

The molecular weights of heparin derivatives were approximated by gel permeation chromatography. Samples were dissolved in an aqueous buffer of 150nM magnesium sulfate (Macron Fine Chemicals) and 10mM Tris base (Sigma-Aldrich) in ddH_2O. The aqueous buffer was also used as the mobile phase in the gel permeation chromatography instrument equipped with a refractive index detector (Shimadzu). Samples were injected into the column (Tosoh Bioscience) at a flow rate of 0.5mL/min (n=3). Retention times were compared to those produced by polyethylene oxide standards in the range of M_p 14,000-73,500 (Waters).

Proton nuclear magnetic resonance (^{1}H NMR) was utilized to determine the shifts observed after each selective desulfation process. Heparin and its desulfated derivatives were solubilized in deuterated water (D_2O) and ^{1}H NMR was measured on a Bruker Avance III 400 spectrometer at 400MHz. The resulting spectra were analyzed by calibrating the signal between 5.15 and 5.55ppm, which corresponds to the combined signals of H1 from all the glucosamine and uronic acid residues. This provided an internal standard which allowed monitoring of the amount of modification to specific protons near sulfation sites.

4.2.2 Cell-Based Bioactivity Assay

4.2.2.1 C2C12 Cell Culture

The mouse myoblast subclone C2C12 cell line (CRL-1772) was purchased from ATCC and plated onto a recovery plate in growth medium consisting of 4.5g/mL glucose Dulbecco's Modified Eagle Medium (DMEM, Cellgro), 10% v/v fetal bovine serum (FBS, Atlanta Biologics), 1% v/v 10,000IU penicillin/10,000μg/mL streptomycin (Mediatech), and 1% v/v 200mM L-glutamine (Cellgro). Plate was subcultured with 0.05% trypsin with ethylenediaminetetraacetic acid (EDTA) before reaching confluency to prevent depletion of myoblastic population in the culture and replated at $1.5x10^5$-$1.0x10^6$ cells/75cm^2. All studies were performed with cells between passages 4-6.

4.2.2.2 BMP-2 Administration and Heat Treatment

Recombinant human BMP-2 expressed in *E. coli* (Peprotech, 26kDa) was resuspended at 100μg/mL in sterile ddH_2O and single-use aliquots were frozen until use. Solutions of 1mg/mL heparin and desulfated heparin derivatives were made in PBS, filter sterilized, and aliquots were frozen until use. Low adsorption tubes (Eppendorf) were used for storage of BMP-2 and heparin.

In preparation of BMP-2 bioactivity, $2x10^4$ C2C12 cells were plated into each well of a 96-well plate in growth medium. Cells were allowed to attach for 8h, at which point, cells were washed with PBS containing 1g/L $CaCl_2$/$MgCl_2$ and switched to the bioactivity assay medium. BMP-2 concentrations were tested at 0-600ng/mL; all bioactivity studies presented here used 500ng/mL, or 150ng/well, BMP-2. Heparin was assumed to have a molecular weight of 18kDa and molar excess of 10 and 100 were used in the studies. Due to the polydisperse nature of the modified heparin species,

equivalent mass concentrations of heparin derivatives were used in the studies. For samples consisting of heparin or heparin derivatives, BMP-2 and heparin were pipetted vigorously before being allowed to incubate at room temperature for 10min to allow interaction between the moieties. Samples for heat treatment were then placed in a 65°C heated water bath for either 2, 5, 10, or 15min. Samples were cooled on ice and basal low serum medium consisting of 4.5g/mL glucose DMEM with 1% v/v FBS was then added to the mixture and transferred to cells. Negative controls consisting of wells free of BMP-2 included the low serum medium and low serum medium supplemented with the same concentrations of heparin or heparin derivatives used in the experimental wells. A schematic of the experimental timeline is shown in Figure 4.1.

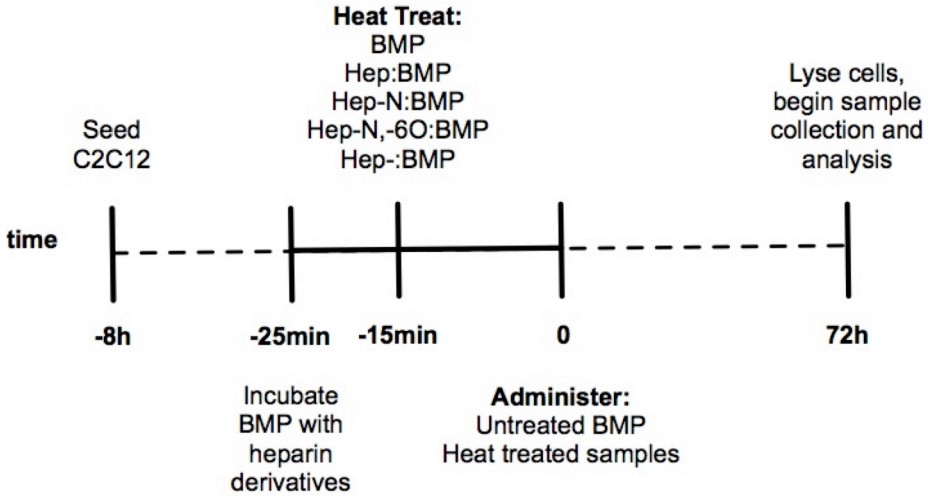

Figure 4.1. Schematic of experimental timeline for cell-based BMP-2 bioactivity assay.

4.2.2.3 BMP-2 Bioactivity Assessment

The C2C12 cells were cultured in the 96-well plate for an additional 72h, at which point, the wells were aspirated, washed twice with PBS with $CaCl_2$/$MgCl_2$ and

incubated with ddH_2O for 20min at room temperature to lyse cells. The plates of cells were frozen, thawed, and mechanically scraped to retrieve cell lysate. Cell lysates were sonicated for 20min and the freeze-thaw-sonicate cycle was repeated once more. Cell lysates were spun down and the supernatants were collected into separate microcentrifuge tubes.

Alkaline phosphate activity (ALP) was assayed using the p-nitrophenol phosphate substrate and a serial dilution of p-nitrophenol standards (0-1000μM). Briefly, 50μL of samples and standards were aliquoted into each well of a clear 96-well plate and incubated with 50μL of 1.5M 2-amino-2-methyl-1-propanol (Sigma-Aldrich) solution at pH 10.25. Then 100μL of a freshly made 1:1 mixture of 20mM p-nitrophenol phosphate disodium salt hexahydrate and 10mM magnesium chloride was added to each well. The assay plate was sealed and incubated at 37°C until a colorimetric change was observed, at which point the assay time was recorded.

In addition, the concentration of double stranded DNA was assayed by the PicoGreen (Invitrogen) assay. Briefly, λ DNA standards (0-4μg/mL) were prepared in RNase/DNase free H_2O. 1x TE buffer was prepared in RNase/DNase free H_2O and the PicoGreen dsDNA reagent was diluted 200-fold in 1x TE buffer. In each well of an opaque 96-well plate, 43μL of sample or standard was incubated with 107μL of 1x TE buffer, and 150μL of PicoGreen solution. All samples were assayed in duplicates. The ALP activity (nmol of p-nitrophenol/mL/min) of each sample was normalized to its dsDNA concentration (μg/mL) and then normalized to the activity level of the positive control of untreated BMP-2 administered to C2C12.

4.2.3 Differential Scanning Fluorimetry (DSF) of Model Protein and Heparin Species

Experiments were performed using a StepOne Plus Real Time polymerase chain reaction System (Applied Biosystems). A melting protocol was designed with a 2min pre-warming step at 31°C and a gradient up to 81°C in steps of 0.5°C as previously reported [201, 299]. Data were collected using the TAMRA dye setting (λ_{ex} 560nm/λ_{em} 582nm), with quencher and reporter dye set to "none". Fluorescence data and derivative data were analyzed by the Protein Thermal Shift software (Applied Biosystems).

DSF plates were prepared such that 10µL volumes were placed within each well, containing 20µM lysine-rich histone (Sigma-Aldrich), 10µM heparin species, 5X of Sypro Orange (Invitrogen) and PBS without $CaCl_2$/$MgCl_2$. Prior to placement in wells, mixtures were prepared in low-binding polypropylene microcentrifuge tubes with enough volume for quadruplicates. Stock solutions of histone and heparins were made separately in PBS. The fluorescent dye Sypro Orange 5,000x (Invitrogen) was diluted 100x in ddH_2O, vortexed until mixed, kept protected from light, and used within 1h. For each mixture, histone was mixed with heparin and PBS and incubated at room temperature for 10min. Finally, Sypro Orange was added to the solution and carefully mixed. Controls consisted of each component (PBS buffer, histone-only, and heparin species only) with 5X Sypro Orange. Aliquots of 10µL of each mixture were placed into each well of a Fast Optical 96-well Reaction Plate (Applied Biosystems) and sealed with Optical Adhesive Film (Applied Biosystems). Plates were briefly centrifuged for 1min at 1000 RPM to remove bubbles and draw all solutions to the bottoms of the wells. Plates were then placed into the PCR instrument for the denaturation experiment with the

assigned melting protocol. Data is presented as representative curves from experiments performed in quadruplicate.

4.2.4 Statistical Analysis

DMMB, M_n, PI, and BMP-2 bioactivity data are presented as mean ± standard deviation. One- and two-way analysis of variance (ANOVA) were used to identify significant differences or interactions. Tukey's *post hoc* multiple comparison test with a significance value set at $p<0.05$ indicated significant differences between individual samples. Statistical analysis was performed with Minitab (v15.1).

4.3 Results

4.3.1 Heparin Modification and Characterization

The DMMB assay was used to assess overall sulfation levels of heparins desulfated by the various protocols. Increasing concentrations of modified heparins were plotted against the absorbance of DMMB. In comparison to the native heparin molecule, Hep^{-N}, $Hep^{-N,-6O}$, and Hep^{-} were approximately 82.2%, 39.2%, and 0.7% as sulfated, indicating a stepwise decrease in sulfation due to the desulfation protocols (Figure 4.2b).

The molecular weight of the heparin species were resolved against a range of PEO standards on a GPC running on an aqueous method. The molecular weight for Hep^{-} was significantly smaller than Hep and Hep^{-N} (Table 4.1). In addition, the polydispersity index (PI) appeared to increase as the overall level of sulfation on heparin decreased (Table 4.1).

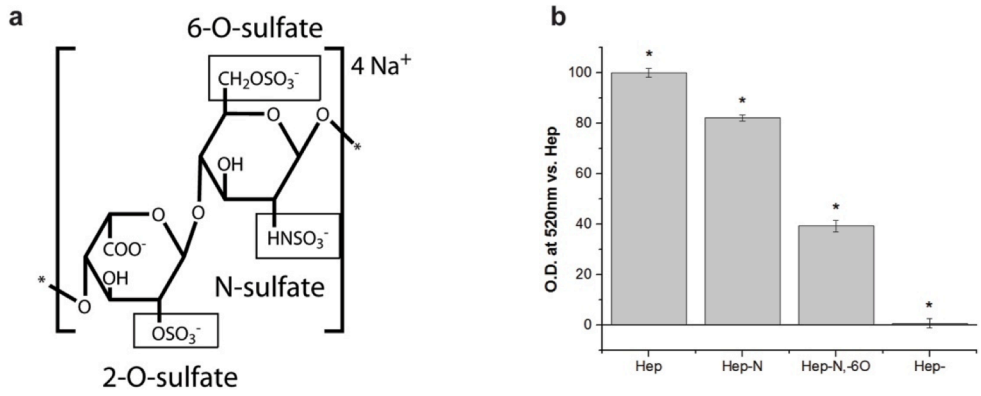

Figure 4.2. Common sulfation positions on heparin disaccharide and effect of desulfation protocols on native heparin. (a) Boxed regions represent positions that are sensitive to the desulfation protocols. (b) Overall sulfation levels of modified heparins compared to native heparin as measured by absorbance of DMMB. * indicates that normalized absorbance of sample was significantly different than all other derivatives, $p \leq 0.05$, n=3, mean ± s.d.

	M_n ± s.d.	**PI ± s.d.**
Hep	25,200±5,500	1.2±0.05
Hep^{-N}	29,400±60	1.3±0.00
$Hep^{-N,-6O}$	22,200±260	1.5±0.03
Hep^{-}	17,800±240$^{\wedge\#}$	1.5±0.01

Table 4.1 Number average molecular weight (M_n) and polydispersity (PI) of heparin species compared to PEG standards. ^ indicates significant difference from Hep, # indicates significant difference from Hep^{-N}. $p \leq 0.05$, n=3, mean ± s.d.

Proton NMR showed specific chemical shifts upon desulfation protocols. Hydrogen atoms on heparin (Figure 4.3) exhibited shifts upon N-desulfation (a), 2-O desulfation (b, c), and 6-O desulfation (d). There was some evidence of 2-O desulfation upon the N-desulfation protocol, and more complete 2-O desulfation upon the 6-O, N-

desulfation protocol. Complete desulfation of heparin exhibits the N-, 2-O, and 6-O desulfation shifts, although in more defined peaks.

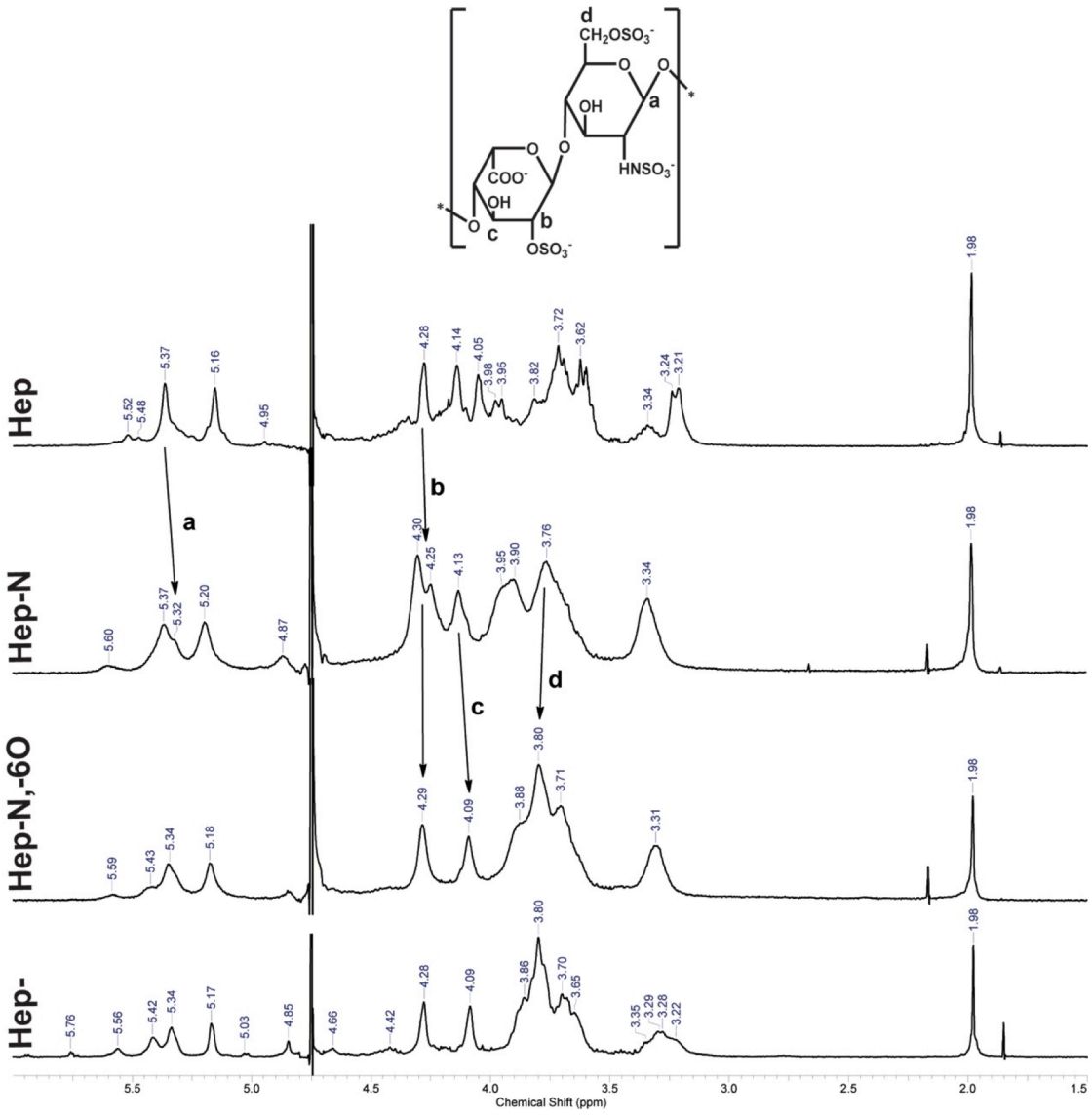

Figure 4.3. ^{1}H NMR spectra for desulfated heparin species. Letters correspond to the position of the hydrogen depicted on the chemical structure. The chemical shifts after N-desulfation suggests changes near the amino group (**a**) and minor 2-O desulfation (**b**). $Hep^{-N,-6O}$ show further 2-O desulfation (**c**) and shifts due to 6-O desulfation (**d**). Spectra of Hep^{-} appears similar to $Hep^{-N,-6O,}$ but with more defined peaks, as well as a more prominent signal near 4.85ppm, indicating the presence of glucuronic acid.

4.3.2 Cell-Based BMP-2 Bioactivity Assay

BMP-2 bioactivity was assessed after heat treatment at 65°C by administering treated samples to C2C12 cells and evaluating for ALP activity after a 3 day incubation period. Each sample was normalized to an ALP activity level induced by untreated BMP-2 in order to minimize differences across plates. Negative controls of low serum (1% FBS) basal medium and medium supplemented with heparin species did not induce significant ALP activity in C2C12 cells over 3 days (Figure 4.4a). When BMP-2 was pre-treated with heat, a significant drop in bioactivity was observed with as short as a 2min heating period compared to untreated ("0min") BMP-2 (Figure 4.4b). When BMP-2 was complexed to 10 molar excess heparin, no drop in bioactivity was detected until the complex was pre-treated with 10min of heat. Also by 10min of heat treatment, the 10:1 complex showed less BMP-2 bioactivity than the 100:1 complex, a feature that was repeated at 15min of heat treatment. Unlike the BMP-2-alone and 10:1 complex, the 100:1 complex did not show a significant decrease in bioactivity over heat treatment times. In addition, the 100:1 complex exhibited significantly higher ALP activity than BMP-2-alone over all heat treatment times. With 15min of heat treatment, the 100:1 complex retained approximately 70% of the ALP activity induced by untreated BMP-2 (Figure 4.4b).

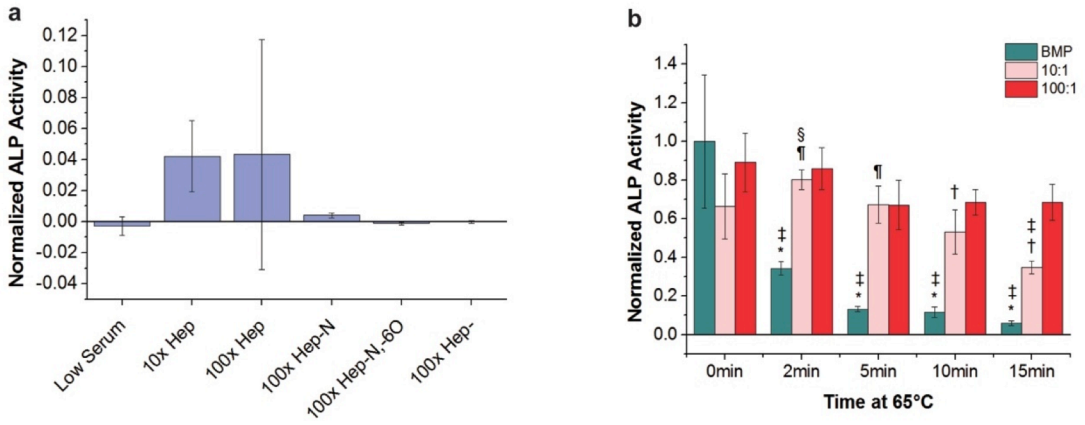

Figure 4.4. Normalized BMP-2 bioactivity levels after pre-treating BMP-2 with heat for various times prior to administration to C2C12 cells. (a) ALP activity for BMP-free control cultures showing no significant differences. (b) BMP-2 saw a significant drop in bioactivity after 2min of heating, while 10:1 heparin:BMP did not exhibit a significant drop until 10min of heating. There were no significant differences in bioactivity of 100:1 heparin:BMP groups over treatment time. All BMP activity values were normalized to an untreated BMP-2 control. * indicates significantly different than other samples within same treatment time, † lower than 100:1 within same treatment time, ‡ different from 0min for same sample, § different from 10min for same sample, ¶ different from 15min for same sample. $p<0.05$, n=4, mean ± s.d.

Initial differences in ALP activity were observed when BMP-2 was co-delivered with chemically desulfated heparin species. Co-delivery with Hep^{-N} or $Hep^{-N,-6O}$ showed significantly lower ALP activity than BMP-2-alone (Figure 4.5). In addition, Hep^{-N} showed lower ALP activity than Hep co-delivery at 0min. Upon heat treatment for both times, BMP-2 was significantly less bioactive than untreated BMP-2. While BMP-2 complexed to Hep showed no significant difference in bioactivity over heating time, Hep^{-N} co-delivery exhibited an initial drop in bioactivity after 2min of heating yet retained approximately 35% of the ALP activity of the untreated BMP-2 positive control after 15min of heating. $Hep^{-N,-6O}$ co-delivery exhibited a lower ALP activity after 15min of heating compared to its unheated control, and was significantly lower than the ALP activity induced by Hep co-delivery. When Hep^{-}, the modification that carries the least amount of sulfation, was co-delivered with BMP-2, it had a similar level of bioactivity

as BMP-2 at 0min (~71% of untreated BMP-2 bioactivity), but had only approximately 17% of bioactivity after 15min of heating. With 15min of heating, BMP-bioactivity is significantly higher when co-delivered with Hep, Hep^{-N}, and Hep$^{-N,-6O}$ when compared to BMP-2-alone.

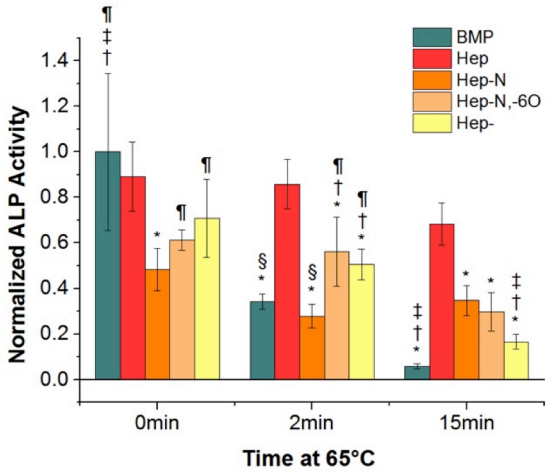

Figure 4.5. Normalized BMP-2 bioactivity over heat treatment time and co-delivery with modified heparins. With 15min of heat treatment, BMP-2 co-delivered with Hep, Hep^{-N}, or Hep$^{-N,-6O}$ showed higher bioactivity than BMP-2 alone. All BMP activity values were normalized to an untreated BMP-2 control. * indicates significantly different than Hep within the same treatment time, † different from Hep^{-N} within the same treatment time, ‡ different from Hep$^{-N,-6O}$ within the same treatment time, § different from 0min of same sample type, ¶ different from 15min of same sample type. $p<0.05$, n=4, mean ± s.d.

4.3.3 DSF of Model Protein and Heparin Species

Differential scanning fluorimetry (DSF) is a method that uses a fluorescent dye that can bind to the core hydrophobic residues of denatured proteins [300]. Upon increasing temperatures, many proteins exhibit an unfolding transition where the hydrophobic dye can bind to core residues, producing an increasing fluorescence signal with increasing temperature. Upon reaching a maximum fluorescence, the fluorescent signal gradually decreases as proteins aggregate at higher temperatures. Fluorescence

spectra can be analyzed by performing the first derivative on data to find the point where the concentration of unfolded protein is in equilibrium with folded protein, also known as the melting temperature (T_m) [300].

Representative fluorescence curve profiles and selected first derivative curves are depicted in Figure 4.6. Heparin and its desulfated derivatives show no change in fluorescence over the tested temperature range (Figure 4.6a, inset), indicating that the glycosaminoglycans do not interact directly with the Sypro Orange dye. Histone alone did not show a clear melting curve, but addition of specific heparins induced a melting profile. Incubation with 10μM heparin induced a sigmoidal fluorescence profile in histone (Figure 4.6a) and a corresponding first derivative melting curve (Figure 4.6b), with an approximate T_m of 39.7±1.1°C. Hep^{-N} also induced a sigmoidal fluorescence profile in histone and melting curve (Figure 4.6a, b), with an average T_m of 45.4±0.8°C. Addition of $Hep^{-N,-6O}$ or Hep^{-} to histone did not produce sharp melting curves (Fig. 3.6a) and exhibited an overall low level of fluorescence, preventing calculation of an accurate T_m.

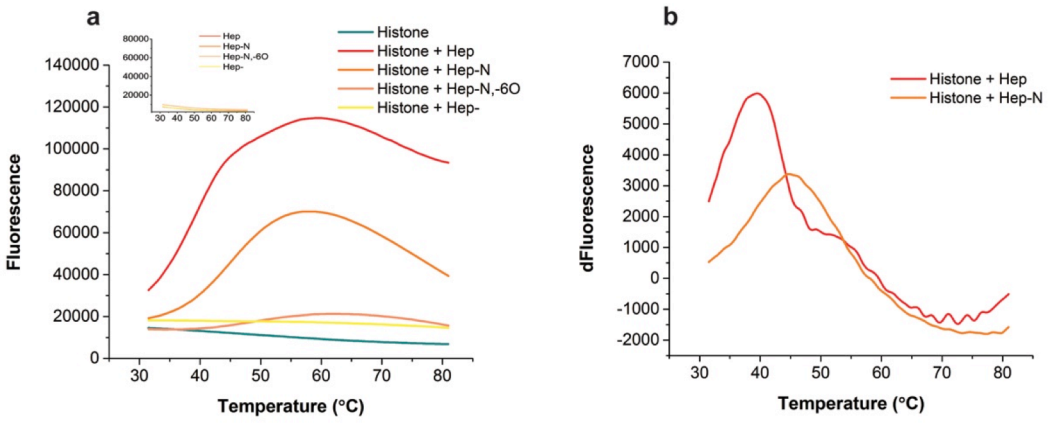

Figure 4.6. Representative fluorescence spectra of histone and heparin derivatives with DSF. (a) Histone fluorescence when incubated with heparin species. Hep and Hep^{-N} induce a conformational change in histone to produce a clear DSF signal. Inset figure shows fluorescence from negative controls of heparin materials alone. (b) First derivative of fluorescence data for histone incubated in Hep and Hep^{-N}. The maximum of each curve represents the T_m. All samples were repeated in quadruplicate.

4.4 DISCUSSION

An established BMP-2 bioactivity assay was used to determine the effect of heparin species of varying sulfation on maintaining BMP-2 bioactivity during thermal stress. Heparin with reduced anti-coagulation activity would be amenable for use in *in vivo* delivery systems and these materials have been developed through selective desulfation [290, 297, 301]. The goal of this study was to determine if sulfation level of heparin correlated to the level of BMP-2 bioactivity after heat treatment and evaluate the interaction between desulfated heparin species and proteins.

In characterizing the desulfated heparin species produced in this study, both overall sulfation level as well as molecular weight changes after chemical treatment were evaluated. For the same mass concentration of heparin species, the DMMB assay showed that overall sulfation level decreased as heparin was N-desulfated, 6-O,N-desulfated, and completely desulfated (Figure 4.2). Heparin was relatively resistant to

chain scission when treated with acidic methanol for complete desulfation, although the product, Hep^{-}, had a significantly lower molecular weight than Hep and Hep^{-N} (Table 4.1). The N-desulfation of heparin was achieved by removing the more reactive N-sulfate groups with a solvent that does not induce hydrolysis at the glycosidic linkages [290]. Proton NMR showed that chemical desulfation produced spectra shifts in expected locations and suggested that the chemical processes were specific. Evidence of iduronic to glucuronic epimerization was noted for Hep^{-} (Figure 4.3), suggesting that desulfation processes may affect heparin conformation.

In these studies, a non-glycosylated version of BMP-2 was used to probe the effect of thermal stress. The benefit of using non-glycosylated BMP-2 in these studies was the suitability in understanding how the protein backbone may be affected by external factors and interactions. Glycosylated BMP-2 has glycans attached to the protein backbone that can affect protein folding and response to thermal stress. The form of BMP-2 used in this study can more readily show the effects of thermal denaturation and provide valuable information on molecules that can stabilize its activity without the confounding effects of glycans.

The results of these experiments show that non-glycosylated BMP-2 was sensitive to heat treatment (bioactivity was reduced to 34±0.03% after a 2min exposure to heat (Figure 4.4) and was protected by heparin co-delivery. The thermal stress of heating at 65°C appeared to cause non-reversible unfolding as bioactivity was not recovered after removal from heat. Native heparin at 100 molar excess was shown to maintain BMP-2 bioactivity at 68±0.09% over 15min of thermal stress compared to 0.06% of BMP-2-alone. While a 10 molar excess of heparin complexed to BMP-2

showed a decrease in bioactivity after 15min of heating, the bioactivity level was significantly higher than BMP-2-alone heated for the same amount of time. Complexes of 10:1 heparin:BMP-2 were a significant improvement in maintaining BMP-2 bioactivity over free BMP-2 and an even higher excess of heparin seems to have additional effects on bioactivity when exposed to thermal stress. This heparin concentration dependence was similar to a past study with FGF-1, in which FGF-1 experienced more thermal stability when incubated with increasing concentrations of heparin [302].

While lower concentrations of heparin were able to change the secondary structure of a model protein (Supplementary figure A.2) an excess of heparin was chosen in order to ensure BMP-heparin interaction. These approximate molar ratio of heparin to protein have been used in a previous study investigating heparin with FGF-2 and a delivery vehicle that showed modulated release with 100:1 heparin:growth factor concentrations [303, 304]. It has been estimated that 5-6 molecules of BMP-2 can be bound to each heparin chain, so there were heparin molecules that were not saturated with BMP in these studies [168]. It is possible that the excess of unoccupied heparin at 100 molar excess may play an additional role in slowing denaturation of BMP-2. In studies of excipients used to stabilize proteins, increasing concentrations of the sugar trehalose was shown to increase the surface tension of the protein solution, which then required greater amounts of energy to change the solvation during denaturation [305].

A 100 molar excess of desulfated heparin species was chosen for BMP-2 bioactivity assays in order to maximize the potential interaction with the growth factor. All the desulfated species at 100 molar excess failed to be as effective as 100:1

Hep:BMP-2 at maintaining BMP-2 bioactivity when exposed to heat (Figure 4.5). While the overall sulfation of Hep^{-N} was ~80% of native heparin (Figure 4.2b), the bioactivity after 2min of heating was ~30% of untreated BMP-2 compared to ~90% of Hep:BMP-2 (Figure 4.5). Bioactivity of BMP-2 after 15min of heating was reduced with all the desulfated derivatives in comparison to 100:1 Hep:BMP-2 (Figure 4.5). Co-delivery with Hep^{-N} and $Hep^{-N,-6O}$ resulted in similar BMP-2 bioactivity levels after 15min of heating, and were higher than the bioactivity of BMP-2 alone, suggesting that there may be protective effects due to residual sulfates on those heparin species. Co-delivery with Hep^{-} exhibited a significantly lower BMP-2 bioactivity level than all other heparin derivatives after 15min of heating. The charged hydroxyl and carboxyl groups on Hep^{-} were not sufficient in maintaining BMP-2 bioactivity at this level of thermal stress, suggesting that there is a sulfation-level dependence on maintaining BMP-2 bioactivity.

It has been suggested previously that desulfated heparin species may not protect BMP-2 bioactivity [306]. However, in that study, samples were not heated and the co-delivery of desulfated samples exhibited comparatively lower ALP activity values than presented here. It is possible that differences in desulfation methods and differences in the heparin concentrations used may have limited the amount of interaction between BMP-2 and the desulfated heparin derivatives in that previous study [306]. In both studies, the heparin backbone conformation may play a role in interactions between heparin and heparin-binding proteins. Heparin is a relatively flexible molecule, able to wrap itself around proteins during binding, driven primarily by the iduronic acid residue that can adopt several conformations [183, 198]. It is possible a change in heparin conformation occurred while undergoing desulfation procedures, as suggested with the

increased presence of glucuronic acid, a hexuronic acid with fewer conformations than L-iduronic acid, in ^{1}H NMR results (Figure 4.3). Any structural difference between Hep^{-}, Hep^{-N} and Hep-$^{N,-6O}$ may influence BMP-2 binding and bioactivity.

In order to understand the interaction between desulfated heparin derivatives and proteins further, differential scanning fluorimetry (DSF) was used to gauge the evidence of heparin-protein complexation. DSF is a high-throughput, low volume method that utilizes a hydrophobic dye to probe thermal unfolding of proteins in the presence of ligands [300]. This technique was used to demonstrate protein stability upon binding to glycosaminoglycans such as heparin and may be used to indicate interactions between proteins and glycosaminoglycans [201, 307]. The ability of a ligand to confer stability is reflected in a sigmoidal melting curve and a shift toward a higher melting temperature (T_m). While amenable for many proteins, some proteins may not produce an adequate signal, whether by not exhibiting a reversible two-state unfolding or exhibiting highly accessible hydrophobic residues that produce high initial background readings [300, 308]. BMP-2 exhibits the latter limitation, causing high initial fluorescence that masked the melting regions. While a technique will need to be optimized in order to study the interactions between desulfated heparin species and BMP-2, DSF was used with a model protein to show how the heparin species may interact with BMP-2.

DSF was used to measure the thermal stability of a positively-charged model protein, lysine-rich histone, in the presence of different heparin species. Lysine-rich histone, consisting primarily of f1 histone, is similar in size (~21.5kDa) to BMP-2 and has a net positive charge at physiological pH. No specific heparin-binding sequence on histone has been identified, but studies have shown that histone can have an altered

diffusion profile into heparin-containing hydrogels, suggesting some level of electrostatic interaction between the molecules [309]. Furthermore, the random coil structure of histone [310] was altered upon binding to Hep and Hep^{-N} (Supplementary figure A.2). Histone itself has been shown to become more structurally defined upon binding to DNA [311], suggesting that it is amenable to studying interactions with acidic heparins.

The denaturation profile of histone alone in DSF analysis shows no obvious transition (Figure 4.6a), which has been observed for certain proteins using the DSF technique [299]. However, in some cases, proteins without clear melting curves can obtain them following interaction with a ligand [299]. When histone was incubated with Hep, its melting profile became more defined, indicating that Hep was able to induce a structural change on histone that influences its unfolding behavior (Figure 4.6a). The sigmoidal melting profile shown in the overall fluorescence (Figure 4.6a) was repeated when histone was incubated with Hep^{-N}. However, $Hep^{-N,-6O}$ and Hep^{-} fail to induce a significant transition in fluorescence with increased temperature. While the absolute values of fluorescence in the melting curves are informative, the shape of the curves is especially telling about the interactions between the heparins and histone. Hep and Hep^{-N} contain more sulfate groups, hence negative charge, for histone to interact with to induce an initial structural change in histone that can be traced through unfolding by DSF. On the other hand, histone incubation with $Hep^{-N,-6O}$ had a much lower signal and broader profile. Addition of Hep^{-} produced melting curves more similar to histone alone. These results indicate that in terms of electrostatic interaction, the amount of sulfation on heparin determines the extent of interaction. When sulfation drops to below 40% of

native heparin, as in the case of $Hep^{-N,-6O}$ and Hep^{-} (Figure 4.2b) the interaction between the heparin derivative and histone become significantly weakened (Figure 4.6a), leading to a lack of sufficient structural change to induce a clear melting transition. This observation is a different perspective on the value of incubating $Hep^{-N,-6O}$ with BMP-2 during thermal stress. It appeared that $Hep^{-N,-6O}$ was effective in protecting BMP-2 from thermal stress up to 15min of heat exposure (Figure 4.5), which suggest that there may be sulfation pattern sequences that BMP-2 recognize.

BMPs are powerful morphogens that can affect many cellular processes and are of interest in regenerative medicine. The ability to improve the half-life of BMP-2 in solution and in delivery systems will enable the delivery of lower doses of BMP-2, resulting in more effective and cost efficient therapeutics. Use of heparin-derived materials with decreased anti-coagulant activity will allow the design of scaffolds that feature high affinity for BMP-2 as well as maintenance of BMP-2 bioactivity. The results of this study can also allow the selection of materials to study the effects of heparin-derivative:BMP-2 complexes either in soluble form, from coacervates, or from scaffolds. Furthermore, fundamental studies to determine how the interaction between heparin derivatives and a positively-charged protein can be disrupted or how these complexes interact with other glycosaminoglycan-based biomaterials can inform the success of these complexes (Supplementary figures A.3.2, A.3.3). Overall, by understanding growth factor interactions with sulfated GAGs, these fundamental results can help design more effective delivery systems.

4.5 CONCLUSIONS

These studies build upon what is currently known about BMP-2 interactions with heparin and seek to establish a role of heparin sulfation level in maintenance of BMP-2 bioactivity. Native heparin maintained a significant portion of BMP-2 bioactivity when exposed to thermal stress and at particularly long times, the effect appeared to be heparin concentration dependent. While desulfated heparin derivatives were not as effective as native heparin in maintaining BMP-2 bioactivity, Hep^{-N} and $Hep^{-N,-6O}$ were beneficial when administered prior to exposure to thermal stress at particularly long times compared to BMP-2-alone. This indicates that sulfation has some effect in maintaining BMP-2 bioactivity, but the backbone structure of the heparin derivatives may also determine the affinity and extent of protective effects they can confer to BMP-2 in solution. Hep and Hep^{-N} were found to induce a conformational change within a model positively-charged protein, suggesting that these heparin species can directly interact with the protein, forming a complex. Taken together, Hep^{-N} has shown the best qualities in terms of retaining high overall sulfation, maintaining BMP-2 bioactivity during heat treatment, and exhibiting evidence of direct interaction with a model protein compared to the other desulfated species. Future development of heparin-derived materials can take advantage of these features in order to most effectively deliver growth factors. The ability of desulfated heparin species to exhibit low anti-coagulant activity, improve the half-life of BMP-2 in solution and in delivery systems, and exhibit affinity to BMP-2 will enable the delivery of lower doses of BMP-2, resulting in more effective and cost efficient therapeutics.

CHAPTER 5

CATHEPSIN ACTIVITY INCREASES IN THE INSERTION REGION OF RAT SUPRASPINATUS TENDON WITH OVERUSE

5.1 Introduction

The etiology of supraspinatus tendinopathy is multifactorial, with impingement by the coracoacromial arch and overuse being commonly cited factors[312]. In regards to animal models pertinent to the study of this pathology, the rat has been shown to have similar shoulder anatomy to humans, with a coracoacromial process that the supraspinatus tendon slides beneath[112]. Tendon overuse in this rat model has shown altered biomechanical properties[313] and decreased gene expression of type I and III collagens.[314] Changes in tendon architecture were also observed with this overuse protocol[313], but mechanisms for the tissue degeneration have not been defined.

Type I collagen is the main extracellular matrix constituent of tendon that imparts the tensile strength necessary for tendon function and can exhibit disrupted organization upon injury[315]. Furthermore, supraspinatus tendons have shown decreased collagen content or expression as a result of degeneration or failed healing[100, 124]. The importance of collagen catabolism as a part of pathology progression in tendinopathy has resulted in a focus on the family of matrix metalloproteinases (MMPs). Previous studies examining the healing of tendon after tendon rupture have found increases in expression and activity of MMP-1[316] and MMP-13,[317] but a range of proteases likely take part in tendon degeneration.

The contributions of cysteine cathepsins, a family of lysosomal and secreted

proteases, are increasingly recognized in tissue maintenance and a variety of degenerative tissue diseases. They have been identified as the most potent mammalian collagenases capable of cleaving types I and II collagens both intrahelically and at the telopeptide regions, whereas other collagenases only cleave at one or the other[318]. Cathepsin K, associated with bone remodeling, has been implicated in collagen proteolysis in osteoarthritis[40], while cathepsin L, potent in cleaving at collagen telopeptide regions, has been found in myopathies[319]. Additionally, cathepsins can play important roles in activating other proteases such as MMPs[320] and the serine proteases urokinase-type plasminogen activator[321]. Sustained expression of these proteases has been linked with chronic tissue degeneration and disease progression[322]. Since cathepsins have a vital role in initializing and significantly contributing to proteolytic cascades, their involvement in tendon degeneration may shed light on the mechanisms of chronic tendon diseases.

With this in mind, a detailed study to examine the role of cathepsins in a rat model of tendon overuse was designed. After up to 8 weeks of decline running on a treadmill, supraspinatus tendons of Dahl Salt Resistant rats were analyzed for differences between the region closest to the osseotendinous junction (the insertion region) and the region encased in muscle (the midsubstance region). Tissue damage was evaluated histologically and contralateral tendons underwent analysis via gelatin zymography. Multiplex cathepsin zymography is a sensitive electrophoretic technique that separates proteases and correlates the gelatin substrate digestion with proteolytic activity,[323] and can be more sensitive than Western blotting[324]. In this study, we hypothesized that the overuse protocol would primarily cause tissue damage at the

insertion region (due to possible impingement from the overlying acromion) and that there would be a concomitant increase in cathepsin activity in the overused tendon.

5.2 Materials and Methods

5.2.1 Rat Model

Twenty-four male Dahl Salt Resistant rats (330±20g initial weight, 12-13 weeks initial age, Harlan Labs) were used in this study, as approved by Georgia Institute of Technology's Institutional Animal Care and Use Committee. Twelve rats were acclimated to the running regime for 2 weeks to run at a final speed of 17m/min at a 10° decline for 1 hour/day for 5 days/week, as described previously[313]. In the experimental group, rats were subjected to overuse exercise for 4 or 8 weeks (n=6/group). Age-matched rats that were allowed cage activity served as controls (n=6/timepoint). At each endpoint, the supraspinatus muscle was detached from the scapula and the humerus was bisected by bone rongeurs. The bone-tendon-muscle units were wrapped individually in saline-soaked gauze and frozen until further processing.

5.2.2 Histological Staining and Scoring

For histological evaluation, tendons were thawed and peritendon tissue and the majority of muscle were removed. Tendons were sharply dissected from their bony attachment. To prepare samples for cryosectioning, tendons were embedded in a 40:60 solution of 20% sucrose:optimum cutting temperature (OCT) compound (Sakura Finetek) solution, placed under vacuum for 10h to increase penetration of embedding medium, and frozen in isopentane chilled by liquid nitrogen.

Therafter, tendons were sectioned with a cryostat (Thermo Scientific CryoStar

NX70) into 10μm sections, longitudinal to the tendon. Slides stained with hemaxotylin (Sigma-Aldrich) and eosin (EMD Chemicals) (H&E) were imaged with a Nikon Eclipse 80i. Slides stained with picrosirius red (Sigma-Aldrich) were imaged with an Olympus BX51 polarized light microscope mounted with an Olympus Camedia C-5060 digital camera. Histological grading of H&E stained sections was carried out using a semi-quantitative scale, similar to the Bonar and Movin scales.[325, 326] Categories for histological scoring included regional variations in cellularity, cell shape, collagen fiber organization, and vascularity (Table 5.1). A 4-point scoring system was used, where 0 indicated normal appearance and 3 a markedly abnormal appearance. Four graders (JL, MG, TER, TM), blinded to the sample types, scored 4 images from each tendon (n=3 tendons/group/timepoint). Within each timepoint, the categorical scores of the control and experimental groups were compared.

5.2.3 Multiplex Cathepsin Zymography

For cathepsin zymography, tendons were isolated from muscle and bone. The tendons were systematically divided into the insertion and midsubstance regions by transecting the tendon at 17% of the total length from the insertion end. This proportion consistently excluded the region encased in muscle from the insertion region and provided enough protein for subsequent assays. Subsequently, samples were diced and homogenized in PlusOne grinding kits (GE Healthcare) in lysis buffer (20 nM Tris–HCl at pH 7.5, 5 mM ethylene glycol-bis(2-aminoethylether)-N,N,N’,N’-tetraacetic acid (Sigma-Aldrich), 150 mM NaCl (BDH), 20 mM β-glycerolphosphate (Alfa Aesar), 10 mM NaF (Sigma-Aldrich), 1 mM sodium orthovanadate (Sigma-Aldrich), 1% Triton X-100 (EMD Chemicals), 0.1% Tween-20 (Fisher Scientific)) with freshly added 0.1 mM

leupeptin (Affymetrix). Samples were subject to zymography as described previously[323]. Supernatants were cleared by centrifugation and collected. Protein quantification of supernatants was performed with a micro BCA kit (Pierce). Cathepsin zymography was performed on tissue lysates. Briefly, non-reducing loading buffer (5X – 0.05% bromophenol blue (Fisher Scientific), 10% sodium dodecyl sulfate (SDS, Amresco), 1.5M Tris (Fisher Scientific), 50% glycerol (EMD Chemicals)) was added to 12μg of protein prior to loading samples into gel. Control and experimental samples from the same timepoint were run on the same gel (n=4/group), with 8.3ng cathepsin V (Enzo Chemicals) as a positive control. Samples were loaded into 12.5% SDS-polyacrylamide (Protogel) gels containing 0.2% gelatin (Sigma-Aldrich) and resolved at 110V at 4°C. Enzymes within gels were renatured in 65mM Tris buffer pH 7.4 with 20% glycerol for 3 washes, 10min each. Gels were then incubated in pH 4 activity buffer (acetate buffer, 1mM ethylenediamine tetraacetic acid (Fisher Scientific), freshly added 2 mM dithiothreitol (Sigma-Aldrich)) for 17h at 37°C. Thereafter, gels were rinsed and stained with Coomassie Blue (Sigma-Aldrich) and imaged with an ImageQuant LAS 4000 (GE Healthcare). To limit variability, samples from the same timepoint were processed in parallel and gels were imaged simultaneously. Densitometry analysis was performed on images using ImageJ (NIH) to quantify the cleared bands that represent proteolytic activity. Values were normalized to the cathepsin V band within the same gel. Values are reported as mean ± standard deviation.

	0	1	2	3
Regional variations in cellularity	Density of cells are uniform throughout field of view	<25% of nuclei exhibit some disorganization (not following fiber direction)	25-50% of nuclei exhibit disorganization in spatial arrangement and show evidence of hypercellularity (<25% of field of view)	>50% of nuclei show a disorganized arrangement and >25% field of view exhibits hypercellularity
Cell shape	Elongated spindle shaped nuclei with no obvious cytoplasm at light microscopy	Increased roundness: some (<25%) nuclei become more ovoid to round in shape without conspicuous cytoplasm	Increased roundness and size: 25-50% of nuclei are round, slightly enlarged and a small amount of cytoplasm is visible	>50% of nuclei are round, large with abundant cytoplasm and lacuna formation (chondroid change)
Collagen fiber organization	Collagen arranged in tightly cohesive well-demarcated and large bundles, possibly with crimping	Separation of individual fibers but demarcated bundles still evident	Separation of fibers with loss of demarcation of bundles giving rise to expansion of the tissue overall	Marked separation of fibers with complete loss of architecture
Vascularity	Inconspicuous blood vessels coursing between bundles	Occasional evidence of capillaries (1 vessel per field of view)	Evidence of capillaries in the form of a cluster of blood vessels (1 cluster per field of view)	Greater than 2 clusters of capillaries per field of view

Table 5.1 Semi-quantitative scoring matrix for H&E sections.

5.2.4 Immunofluorescence Staining

For immunofluorescence, slides were fixed in acetone (BDH), blocked with 2% normal goat serum (Vector Labs) for 1h and incubated with 1:100 dilution rabbit anti-rat cathepsin K (Santa Cruz Biotechnology) or L (Abcam) primary antibody overnight at 4°C in a humidified chamber. Goat anti-rabbit secondary antibody (Invitrogen) at 1:200 dilution was applied and sections were counterstained with 4',6-diamidino-2-phenylindole dihydrochloride (DAPI, Anaspec) and imaged with a Nikon Eclipse

TE2000-U.

5.2.5 Statistical Analysis

Categorical scores from histological evaluation were compared between the control and running groups by the non-parametric Mann-Whitney test. Data from cathepsin zymography were Box-Cox transformed and analyzed by t-tests on a per zymogram basis. All statistical analyses were evaluated at a statistical significance level of $p<0.05$. Statistical analysis was performed with Minitab software.

5.3 Results

5.3.1 Histological Imaging and Scoring

H&E stained histological sections revealed that tissue-level changes were more prominent in the insertion regions of the tendons compared to the midsubstance regions. The 4-week control tendon (Figure 5.1a) showed tightly packed fibers and aligned cells at the insertion region. The 4-week overuse insertion region (Figure 5.1b) showed minor collagen disorganization, as evidenced by the appearance of demarcated fibers with less dense staining between them, but collagen fiber bundles remained largely intact. The 8-week control insertion region displayed mostly intact collagen bundles with sparse and aligned tenocytes (Figure 5.1c). By 8 weeks of overuse, collagen fiber thinning and separation from larger bundles was more obvious in the tendon insertion region (Figure 5.1d) compared to the age-matched control (Figure 5.1c). In contrast to the changes observed at the insertion regions, the midsubstance regions, where tendon is encased in muscle, exhibited similar morphology across time and condition: tightly packed collagen fibers with elongated tenocytes oriented along the axis of the tendon (Figure 5.1e-h).

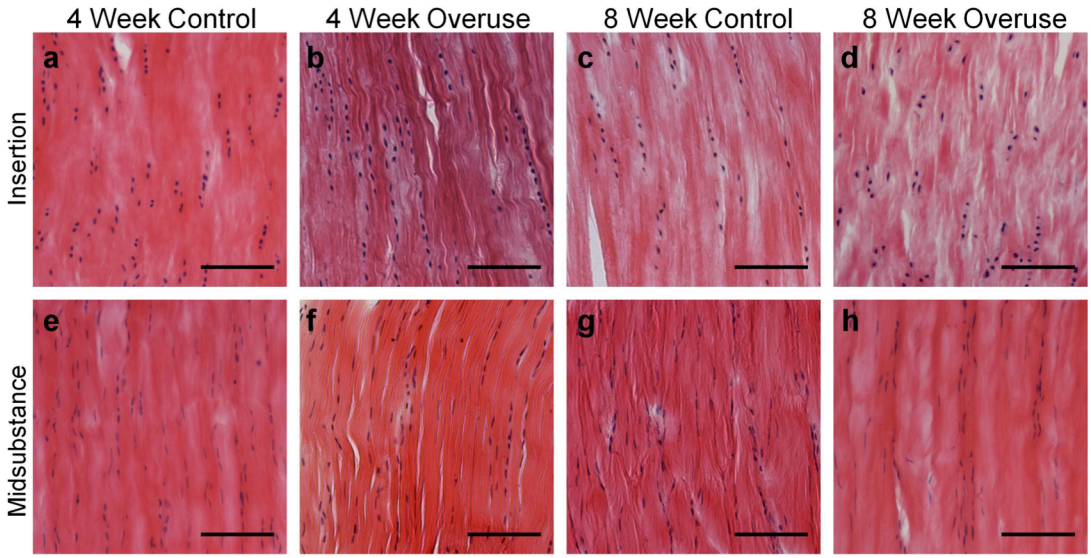

Figure 5.1 Changes to supraspinatus tendon structure obvious by 8 weeks of overuse. The insertion region of the 4-week control (a) and 8-week control (c) tendons are contrasted with insertion region of the 4-week overuse (b) and 8-week overuse (d) tendons. The tissue structures of the midsubstance regions (e-h) were comparable across all groups. n=2, scale bar=100μm.

H&E-stained control and experimental samples evaluated within each timepoint by the semi-quantitative scoring system (Table 5.1) showed significant differences only at the insertion region. For the 4-week group, although the medians were the same between overuse and control group, the distribution in scores for cell shape at the insertion region was significantly different, with more instances of cell roundness (as indicated by nuclei shape) noted in the overuse group (Table 5.2). More regional variation in cellularity was observed in the 4-week control insertion region compared to the overuse group, suggesting that a portion of cells in control tendons were not as uniformly distributed. For the 8-week group, both cell shape and fiber organization scores were significantly different (Table 5.2). The insertion region of the 8-week overuse group showed more cells with increased roundness and size (Figure 5.1) than

the control group. Additionally, in regards to collagen fiber organization, the insertion region of the 8-week overuse group showed more instances of fiber separation than the control group. Vascularity, denoted by clusters of capillaries, was rarely noted by the observers in the tendon sections and assigned scores did not show any significant difference between overuse and control groups.

	4 Week Insertion		8 Week Insertion	
	Control	**Overuse**	**Control**	**Overuse**
Regional variations in cellularity	2 (0, 3)	1 (0, 3) *	1 (0, 3)	1 (0, 3)
Cell shape	1 (0, 3)	1 (1, 3) *	1 (0, 3)	2 (0, 3) *
Fiber organization	2 (0, 3)	2 (0, 3)	0 (0, 2)	1 (0, 3) *
Vascularity	0 (0, 1)	0 (0, 1)	0 (0, 1)	0 (0, 1)

Table 5.2. Summary of categorical histology scores of control and overused tendon at the insertion region. Data presented as median (range), * significantly different than control within the same timepoint; $p<0.05$

Picrosirius red stained sections imaged under circular polarized light exhibit yellow to red staining characteristic of large and organized collagen fibers (Figure 5.2). While the crimping pattern of the control insertion region was uniform and uninterrupted across the section (Figure 5.2a), the overuse insertion region showed less collagen packing and disturbed crimping (Figure 5.2b, boxes).

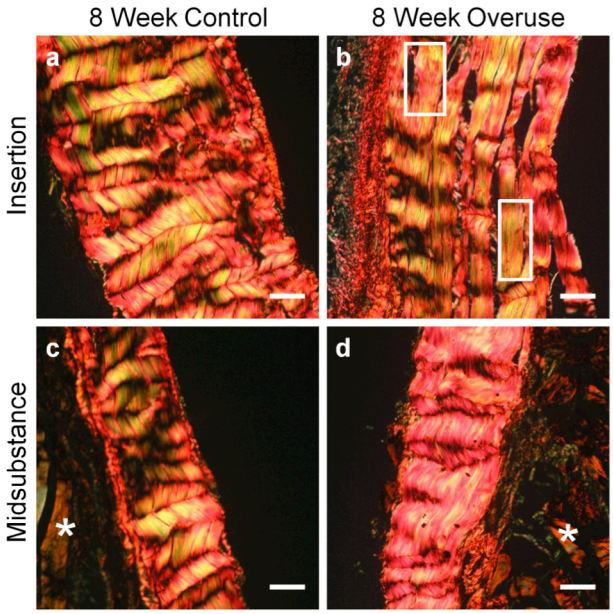

Figure 5.2 Picrosirius red-stained sections of tendons observed under circular polarized light microscopy. 8-week control (A) group contrast with the overuse group (B; boxes indicate disturbed crimp pattern). The midsubstance regions of the control (C) and overuse (D) groups were comparable. * indicates muscle, n=2, scale bar=50μm.

5.3.2 Multiplex Cathepsin Zymography

Incubation of the zymography gels in pH 4 activity buffer during the overnight assay period selects for murine cathepsin L over the other cathepsins, producing an active band between 25 – 35 kDa[323], and this activity was detected in all of the tendon samples as evidenced by the less dense bands in the gelatin gels (Figure 5.3a, d). Zymograms exhibited high molecular weight bands (50-75kDa) bands for some samples (Figure 5.3a), which were attributed to cathepsin K bound to extracellular matrix, as was seen in osteoclasts in previous studies[327]. Densitometric quantification of band intensities determined that by 4 weeks, the activity of cathepsins L and K were higher in the insertion region of the overuse group compared to the control group by 1.8-fold and 4.2-fold, respectively (Figure 5.3b,c, n=3-4, $p<0.05$). Additionally, by 8 weeks,

cathepsin L activity was 1.8-fold higher in the insertion region of the overuse group compared to age-matched controls (Figure 5.3e), although there was no longer a statistically significant increase for cathepsin K (Figure 5.3f). No significant differences were observed for cathepsin activity in the midsubstance regions between the overuse and control groups for either timepoint or cathepsins (Figure 5.3b, e).

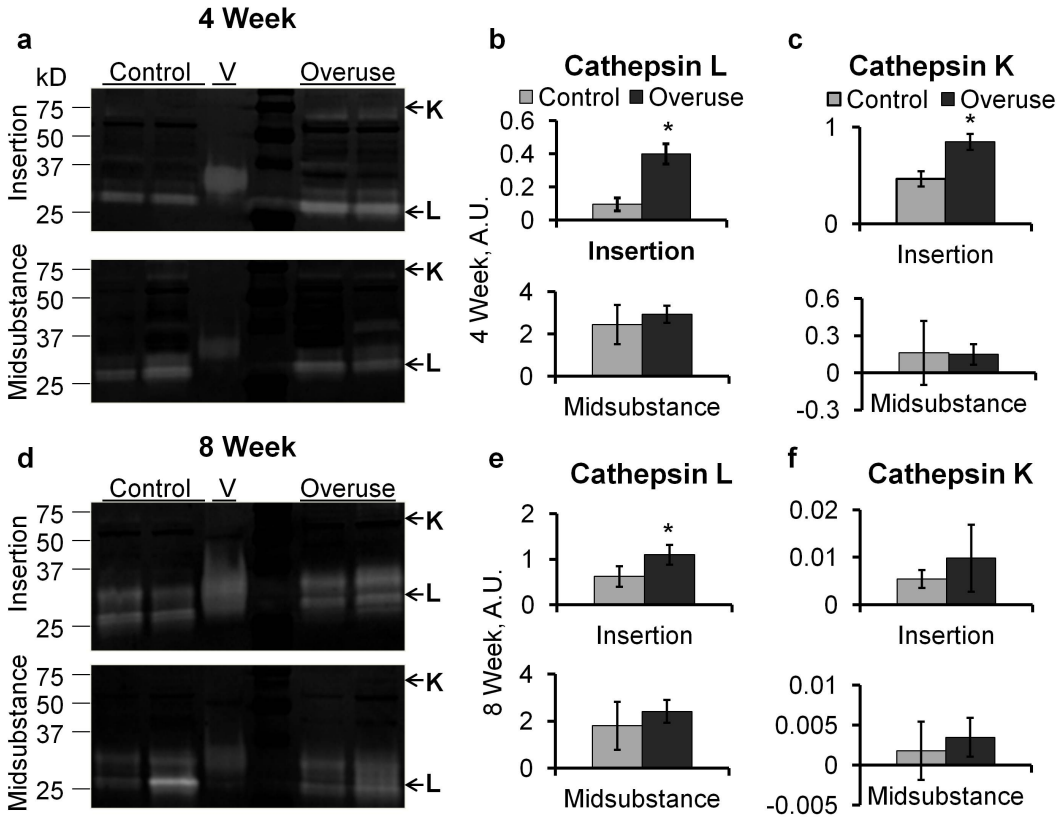

Figure 5.3 Cathepsin activity in supraspinatus tendon. Representative zymography gels (a, d) depict location of cathepsin K (higher molecular weight) and L (lower molecular weight). Cathepsin L activity in 4-week overuse (b) and 8-week overuse (e) tendons compared to age-matched controls. Cathepsin K activity in 4-week overuse (c) and 8-week overuse (f) tendons compared to age-matched controls. n=3-4, * indicates significantly greater activity over control at the same time point ($p<0.05$).

5.3.3 Immunofluorescence Staining

Immunofluorescence staining was employed in order to confirm the presence of cathepsin L and K. Positive staining was confirmed with sections of rat spleen and

negative staining was conducted without the primary antibody (data not shown). Staining revealed that cathepsin staining was localized within or in close proximity to the cell. The tendon midsubstance regions showed similar positive levels of staining for overused and control tendons (data not shown), while there were more marked differences in staining at the insertion regions. For cathepsin L staining at the insertion regions, the 4- and 8-week controls showed similarly low levels of cathepsin staining (Figure 5.4a, b). The 4-week and 8-week overuse group (Figure 5.4e, f), showed more intense and uniformly distributed staining at the insertion region compared to their age-matched controls (Figure 5.4a, b). Cathepsin K staining was slightly more variable in the 4-week overuse group (Figure 5.4g), but overall showed more positive staining than seen in the controls (Figure 5.4c). The 8-week overuse group (Figure 5.4h) also exhibited more positive cathepsin K staining than in the controls (Figure 5.4d).

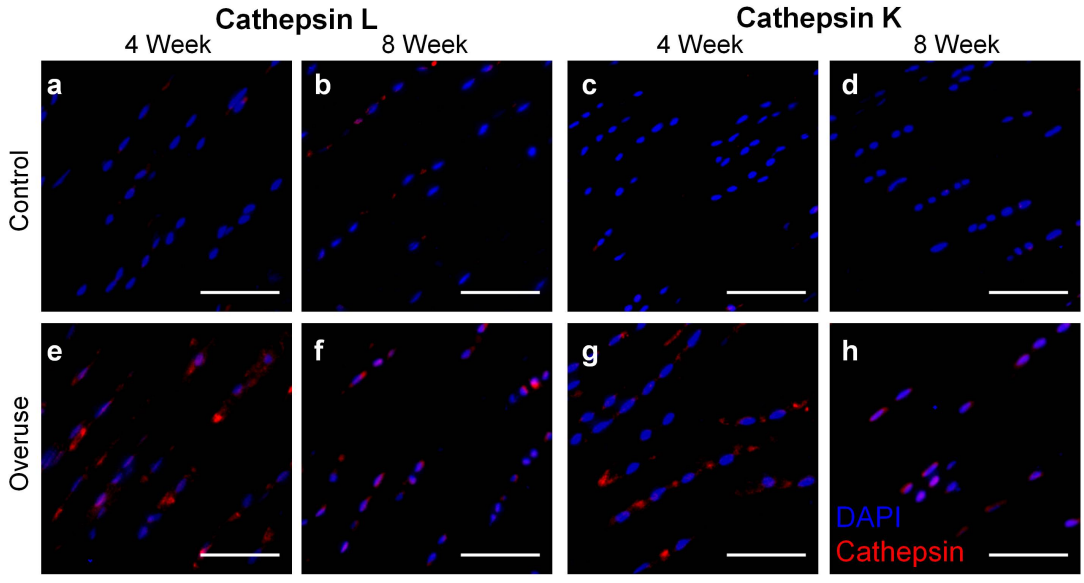

Figure 5.4. Immunofluorescence staining of cathepsin localization in supraspinatus tendons. Cathepsin L staining (red) in the insertion regions of the 4-week (b) and 8-week (f) overused tendons compared to controls (a, e). Cathepsin K staining (red) in the insertion regions of the 4-week (d) and 8-week (h) overused tendons compared to their controls (c, g). Cell nuclei are shown in blue. n=2, scale bar=50μm.

5.4 DISCUSSION

This study demonstrated the effects of overuse on cysteine cathepsin activity in supraspinatus tendon. A well-established rat overuse protocol[101, 313, 328] that features acromial impingement on the supraspinatus tendon was adapted for use with an inbred strain of rat to allow for the possibility to explore autologous cell therapy for overuse injuries in future studies. The inbred Dahl Salt Resistant rat strain was chosen for this study for their greater weight compared to other inbred strains. With the inbred rat strain, from histological analysis, we attain evident damage to the supraspinatus tendon after overuse. While significant damage occurred by 4 weeks of overuse in outbred strains[313], only minor histological damage was observed by 4 weeks in this study, possibly due to the lower weight of inbred versus outbred strain of rats. However, by 8 weeks of overuse, the insertion region of the supraspinatus tendon displayed obvious changes to the fiber organization and cell shape (Figure 5.1). Fiber separation from bundles and increased cell rounding were more evident by 8 weeks of overuse compared to the 4-week overuse group, indicating that increased time of overuse can cause accumulation of damage. Comparisons between the insertion regions of the 8-week group showed differences in crimping pattern at the insertion (Figure 5.2). While the insertion region of the control tendon demonstrated tightly packed fibers with periodic and cohesive crimping, the insertion of the overuse tendon exhibited regions with flattened crimps and a loss of the periodicity of crimping. Reduction in tendon crimping can result from exercise-induced microtrauma[329], and may be a macroscopic representation of collagen disruption that can ultimately alter biomechanical properties[313]. By confirming the tendon tissue damage by H&E staining and polarized

light microscopy, we determined that this rat model was appropriate to study the molecular level changes in tendon overuse.

The insertion region of the tendon is clinically relevant, as most damage and tears occur in this region, reflecting the complex mechanical forces imparted to this region[330]. Histological scoring displayed the differences between the overuse and control groups at the insertion region. Primary differences in scoring indicated observable changes to cell shape, which was detected by the 4-week timepoint, and fiber organization, which was observed by 8 weeks. Cell shape, reflected by the shape of nuclei, appeared to be rounder near the insertion of the overuse group, as noted previously[331]. The scoring results also further confirmed the disruption in collagen organization compared to controls at the insertion region by 8 weeks of overuse, potentially contributing to the decreased alignment of cells observed (Figure 5.1). The extent of tissue damage by 8 weeks period indicates a demonstrable overuse pathology. There was no observable neovascularization in the tissue sections, which may indicate that tendinopathy can occur without changes to vascularity as suggested previously[325]. While neovascularization has been observed in other studies, it may be a feature of a later stage of healing in response to tendon damage by other means such as tendon detachment[315].

Our novel multiplex cathepsin zymography method has resulted in the first quantitative report that protease activity is upregulated specifically at the insertion region of overused tendon. Additionally, this is one of the few studies that has examined cathepsin expression in tendon. Previously, cathepsin D was detected only by immunohistochemistry within the granulation tissue of torn rotator cuff[332] and was

hypothesized to activate other chemical mediators. However, in this study, in the absence of granulation tissue, increased activity of cathepsin K and L were found within overused tendons (Figure 5.3). The specificity and sensitivity of gelatin zymography allows detection of femtomole quantities of cathepsin K[324] and detects only the active form of enzymes, which distinguishes it from antibody-based techniques and makes it ideal for use in tissue samples with low protein amounts, such as rat tendon.

The increased expression of molecules such as nitric oxide synthase[328] or heat shock protein[101] early in tendon overuse can help discern molecular events in disease progression. In the same vein, in this study, detection of increased cathepsin K and L activity over controls by 4 weeks (Figure 5.3a, b, c) via zymography occurred before observable tissue damage. Other animal models have exhibited early cathepsin gene expression changes prior to the onset of orthopaedic diseases. In a transgenic Del1 osteoarthritis mouse model, higher cathepsin K mRNA levels were observed 3 months before disease onset[333]. In UTU17 transgenic mice, which constitutively overexpresses the cathepsin K gene, early cathepsin K production was found in the synovial lining ahead of severe cartilage degeneration 5 months later[334]. These studies suggest that cathepsin K expression precedes many observable tissue changes that describe disease onset. It has been suggested that cathepsin K plays a major role in initiating fibrillar collagen degradation by exposing a greater number of sites for other collagenases to work and sustain the degradation[318]. In our study, cathepsin K exhibited a temporal response with overuse, with high activity at 4 weeks at the tendon insertion and minor activity by 8 weeks compared to age-matched controls (Figure 5.3f). While cathepsin K staining was positive by immunofluorescence for both timepoints,

antibodies generally do not distinguish between the inactive proform of the enzyme and the proteolytically active mature form of the enzyme.

In contrast to early cathepsin expression that may start the cascade of tissue degradation, sustained cathepsin overexpression can cause accumulation of damage over time, which has been shown in an osteoarthritis mouse model with cathepsin K overexpression[335]. In the study presented here, at 8 weeks of overuse, cathepsin L activity remained higher in the overuse group than control tendons at the insertion, indicating that protein digestion remained elevated over time (Figure 5.3e). This sustained higher cathepsin L activity may suggest its importance in contributing to increased extracellular matrix degradation.

Cathepsin K and L perform optimally at slightly acidic pH, which reinforces their roles in collagen degradation via local secretion or within the lysosomal compartments of tendon fibroblasts (Figure 5.4). These cathepsins can have interconnected functions with each other and with other proteases such as MMPs and serine proteases[320, 321], which are typically regulated by protease inhibitors. However, with certain diseases, protease activity can become misregulated and it may be beneficial to administer protease inhibitors to control tissue degeneration. Cathepsin activity in overused tendon may be a potential molecular target and has been explored in other orthopaedic diseases such as osteoporosis[336]. Administration of cathepsin inhibitors in osteoporosis studies have shown decreased collagen resorption markers and increased bone strength[337]. Since cysteine cathepsin inhibitors have been shown to be promising in other diseases, delivery of cathepsin inhibitors may be a promising method to slow the progression of collagen destruction in degenerative tendon disorders. One

cysteine cathepsin of interest is cystatin C, an extracellular cathepsin inhibitor that binds to cathepsins [134]. It is positively-charged at physiological pH, making it a potential therapeutic to deliver through affinity biomaterials (Supplementary figure A.4).

The results shown here represent a fundamental study on the role of a new class of enzymes within overused tendon, but questions still remain. Additional studies will need to be conducted to establish the specific roles and timecourse of cathepsins in the progression of clinical tendinopathy. This involves evaluating the timecourse of cathepsin K expression and correlating degree of matrix turnover with cathepsin activity during overuse. And in the same vein, in order to evaluate the potency of cathepsins in tendon degeneration, it will be important to study local and selective cathepsin inhibition within overused tendon.

5.5 Conclusions

Cathepsin activity is a novel potential mechanism for tendon degeneration that has not been shown previously in tendon overuse. Differences in tissue structure and quantitative cathepsin activity were greatest at the insertion region, where most tendon ruptures occur[330]. Understanding the role of cathepsins in tendon overuse may help develop treatment plans to prevent tendon rupture by the local application of cathepsin inhibitors. While it is recognized that tendinopathy represents a range of pathologies[338], in this study, cathepsin upregulation relatively early and in specific areas of the tendon suggest that these proteases may play a very important role in the cascades of events that occur prior to tendon failure and make them an exciting potential target for future molecular therapies.

CHAPTER 6

CONCLUSIONS AND RECOMMENDATIONS

6.1 Summary

Over 200,000 Americans per year require shoulder surgery to repair the rotator cuff, with the volume of repairs likely increasing as the current population ages [3]. Surgical repair can alleviate symptomatic shoulder dysfunction, but the rate of revision surgeries can be as high as 57% and do not address the underlying pathophysiology [4]. A physiologically relevant animal model to understand tendon degeneration and tissue engineering strategies to improve the current outcomes of tendon reattachment repairs represent a multi-faceted approach to treating rotator cuff tendinopathy.

Since poor tendon-bone integration is a leading cause for revision surgery, the introduction of reparative cells or bioactive factors can help accelerate early stages of healing and stabilize the tendon-bone interface [5-7]. Mesenchymal stem cells (MSCs) are multipotent progenitor cells that are capable of differentiating into bone, cartilage, and fibrous tissues [13]. While direct injection of MSCs into tendon defects has had limited success, use of biomaterial carriers and preculture of MSCs are alternatives to improve retention and tissue repair [12, 14, 151]. *In vitro* conditioning of MSCs by coculturing MSCs within a 3D hydrogel with a differentiated cell type may direct MSCs toward a desired phenotype that can stabilize the tendon-bone interface. Furthermore, the design of the hydrogel can affect the cell microenvironment, determine the presentation of soluble signals, and ultimately determine the efficacy of preculturing

MSCs within a 3D scaffold. Due to their versatile functions, glycosaminoglycans (GAGs) have garnered interest for use as biomaterials in tissue engineering applications.

Heparin is a highly-sulfated GAG that has been implicated in biological processes such as tissue morphogenesis, regulation of growth factor availability, and protection of growth factors from denaturation [30, 205, 217]. Translation of heparin biomaterials *in vivo,* however, is hampered by its anti-coagulant property [289]. Selective desulfation of heparin has been shown to significantly decrease its anticoagulant activity [290] and may allow the retention of its other biological roles for tissue engineering applications.

There were 2 overall goals of this dissertation: 1) evaluate heparin and desulfated heparin derivatives as biomaterials for MSC encapsulation and growth factor carriers, and 2) characterize a rotator cuff overuse animal model for histological and enzymatic changes. To achieve this, heparin was chemically modified to allow covalent attachment within a synthetic hydrogel network and subsequently used in encapsulating MSCs for coculture with osteoblasts. Upon finding out that sulfation level can affect overall coculture results, soluble desulfated heparin derivatives were examined for their BMP-2 protection capacity and protein interactions. Finally, to understand the cellular and molecular changes that occur in overused tendon prior to tendon rupture, the supraspinatus tendons of an inbred strain of rat were evaluated after 4 and 8 weeks of downhill treadmill running.

In Chapter 3, synthetic poly(ethylene glycol)-based hydrogels with varying concentrations of heparin methacrylamide were designed to determine if immobilized heparin influenced the levels of osteogenic markers of encapsulated MSCs when

cocultured with monolayers of osteoblasts. MSCs encapsulated with 10% wt. heparin-containing hydrogels exhibited significant increases in alkaline phosphatase (ALP) activity and calcium accumulation by 21 days when cocultured with osteoblasts compared to cocultures with MSCs. Five times more MSCs were encapsulated in hydrogels than osteoblasts in monolayers, suggesting that the hydrogel format can be amenable for pre-treating a large population of MSCs. However, with hydrogels containing the highest amount of heparin, mineralization was observed to occur primarily on the edges of the hydrogels, suggesting that MSC response to coculture was not uniform throughout the depth of the hydrogels. Subsequent model protein pull-in studies showed that high amounts of immobilized heparin can affect the distribution of soluble positively-charged proteins within bulk hydrogels.

In order to overcome the diffusional barriers seen in Chapter 3 and to ablate the anti-coagulant activity of native heparin, desulfated heparin derivatives were synthesized and evaluated by their protein interactions. In Chapter 4, selective desulfation of heparin was performed according to established protocols to produce N-desulfated heparin (Hep^{-}_{N}), 6-O, N-desulfated heparin ($Hep^{-N,-6O}$) and entirely desulfated heparin (Hep^{-}) [290, 296, 297, 301]. Non-glycosylated BMP-2, a heparin-binding growth factor, was heat treated with or without heparin species prior to administration to the C2C12 cell line to determine growth factor bioactivity. Native heparin was the most effective in protecting BMP-2 bioactivity against thermal denaturation, as evidenced by significantly higher alkaline phosphatase (ALP) activity across different heat treatment times. Incubation of BMP-2 with heparin derivatives of intermediate sulfation levels resulted in higher bioactivity compared to BMP-2 alone only after the longest heat treatment time. Protein

interaction with heparin species was indirectly measured by differential scanning fluorimetry and showed that Hep and Hep^{-N} could induce conformational changes in a model protein, suggesting a specific interaction between these heparin species and protein. This study demonstrated that small changes to the sulfation level of heparin will continue to allow direct interaction with proteins, but desulfation could have large effects on the protective features of heparin.

The development of tissue engineering techniques to improve tendon-bone integration after tendon reattachment is one approach to treating tendon injury. Another is to understand what causes tendon degeneration in order to prevent progression of tendinopathy. In Chapter 5, an established overuse protocol was characterized for the inbred Dahl Salt Resistant strain of rat. The supraspinatus tendon was analyzed by cathepsin zymography and histology at 4 and 8 weeks of overuse. Minor tissue damage was observed by 4 weeks, but tissue disorganization was more obvious by 8 weeks of overuse and was localized at the insertion region of the tendon. Cathepsin zymography revealed higher cathepsin L activity in the insertion region of the tendon of overused shoulders compared to non-running controls at both 4 and 8 weeks. These findings validated the use of the Dahl Salt Resistant rat for developing a supraspinatus tendon overuse injury in an area that experiences the most tendon tears. Furthermore, these results revealed a potential new mechanism for tendon degeneration caused by overuse.

6.2 Conclusions

The research presented in this dissertation advances understanding of the role of sulfation in developing heparin-based biomaterials and provides insight into a novel,

potential mechanism of tissue degradation in tendon overuse. The results of these studies suggest that heparin 1) interacts with charged soluble factors to enhance paracrine signaling and 2) its sulfation level can affect the protection conferred to growth factors in a denaturing environment. Furthermore, the characterization of the *in vivo* overuse model was critical in establishing baseline tissue damage and identifying cathepsin activity within overused tendon.

The numerous docking sites for protein on heparin [30, 339] was used as an opportunity to develop covalently crosslinked heparin-containing hydrogels to enhance dynamic soluble factor treatment of MSCs. Heparin, with its multiple carboxyl groups, is amenable to methacrylamide (MAm)-group functionalization that allows for the formation of a covalent crosslinked network. Heparin addition to hydrogels have been shown to control the release of proteins (Supplemental figure A.1) [231, 232], but its use for sequestering multiple soluble factors from a defined coculture environment is relatively unexplored.

In Chapter 3, a coculture experiment was described to allow dynamic signaling between encapsulated MSCs and monolayers of osteoblasts. The presence of members of the BMP family is likely in this coculture system since it has been established that osteoblasts can secrete BMP-2, BMP-4, and BMP-7, which are known to induce osteogenesis in MSCs [273, 274]. Cocultures were compared to the cocultures of encapsulated MSCs with monolayers of MSCs and all data were expressed as a difference between the values of cell-laden hydrogels and acellular hydrogels of the same polymer composition cultured in parallel. Effects of osteoblast coculture on ALP activity were apparent by day 1, and MSCs encapsulated in 10% wt. heparin

methacrylamide (MAm) hydrogels showed the largest time-dependent increase in ALP activity by 21 days with a 5-fold increase over day 1 (Figure 3.5a). While all cell-laden hydrogels accumulated calcium over 21 days, the 10% wt. heparin MAm samples cocultured with osteoblasts showed an over 50-fold increase in calcium content from day 14 and were significantly higher than MSC coculture controls on the same day (Figure 3.5b). All samples cocultured with osteoblasts showed significantly higher calcium accumulation by 21 days compared to samples cocultured with MSCs. Results of elevated ALP activity and calcium accumulation observed in samples cocultured with osteoblasts suggests that heparin interacted with osteoblast-secreted factors to mediate MSC-directed ALP production and mineralization not seen in controls. Previous research has shown that specific BMP interaction with heparin results in the augmentation of the biological activity of BMPs, as reflected in the production of mineralized tissue or induction of osteoblastic differentiation of MSCs [34, 249, 275], which makes these hydrogel formulations particularly suited to enhancing pro-osteogenic signaling from nearby cells.

The differences in mineralization patterns between hydrogels cocultured with osteoblasts suggested that heparin may prevent uniform pre-treatment of cells in a bulk hydrogel containing 10% wt. heparin MAm (Figure 3.6). It was observed that the presence of heparin reduced diffusion of positively-charged molecules, such as the model protein histone, into the hydrogel, particularly into the 10% wt. heparin MAm formulation (Figure 3.7). This phenomenon was not observed when hydrogels were allowed to absorb the similarly sized, negatively-charged protein casein. Protein transport is limited by molecular size and by charge interactions between proteins and

extracellular matrix (ECM) molecules [285]. An *in vivo* study showed that the presence of heparan sulfate in the ECM could decrease the effective diffusion coefficient of polyanion-binding lactoferrin through tissues by ~60%, indicating that the effective charge of heparin can affect the diffusion of charged molecules in our system [286]. To prevent non-uniform treatment of cells, the heparin-containing hydrogels would either have to be reduced in geometry, include less heparin, or include heparin that has lower affinity for proteins. Selective desulfation of heparin can modulate its affinity to proteins [340] with the addition of reducing the anti-coagulation activity [290, 340] for *in vivo* translation.

Chapter 4 highlights the selective desulfation of heparin to produce Hep^{-N}, $Hep^{-N,-6O}$, and Hep^{-}, with minimal change to overall chain length (Figure 4.1). Non-glycosylated BMP-2 was very heat unstable, exhibiting a bioactivity level ~34% after a 2min exposure to heat (Figure 4.4). The thermal stress of heating at 65°C appeared to cause non-reversible unfolding as bioactivity was not recovered after removal from heat. Addition of native heparin at 100 molar excess to BMP-2 prior to heating was shown to maintain BMP-2 bioactivity at ~68% over 15min of thermal stress compared to ~0.1% of BMP-2-alone. Complexes of 10:1 heparin:BMP-2 were a significant improvement in maintaining BMP-2 bioactivity over free BMP-2, but exhibited significantly lower bioactivity than 100:1 after 15min of heat treatment (Figure 4.4).

An excess of heparin was chosen in order to ensure BMP-heparin interaction. These approximate molar ratio of heparin to protein have also been used in a previous study investigating heparin with FGF-2 [303] and a delivery vehicle that has shown modulated release with 100:1 heparin:growth factor concentrations [304]. It has been

estimated that 5-6 molecules of BMP-2 can be bound to each heparin chain [168], so there were heparin molecules that were not saturated with BMP in these studies. It is possible that the excess of unoccupied heparin at 100 molar excess may play additional roles in slowing denaturation of BMP-2.

All the desulfated derivatives at 100 molar excess failed to be as effective as 100:1 Hep:BMP-2 at maintaining BMP-2 bioactivity when exposed to heat. While the overall sulfation of Hep^{-N} is approximately 82% of native heparin, the bioactivity of BMP-2 with Hep^{-N} after 2min of heating, which may represent moderate thermal stress, is approximately 30% of untreated BMP-2. Incubation of Hep^{-N} or $Hep^{-N,-6O}$ with BMP-2 prior to 15min of heating resulted in similar bioactivity levels, which was significantly lower than 100:1 Hep:BMP-2 but significantly higher than BMP-2 alone and BMP-2 incubated with Hep^{-}. These results indicate that overall sulfation is not the only factor in maintaining BMP-2 stability as relatively small changes to sulfation can significantly affect the maintenance of BMP-2 bioactivity. However, Hep^{-N} and $Hep^{-N,-6O}$ may retain sufficient sulfation to protect growth factors in denaturing environments. Differential scanning fluorimetry (Figure 4.6) and circular dichroism (Supplementary figure A.2) data show that Hep and Hep^{-N} produce conformation changes in histone, indicating that these heparin species can directly complex to protein. Furthermore, N-desulfated heparin has been shown to be amenable to osteogenic differentiation [219] and exhibits reduced anti-coagulation activity [290], indicating that this heparin derivative shows beneficial features as a biomaterial.

Characterization of a relevant tendon overuse animal model was presented in Chapter 5. The inbred Dahl Salt Resistant strain of rat was subjected to up to 8 weeks of

downhill running and the supraspinatus tendons were analyzed by histology and cathepsin zymography. Histological scoring demonstrated that collagen disorganization and increased rounding of cells was apparent after 8 weeks of downhill running at the insertion region compared to controls (Table 5.1), and demonstrated that increased period of overuse caused accumulation of damage. The increased observations of rounded cells is similar to what has been shown in outbred rats subjected to downhill running, in which repeated passing through the acromion can cause the tendon to exhibit a compression-induced, cartilaginous phenotype [99, 115]. Comparisons between the insertion regions of the 8-week group under circular polarized microscopy showed differences in crimping pattern (Figure 5.2). While the control tendons demonstrated tightly packed fibers with periodic and cohesive crimping, the insertion of the overused tendons exhibited regions of flattened crimps and a loss of the periodicity of crimping. These changes may indicate collagen disruption due to overuse [341].

Samples from the insertion region of overused tendon at both time points consistently showed active cathepsin L bands between 25-35kDa that were 1.8-fold higher in activity than controls (Figure 5.3a, d). Furthermore, there was evidence of high molecular weight bands (50-75kDa) from the insertion regions of 4 week overuse tendons, which were attributed to cathepsin K bound to extracellular matrix, as seen in osteoclasts in previous studies [342]. Evidence of active cathepsins in tendon overuse had not been previously demonstrated and may represent a novel mechanism for tendon degeneration.

Cathepsins are potent proteases that can play major roles in initiating fibrillar collagen degradation or destabilizing the collagen network [139, 343]. They have been

described in orthopaedic cell types such as synovial fibroblasts that become activated during rheumatoid arthritis, inducing the degradation of aggrecan and type I and II collagen [344-346]. While inflammatory environments have been shown to directly induce cathepsin secretion [347], it was demonstrated that mechanical stress could upregulate the expression of cathepsin B in chondrocytes [348]. Tendon overuse caused an early increase in cathepsin K activity, suggesting that it may play a role in initiating fibrillar collagen degradation, making it easier for other collagenases to sustain the degradation [139]. A sustained increased activity of cathepsin L over the 8-week running period indicates that protein digestion remains elevated over time, leading to accumulated collagen degradation.

6.3 Future Directions

The findings in this dissertation provide significant insight to understanding tendon overuse in a physiologically relevant animal model and to the development of heparin-based biomaterials for coculture applications and growth factor delivery. The goal of Specific Aim I and II was to develop techniques that can be used to improve tendon to bone integration through the use of heparin-based materials. The results of those studies contribute fundamental concepts about the effects of heparin sulfation on hydrogel properties and protective effects against protein denaturation. In Aim III, the tendon overuse model was characterized in order to establish an inbred strain of rat for this overuse protocol for future cellular therapies and to better understand tendon degeneration prior to tendon rupture. The studies highlighted above serve as a

foundation for future studies that use GAG-based biomaterials to slow the progression of tendon degeneration or improve the fixation of tendon to bone after rupture.

Future work can expand on the research presented here in order to improve tendon to bone integration after tendon rupture and to develop therapeutics to prevent tendon degeneration. Hydrogels of heparin derivatives can aid in pre-treating cells prior to implantation. The study of soluble heparin derivatives with BMP-2 provided insight on the effect of sulfation level on maintaining growth factor bioactivity. Hep^{-N}, $Hep^{-N,-6O}$, and Hep^{-} can be chemically modified to allow covalent crosslinking into hydrogels such that the differing levels of sulfation can be presented in 3D. These hydrogels may improve the coculture technique presented in Chapter 3 by allowing more uniform distribution of soluble factors and a more uniform cell response. Since selective desulfation may affect the GAG backbone, it would be interesting to see if desulfated heparin derivatives affect cell response in coculture. Desulfated chondroitin sulfate, chondroitin, was able to enhance the chondrogenic response of encapsulated MSCs in comparison to chondroitin sulfate when treated with chondrogenic medium, possibly by decreasing the affinity of the growth factor to the scaffold to allow growth factor induced signaling [349].

Development of a natural enthesis or insertion between tendon and bone remains a goal after tendon reattachment surgeries. While allowing some mineralization on a reattached tendon may quickly improve the strength of integration between tendon and bone, too much ectopic mineralization may cause other complications that may resemble calcific tendinopathy [350, 351]. Another approach to bridging the tendon to bone interface is by delivering cocultured cells within GAG-based hydrogels into the interface

region. The delivered cells would ideally form a fibrochondrocytic phenotype that transitions from tendon into bone. The desired cell type will determine the type of GAG-based hydrogel to use in coculture. In order to stabilize the fibrocartilage phenotype [17, 350], hydrogels of chondroitin-4-sulfate may be conducive for cell maintenance [218]. In Chapter 3, MSCS were cocultured with osteoblasts, but MSCs may be cocultured with other cell types such as tenocytes that may provide the necessary cues to bridge the tendon to bone gap [352, 353].

The spatial organization of MSCs during coculture can affect differentiation capacity of MSCs. Chondrogenic differentiation of MSCs can be improved when cultured as aggregates [354]. In order to use this cell culture environment, desulfated heparin species can be developed into microspheres and incorporated into cell spheroids. Microspheres may be used to sequester growth factors from the cell culture medium or from neighboring cells. This alternative format avoids the potential diffusional limitations due to the bulk heparin hydrogels and can be amenable to delivery to the tendon-bone interface.

In lieu of cellular delivery, delivery of bioactive factors such as BMPs from heparin-containing hydrogels may help direct endogenous cell responses [21, 50]. With a library of desulfated heparin derivatives, delivery systems can be developed with varying affinity for proteins, thereby controlling their release. Heparin-containing hydrogels can also bind multiple growth factors for delivery, which may improve the biological outcome in complex tissues. By being able to control the spatiotemporal release of soluble factors through biomaterial selection and design of the scaffold, control over molecules such as mitogens, growth factors, and morphogens, may more

closely replicate biological processes [355, 356]. In another biomaterial approach, polyelectrolyte multilayers can be formed from sequential physisorption of anionic and cantionic polymers and do not require harmful processing of the material, allowing growth factor incorporation between layers [357]. Inclusion of heparin species as the anionic layer in polyelectrolyte multilayers can help protect growth factors such as BMP from loss of bioactivity while also controlling the release of BMP [358]. Furthermore, these materials are conformal, allowing delivery with scaffolds of complex geometry [359]. These polyelectrolyte multilayers have been shown to induce tissue integration and recruit progenitor cells to a cell free scaffold [359], suggesting that these materials may be amenable for study at the tendon-bone interface.

Increase in cathepsin activity within overused tendon is a novel finding for this animal model and is a promising target for therapeutics. Currently, we are collecting human tendon samples that are typically discarded after debridement or supraspinatus tendon reattachment procedures to determine if differences in cathepsin activity are related to the chronicity of the tendon injury. Preliminary results show that active cathepsins exists within torn supraspinatus tendon, but more samples will be analyzed and cross-referenced with type of tear (acute versus chronic), gender, and age to better understand the profile of cathepsin activity. If increased cathepsin activity is a significant feature in human rotator cuff tears, the animal model will prove extremely useful in testing whether cathepsin inhibition can affect the progression of tendon degeneration.

Cathepsins have been found to have interesting interactions with glycosaminoglycans; studies have shown that GAGs may contribute to the inhibition or

activation of cathepsins. Chondroitin sulfate and heparin have been purported to aid in activating pro-cathepsn B and L by helping to destabilize the inhibitory peptide sequence [133, 360-362]. However, these studies utilized tissue-derived cathepsins, which may have contained other cathepsins as contaminants. In a more recent study, cathepsin L and B were shown to be inhibited in the presence of chondroitin sulfate [363]. Dissimilarly, chondroitin sulfate formed highly active complexes with cathepsin K to degrade collagen. Furthermore, incubation of cathepsin K with heparin sulfate or heparin inhibited its activity. In light of these results, the use of heparin-based materials may prove advantageous in inhibiting the activities of specific cathepsins where they are expressed *in vivo*. How heparin and desulfated heparin species modulate the activity of cathepsin L and K will need to be evaluated, but the design of materials that can affect the autocatalysis of cathepsins is an exciting prospect.

Active cathepsins are inhibited by the constitutively secreted cystatins, but deficiencies in cystatins may cause excessive tissue damage [364]. Administration of cystatin C can determine if extracellular cathepsin activity is a prominent feature of tendon overuse. Cystatin C is positively-charged at physiological pH and in a preliminary study, its release was modulated by encapsulating the inhibitor within heparin-containing hydrogels (Supplementary figure A.4). If cathepsin L activity is determined to be located within the lysosomes, intracellular inhibitors such as E64 may be used to evaluate the effect of cathepsin inhibition [365].

Determination of the role and timescale of cathepsin activity within tendon overuse can be a significant advancement in preventing and treating tendon diseases. Cathepsin K activity was detected early and cathepsin L showed sustained activity over

time within our animal model. If cathepsin expression can be reliably detected at different (early to chronic) stages of tendon degeneration, diagnostic probes can be developed to help detect tendons that may be susceptible to rupture. Currently, partial tears in tendon are difficult to detect with diagnostic imaging [366, 367]. The advent of fluorescent or near infrared probes for specific enzymes within tissues may help detect early tendinopathic changes. A near infrared probe that remained quenched in its native state, but became fluorescent upon enzyme cleavage was detected in femtomole quantities by fluorescence-mediated tomography [368]. A similar probe was used to detect active cathepsin K, and was able to show the location of cathepsin K near macrophages where elastin damage was evident [369]. Early diagnosis of tendinopathy can help identify and implement conservative treatments that prevent progression of the tendon degeneration.

The benefits of having a consistent tendon overuse animal model allows us to adjust therapeutic parameters in order to best address the tendon degeneration. Heparin is just one GAG in a family of many, including chondroitin sulfate, dermatan sulfate, keratan sulfate and hyaluronan [181]. Hyaluronan, a non-sulfated GAG, has received attention in the field of biomaterials for being able to bind to the cell surface receptor CD44, exhibiting a relatively fast turnover rate, and participating in wound healing and inflammation [370-372]. The studies presented in this thesis have shown the importance of sulfation level on heparin, but this concept of understanding how molecular changes affect cell and protein interaction can be extended to many of the above materials. Sulfation position and presentation of GAG can have significant effects on cell responses. Both chondroitin-6-sulfate (C-6-S) and chondroitin-4-sulfate (C-4-S) were

able to promote wound closure in a 2D wound model, but only C-4-S promoted wound contraction in a 3D wound model [373], suggesting that fibroblasts can sense sulfation level differences as well as presentation of GAG.

The research presented in this thesis contributes significant concepts for the development of future heparin-based biomaterials and exciting opportunities to test therapeutics in an *in vivo* tendon overuse model. Heparin-derived materials have attractive biological features that can be engineered to be safe *in vivo* and efficacious for growth factor delivery. Culturing MSCs in heparin-containing hydrogels is a valuable technique for controlling the presentation of soluble factors to encapsulated cells and has potential for efficiently pre-treating a large population of cells. Selective desulfation of heparin enables studies on the effect of sulfation on protein interaction. In this thesis, it was shown that the level of sulfation on heparin can affect the bioactivity of BMP-2 in denaturing conditions. This will affect the choice of heparin species for biomaterial development. Finally, an inbred animal model for tendon overuse was characterized, featuring a novel potential mechanism of tissue degradation that may become a future therapeutic target. Overall, the research presented here provides the framework for developing GAG-based materials that take into consideration molecular interactions with proteins in order to develop the most efficacious delivery system for cells and growth factors. Furthermore, characterization of an *in vivo* overuse injury provides a test bed for targeted therapeutics that will advance the understanding of tendinopathy.

APPENDIX A

SUPPLEMENTARY FIGURES

A.1 Release of Platelet-Derived Growth Factor-BB From Heparin-Containing Hydrogels

A.1.1 Materials and Methods

A.1.1.1 Encapsulation of platelet-derived growth factor-BB

Recombinant rat platelet-derived growth factor-BB (PDGF-BB, R&D Systems) was resuspended as a working stock solution of 50μg/mL. Heparin MAm synthesis and hydrogel parameters are described in detail in Chapter 3. PDGF-BB was mixed into the macromer solution prior to photoinitiated crosslinking. After polymerization, hydrogels were placed in PBS and the entire supernatant was collected on days 1, 3, 5, 7, and 9. A rat PDGF-BB Immunoassay Kit (R&D Systems) was used to detect the amount of PDGF-BB released. A theoretical initial amount of 69.4ng of PDGF-BB was encapsulated within each hydrogel, representing a 1:1,000 molar ratio of PDGF-BB to heparin in the 10% heparin MAm hydrogels.

A.1.1.2 Statistical Analysis

A two-way analysis of variance (ANOVA) was used to determine statistical differences of groups and subsequent one-way ANOVAs were used to determine differences across time for each hydrogel type and differences across hydrogel type for each timepoint. Tukey's *post hoc* test was used with a significance set at $p \leq 0.05$.

A.1.2 Results

PDGF-BB was released in a burst from 0% heparin MAm hydrogels, showing no significant difference in cumulative PDGF-BB amount between timepoints (Figure A.1). The PDGF-BB released from 1% heparin MAm hydrogels on day 1 was significantly lower than the cumulative values at all other timepoints. Release of PDGF-BB from 10% heparin MAm hydrogels was very low on day 1 and showed no significant differences across time. At day 1, the amount of PDGF-BB released from 0%, 1%, and 10% heparin MAm hydrogels were significantly different from each other. At all other timepoints thereafter, only the cumulative amount from 10% heparin MAm hydrogels was significantly lower than the amounts from 0% and 1% heparin MAm hydrogels.

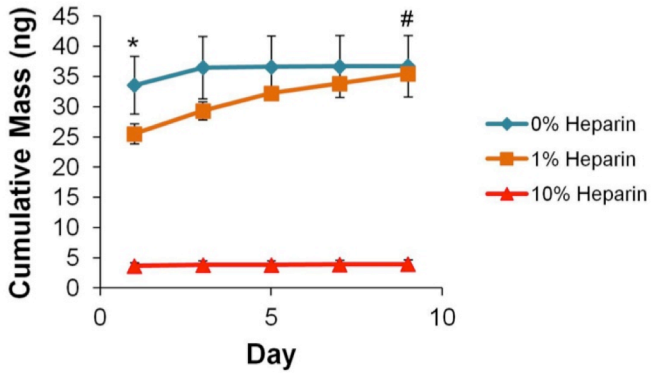

Figure A.1 Heparin-containing hydrogels can control release of positively-charged PDGF-BB. Increasing amounts of heparin from 1% to 10% within the hydrogel drastically reduced the amount of growth factor released into solution. While 0% heparin MAm hydrogels exhibited a burst release with no subsequent release, 1% heparin MAm hydrogels showed a lower burst release with subsequent release. Hydrogels of 10% heparin MAm appeared to prevent release of PDGF-BB. n=3±s.d., * indicates significantly higher PDGF release from 0% heparin MAm hydrogels than from 1% and 10% heparin MAm hydrogels, # indicates significantly less release of PDGF from 10% heparin MAm hydrogels compared to 0% and 1% heparin MAm hydrogels.

A.2 Heparin-Induced Secondary Structure Changes in Histone

A.2.1 Materials and Methods

Ultraviolet circular dichroism (CD) spectra were recorded on an OLIS DSM 17 CD spectrophotometer with OLIS 14 CD software. The sample chamber was maintained at 20°C and spectra were collected over 190-260nm from a demountable quartz cuvette (Starna) with a pathlength of 0.5mm.

Lysine-rich H1 histone (Sigma-Aldrich) and heparin derivatives (Hep, Hep^{-N}, $Hep^{-N,-6O}$, Hep^{-}) were reconstituted at 1mg/mL in 1% v/v 1X PBS in ddH_2O. Different concentrations of heparin derivatives were evaluated to minimize deviations from baseline spectra. Spectra of individual components and mixtures were recorded at final concentrations of 100µg/mL histone and 5µg/mL heparin derivatives. Spectra were smoothed by least squares fit and were translated such that the millidegree reading was 0 at 260nm. Results are expressed as an average of 10 readings as molar ellipticity with units in deg * cm^2/dmol.

A.2.2 Results

A concentration of 5µg/mL of heparin species worked well for Hep, Hep^{-N}, and $Hep^{-N,-6O}$. The same concentration for Hep^{-} produced a signal that may have affected the spectra collected as a mixture with histone, so was not included in these results. Histone protein displays a predominant random coil configuration with a minimum between 200-205nm (Figure A.2). When Hep or Hep^{-N} was incubated with histone, an obvious positive shift in the spectra was observed. When $Hep^{-N,-6O}$ was incubated with histone, no such shift was observed.

These results suggest that Hep or Hep^{-N} can interact with histone to induce a change in in its peptide bond configuration, or secondary structure. The shift may signal a loss in random coil amount, but it is currently unclear how these shifts affect corresponding amounts or configurations of α-helices or β-sheets within histone. Addition of Hep$^{-N,-6O}$ does not seem to induce a large change in secondary structure when compared to Hep, and Hep^{-N}.

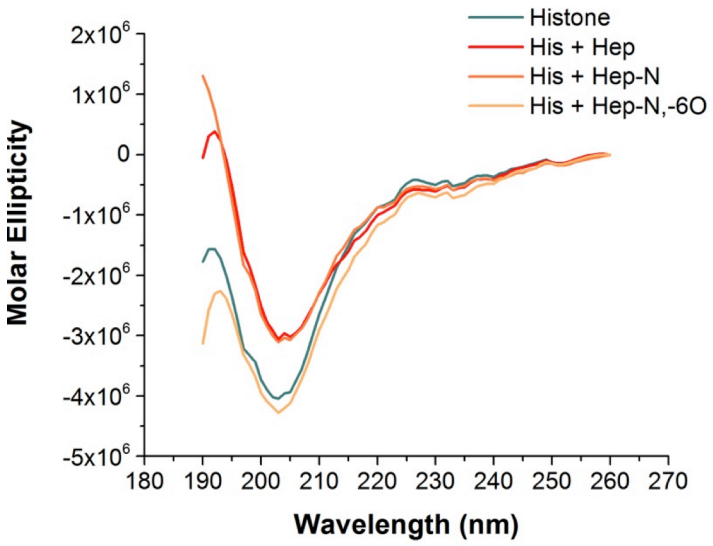

Figure A.2 Far UV CD spectra of histone-alone and in mixtures containing heparin derivatives. Addition of Hep or Hep^{-N} shifted the spectra of histone, suggesting a change in secondary structure due to these ligands. Addition of Hep$^{-N,-6O}$ did not produce the same shift.

A.3 Interactions of Soluble Histone:Heparin Complexes with Heparin-Containing Hydrogels

A.3.1 Materials and Methods

A.3.1.1 Characterization of histone:heparin complexes and hydrogels

A range of histone:heparin mass ratio were formulated in order to identify soluble complexes. Histone and heparin stock solutions were made at 1mg/mL in 1X PBS. Mixtures were pipetted into clear 96-well plates and the absorbance at 420nm was recorded.

Hydrogels (90% wt H2O) of 0%, 10%, or 100% heparin MAm were fabricated with the remaining amount composed of poly(ethylene glycol)-diacrylate (MW~3,400). After crosslinking by ammonium persulfate and TEMED, hydrogels were allowed to swell overnight and weighed. Thereafter, the hydrogels were lyophilized and weighed once more. The swelling ratio was calculated as the ration between the swollen hydrogel weight and the lyophilized hydrogel weight.

A.3.1.2 Pull-in study

For pull-in studies, a complex ratio of 35 molar excess of heparin to histone was chosen. After 0%, 10%, and 100% heparin MAm hydrogels were fabricated, they were placed in a histone or complex solution containing fluorescein-tagged histone for 24 hours. Then hydrogels were imaged by confocal microscopy ($n \geq 3$) and the average fluorescence across the depth for each hydrogel group was computed. Representative images and graphs of fluorescence values are shown up to half the hydrogel depth, as fluorescence attenuation was apparent with greater depths.

A.3.1.3 Hydrogel supernatant analysis

The supernatants from pull-in studies were analyzed for remaining heparin and protein in solution. The complex solutions were analyzed for heparin by DMMB and protein was assayed by BCA. Histone-only solutions were analyzed by BCA assay.

A.3.1.4 Statistical Analysis

Max fluorescence in hydrogels after histone or complex pull-in was analyzed by t-test within each hydrogel formulation. Data from supernatants were analyzed by one-way ANOVA. All data were analyzed with a significance level of $p \leq 0.05$.

A.3.2 Results and Discussion

A large range of soluble complexes could be formed, with turbidity appearing only in the region around where histone and heparin concentrations were equivalent (Figure A.3.1a). The experiments in this study utilized concentrations of heparin and histone that fell within the heparin-rich zones. Heparin-containing hydrogels could be formed without significant changes to the swelling ratio (Figure A.3.1b), indicating that differences observed in diffusion could be attributed to differences in relative charge within the hydrogel.

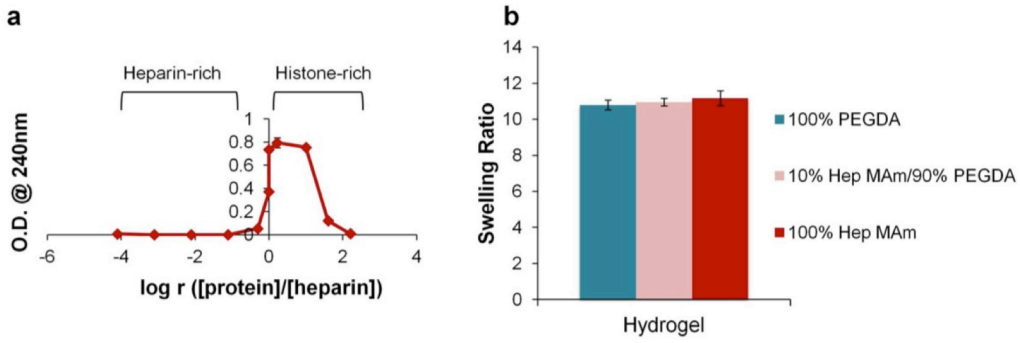

Figure A.3.1 Characterization of complexes and hydrogels. (a) Turbidity measurement of different concentration ratio of heparin and histone. (b) Swelling ratio of hydrogels.

From analysis of the remaining supernatant, no significant differences in heparin concentration were observed between the different hydrogel types (Figure A.3.3a), suggesting that complexed histone did not have appreciable affinity to the different hydrogel formulations. However, the protein assay revealed that less complexed histone remained in the supernatant when 100% heparin MAm hydrogels were incubated in it (Figure A.3.3b), suggesting some pull-in of complexes into these hydrogels. These results suggest that complexes may decomplex as histone is sequestered into the 100% heparin MAm hydrogels while heparin remains in the supernatant.

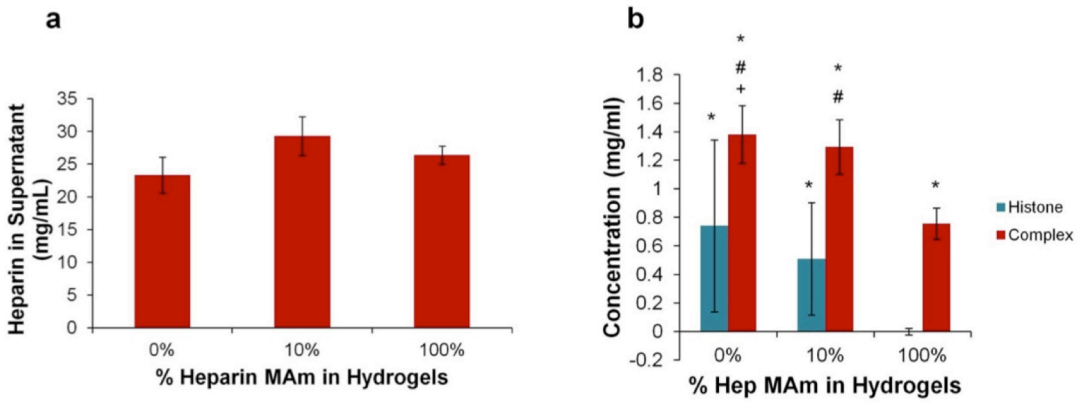

Figure A.3.2 Analysis of supernatants from pull-in study. (a) Remaining heparin in solution after pull-in study incubation showed no significant differences across the different hydrogel types. (b) BCA analysis showed that less histone remained in solution when incubated with 100% heparin MAm hydrogels, yet more remained when histone was complexed to heparin. n=3±s.d., * indicates significantly higher than histone remaining from incubation with 100% heparin MAm hydrogels, # indicates significantly higher than complexed histone incubated with 100% heparin MAm hydrogels, and + indicates significantly higher than histone incubated in 10% heparin MAm hydrogels ($p \leq 0.05$).

Histone and complexes were relatively well distributed across the depth of a hydrogel containing 0% heparin MAm (Figure A.3.2). However, when hydrogels contained 10% heparin MAm, the maximum intensity of histone was 1.9 times higher than complexes within the same hydrogel formulation ($p \leq 0.05$) and the histone-only

samples appeared to distribute primarily to the surfaces of the hydrogels. This lack of accumulation of complexed histone in the 10% heparin MAm hydrogels suggests that the complex has less affinity for heparin MAm, in contrast to results for free histone. The maximum intensity of the complex was not significantly different from histone pulled into 100% heparin MAm hydrogels, although the distribution appeared broader. The similar distribution of free and complexed histone in the 100% heparin MAm hydrogels may indicate instability of the complexes such that at high heparin MAm concentrations, competition may occur between soluble and immobilized heparin. This may lead to decomplexing between soluble heparin and histone.

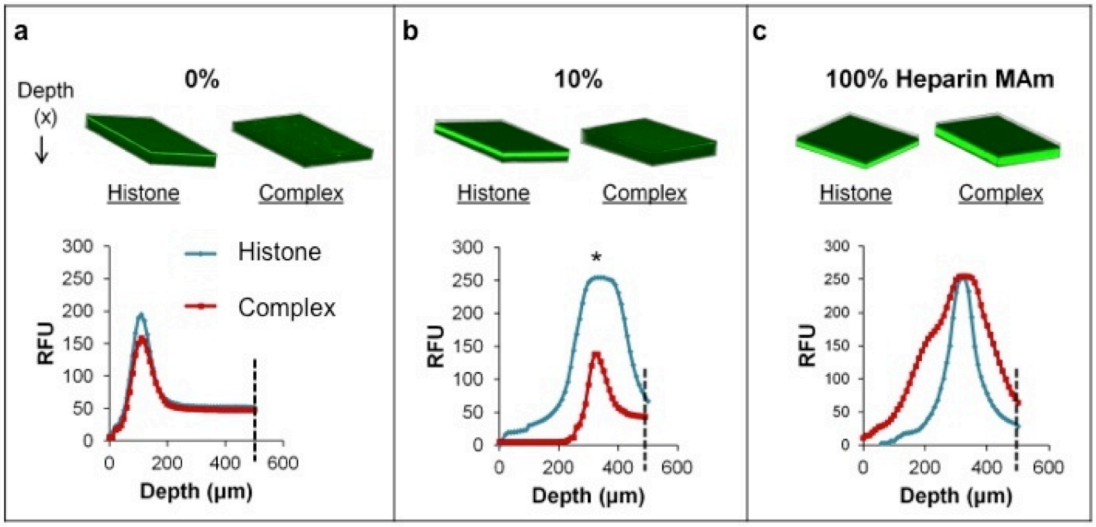

Figure A.3.3 Distribution of fluorescently-tagged histone and complexes of histone after pull-in in hydrogels of increasing amounts of heparin MAm. (a) Distribution of histone and complexes in 0% heparin MAm hydrogel show no differences in peak fluorescence or overall distribution. (b) Histone appears to distribute primarily to the surfaces of the hydrogel and its peak fluorescence is higher than complexed histone in 10% heparin MAm hydrogels. (c) High peak fluorescence was observed for both histone and complexed histone. n=3±s.d., * indicates significant difference in peak fluorescence between histone and complexed histone.

A.4 Release of Cystatin C from a Heparin-Containing Hydrogel

A.4.1 Materials and Methods

A.4.1.1 Hydrogel Fabrication

Oligo(polyethylene glycol) fumarate 10K and poly(ethylene glycol)-diacrylate 3.4K were used as a mixture of 50:50 by weight. Heparin MAm was incorporated in amounts of 0% and 50% weight of total dry weight of polymer and subsequently dissolved in PBS with 0.018M ammonium persulfate/N, N, N', N'-tetramethylethylenediamine for an initial water content of 90% (w/w). Macromer solutions were dispensed in 30 μL amounts into PTFE (Teflon) wells and allowed to crosslink for 10 minutes at 37°C. Resulting hydrogel disks were 6 mm in diameter and ~1 mm thick.

A.4.1.2 Cystatin C Release from Hydrogels

Hydrogels were fabricated and allowed to swell overnight in PBS in wells of a 48-well plate. Hydrogels were subsequently lyophilized for a day to remove all liquid in the samples. Following lyophilization, each hydrogel was incubated with 15μL of 6.7ng/μL cystatin C at 4°C for 1 day to allow protein absorption into the hydrogel. The next day, 300μL of PBS with 1% BSA was added to each well and immediately collected for the day 0 time point. The supernatant was replenished and the procedure of collecting and replenishing the supernatant was repeated every day for up to 5 days.

The cystatin C in supernatants was detected by Western blot. Samples, control, and ladder were loaded into a 12.5% polyacrylamide SDS-PAGE gel and run at 200V. Protein bands were transferred from the gel to a nitrocellulose membrane by electroblotting with a semi-dry method. The membrane was blocked with Odyssey

blocking buffer and incubated with primary rabbit polyclonal cystatin C antibody overnight at 4°C. The membranes were washed and incubated with 1:5000 dilution of fluorescent secondary anti-rabbit antibody for 1 hour. Blots were imaged and image files were processed with Adobe Photoshop and analyzed with ImageJ. Results are shown as mean ± standard deviation. Statistical significance was determined using a 2-sample t-test, $p \leq 0.05$.

A.4.2 Results

Cystatin C release occurred in a burst release from both 0% and 50% heparin hydrogels on day 1. However, significantly lower amounts of cystatin was cumulatively released from the 50% heparin hydrogels by 5 days.

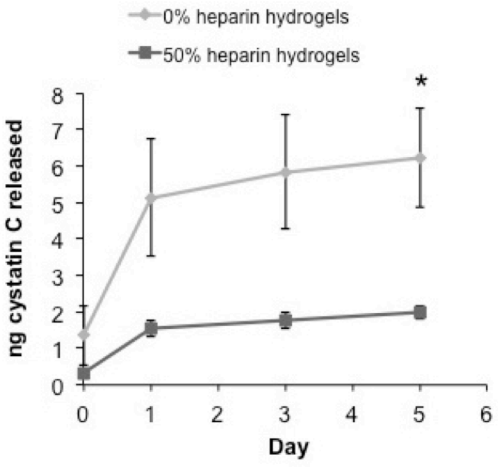

Figure A.4 Release of cystatin C over 5 days from hydrogels. Crosslinking 50% wt. heparin MAm into the hydrogel can significantly reduce the release of cystatin C over 5 days. * indicate that 0% heparin hydrogels released more cystatin than 50% heparin hydrogels. $p \leq 0.05$, n=3; mean ± s.d.

REFERENCES

[1] National Institute for Occupational Safety and Health. Musculoskeletal disorders and workplace factors: A critical review of epidemiologic evidence for work-related musculoskeletal disorders of the neck, upper extremity, and low back; Washington, D.C.: U.S. Department of Health and Human Services; 1997.

[2] Józsa LG, Kannus P. Human Tendons: Anatomy, Physiology, and Pathology. Champaign, IL: Human Kinetics Publishers; 1997.

[3] Colvin AC, Egorova N, Harrison AK, Moskowitz A, Flatow EL. National trends in rotator cuff repair. J Bone Joint Surg Am. 2012;94:227-33.

[4] Boileau P, Brassart N, Watkinson DJ, Carles M, Hatzidakis AM, Krishnan SG. Arthroscopic repair of full-thickness tears of the supraspinatus: does the tendon really heal? J Bone Joint Surg Am. 2005;87:1229-40.

[5] Bigliani LU, Cordasco FA, McIlveen SJ, Musso ES. Operative treatment of failed repairs of the rotator cuff. J Bone Joint Surg Am. 1992;74:1505-15.

[6] Cummins CA, Murrell GAC. Mode of failure for rotator cuff repair with suture anchors identified at revision surgery. J Shoulder Elb Surg. 2003;12:128-33.

[7] Kovacevic D, Rodeo SA. Biological Augmentation of Rotator Cuff Tendon Repair. Clin Orthop Relat Res. 2008;466:622-33.

[8] Liu SH, Baker CL. Arthroscopically assisted rotator cuff repair: Correlation of functional results with integrity of the cuff. Arthroscopy. 1994;10:54-60.

[9] Benjamin M, Toumi H, Ralphs JR, Bydder G, Best TM, Milz S. Where tendons and ligaments meet bone: attachment sites ('entheses') in relation to exercise and/or mechanical load. J Anat. 2006;208:471-90.

[10] Alhadlaq A, Mao JJ. Tissue-engineered osteochondral constructs in the shape of an articular condyle. J Bone Joint Surg Am. 2005;87:936-44.

[11] Holland TA, Bodde EWH, Baggett LS, Tabata Y, Mikos AG, Jansen JA. Osteochondral repair in the rabbit model utilizing bilayered, degradable oligo(poly(ethylene glycol) fumarate) hydrogel scaffolds. J Biomed Mater Res A. 2005;75:156-67.

[12] Phillips JE, Burns KL, Le Doux JM, Guldberg RE, García AJ. Engineering graded tissue interfaces. Proc Natl Acad Sci USA. 2008;105:12170-5.

[13] Kolf CM, Cho E, Tuan RS. Biology of adult mesenchymal stem cells: regulation of niche, self-renewal and differentiation. Arthritis Res Ther. 2007;9:204.

[14] Chong AKS, Ang AD, Goh JCH, Hui JHP, Lim AYT, Lee EH, et al. Bone marrow-derived mesenchymal stem cells influence early tendon-healing in a rabbit achilles tendon model. J Bone Joint Surg Am. 2007;89:74-81.

[15] Castano-Izquierdo H, Alvarez-Barreto J, van den Dolder J, Jansen JA, Mikos AG, Sikavitsas VI. Pre-culture period of mesenchymal stem cells in osteogenic media influences their in vivo bone forming potential. J Biomed Mater Res A. 2007;82:129-38.

[16] Farrell E, Both SK, Odörfer KI, Koevoet W, Kops N, O'Brien FJ, et al. In-vivo generation of bone via endochondral ossification by in-vitro chondrogenic priming of adult human and rat mesenchymal stem cells. BMC Musculoskelet Disord. 2011;12:31.

[17] Hashimoto Y, Yoshida G, Toyoda H, Takaoka K. Generation of tendon-to-bone interface “enthesis” with use of recombinant BMP-2 in a rabbit model. J Orthop Res. 2007;25:1415-24.

[18] Rodeo SA, Suzuki K, Deng XH, Wozney J, Warren RF. Use of recombinant human bone morphogenetic protein-2 to enhance tendon healing in a bone tunnel. Am J Sports Med. 1999;27:476-88.

[19] Fiedler J, Röderer G, Günther K-P, Brenner RE. BMP-2, BMP-4, and PDGF-bb stimulate chemotactic migration of primary human mesenchymal progenitor cells. J Cell Biochem. 2002;87:305-12.

[20] Lind M, Eriksen EF, Bünger C. Bone morphogenetic protein-2 but not bone morphogenetic protein-4 and -6 stimulates chemotactic migration of human osteoblasts, human marrow osteoblasts, and U2-OS cells. Bone. 1996;18:53-7.

[21] Noël D, Gazit D, Bouquet C, Apparailly F, Bony C, Plence P, et al. Short-term BMP-2 expression is sufficient for in vivo osteochondral differentiation of mesenchymal stem cells. Stem Cells. 2004;22:74-85.

[22] Rauch C, Brunet AC, Deleule J, Farge E. C2C12 myoblast/osteoblast transdifferentiation steps enhanced by epigenetic inhibition of BMP2 endocytosis. Am J Physiol Cell Physiol. 2002;283:C235-C43.

[23] Rickard DJ, Sullivan TA, Shenker BJ, Leboy PS, Kazhdan I. Induction of rapid osteoblast differentiation in rat bone marrow stromal cell cultures by dexamethasone and BMP-2. Dev Biol. 1994;161:218-28.

[24] Yamaguchi A, Katagiri T, Ikeda T, Wozney JM, Rosen V, Wang EA, et al. Recombinant human bone morphogenetic protein-2 stimulates osteoblastic maturation and inhibits myogenic differentiation in vitro. J Cell Biol. 1991;113:681-7.

[25] Beitzel K, McCarthy MBR, Cote MP, Durant TJS, Chowaniec DM, Solovyova O, et al. Comparison of mesenchymal stem cells (osteoprogenitors) harvested from proximal humerus and distal femur during arthroscopic surgery. Arthroscopy. 2013;29:301-8.

[26] Uhthoff HK, Trudel G, Himori K. Relevance of pathology and basic research to the surgeon treating rotator cuff disease. J Orthop Sci. 2003;8:449-56.

[27] Carragee EJ, Hurwitz EL, Weiner BK. A critical review of recombinant human bone morphogenetic protein-2 trials in spinal surgery: emerging safety concerns and lessons learned. Spine J. 2011;11:471-91.

[28] Laub M, Chatzinikolaidou M, Jennissen HP. Aspects of BMP-2 binding to receptors and collagen: Influence of cell senescence on receptor binding and absence of high-affinity stoichiometric binding to collagen. Mat-wiss u Werkstofftech. 2007;38:1019-26.

[29] Shields LBE, Raque GH, Glassman SD, Campbell M, Vitaz T, Harpring J, et al. Adverse effects associated with high-dose recombinant human bone morphogenetic protein-2 use in anterior cervical spine fusion. Spine. 2006;31:542-7.

[30] Capila I, Linhardt RJ. Heparin-protein interactions. Angew Chem Int Ed 2002;41:391-412.

[31] Schlessinger J, Plotnikov AN, Ibrahimi OA, Eliseenkova AV, Yeh BK, Yayon A, et al. Crystal structure of a ternary FGF-FGFR-heparin complex reveals a dual role for heparin in FGFR binding and dimerization. Mol Cell. 2000;6:743-50.

[32] Nakaoka R, Hsiong SX, Mooney DJ. Regulation of chondrocyte differentiation level via co-culture with osteoblasts. Tissue Eng. 2006;12:2425-33.

[33] Richardson SM, Walker RV, Parker S, Rhodes NP, Hunt JA, Freemont AJ, et al. Intervertebral disc cell-mediated mesenchymal stem cell differentiation. Stem Cells. 2006;24:707-16.

[34] Benoit DSW, Collins SD, Anseth KS. Multifunctional hydrogels that promote osteogenic hMSC differentiation through stimulation and sequestering of BMP2. Adv Funct Mater. 2007;17:2085-93.

[35] Caplan AI. Adult mesenchymal stem cells for tissue engineering versus regenerative medicine. J Cell Physiol. 2007;213:341-7.

[36] Urban JPG, Roberts S. Degeneration of the intervertebral disc. Arthritis Res Ther. 2003;5:120-30.

[37] Nakamura S, Ishihara M, Obara K, Masuoka K, Ishizuka T, Kanatani Y, et al. Controlled release of fibroblast growth factor-2 from an injectable 6-O-desulfated heparin hydrogel and subsequent effect on in vivo vascularization J Biomed Mater Res A. 2006;78:364-71.

[38] Taipale J, Keski-Oja J. Growth factors in the extracellular matrix. FASEB J. 1997;11:51-9.

[39] Costa AG, Cusano NE, Silva BC, Cremers S, Bilezikian JP. Cathepsin K: its skeletal actions and role as a therapeutic target in osteoporosis. Nat Rev Rheumatol. 2011;7:447-56.

[40] Dejica VM, Mort JS, Laverty S, Percival MD, Antoniou J, Zukor DJ, et al. Cleavage of type II collagen by cathepsin K in human osteoarthritic cartilage. The American journal of pathology. 2008;173:161-9.

[41] Li Z, Yasuda Y, Li W, Bogyo M, Katz N, Gordon RE, et al. Regulation of collagenase activities of human cathepsins by glycosaminoglycans. J Biol Chem. 2004;279:5470-9.

[42] Soslowsky LJ, Thomopoulos S, Tun S, Flanagan CL, Keefer CC, Mostow J, et al. Neer Award 1999. Overuse activity injures the supraspinatus tendon in an animal model: A histologic and biomechanical study. J Shoulder Elb Surg. 2000;9:79-84.

[43] Benjamin M, Kaiser E, Milz S. Structure-function relationships in tendons: a review. J Anat. 2008;212:211-28.

[44] Elliott DH. Structure and function of mammalian tendon. Biol Rev. 1965;40:392-421.

[45] Shadwick RE. Elastic energy storage in tendons: Mechanical differences related to function and age. J Appl Physiol. 1990;68:1033-40.

[46] Kannus P. Structure of the tendon connective tissue. Scand J Med Sci Sports. 2000;10:312-20.

[47] Voleti PB, Buckley MR, Soslowsky LJ. Tendon healing: Repair and regeneration. Annu Rev Biomed Eng. 2012;14:47-71.

[48] Józsa L, Lehto M, Kvist M, Bálint JB, Reffy A. Alterations in dry mass content of collagen fibers in degenerative tendinopathy and tendon-rupture. Matrix. 1989;9:140-6.

[49] Kjaer M. Role of extracellular matrix in adaptation of tendon and skeletal muscle to mechanical loading. Physiol Rev. 2004;84:649-98.

[50] Sharma P, Maffulli N. Tendon injury and tendinopathy: Healing and repair. J Bone Joint Surg Am. 2005;87:187-202.

[51] Ritty TM, Ditsios K, Starcher BC. Distribution of the elastic fiber and associated proteins in flexor tendon reflects function. Anat Rec. 2002;268:430-40.

[52] Rosenbloom J, Abrams WR, Mecham RP. Extracellular matrix 4: The elastic fiber. FASEB J. 1993;7:1208-18.

[53] Vogel KG, Heinegård D. Characterization of proteoglycans from adult bovine tendon. J Biol Chem. 1985;260:9298-306.

[54] Danielson KG, Baribault H, Holmes DF, Graham H, Kadler KE, Iozzo RV. Targeted disruption of decorin leads to abnormal collagen fibril morphology and skin fragility. J Cell Biol. 1997;136:729-43.

[55] Derwin KA, Soslowsky LJ, Kimura JH. Proteoglycans and glycosaminoglycan fine structure in the mouse tail tendon fascicle - Derwin - 2006 - Journal of Orthopaedic Research - Wiley Online Library. J Orthopaed Res. 2001.

[56] Yoon JH, Halper J. Tendon proteoglycans: Biochemistry and function. J Musculoskelet Neuronal Interact. 2005;5:22-34.

[57] Robbins JR, Evanko SP, Vogel KG. Mechanical loading and TGF-β regulate proteoglycan synthesis in tendon. Arch Biochem Biophys. 1997;342:203-11.

[58] Hayem G. Tenology: a new frontier. Joint Bone Spine. 2001;68:19-25.

[59] Moore MJ, De Beaux A. A quantitative ultrastructural study of rat tendon from birth to maturity. J Anat. 1987;153:163-9.

[60] McNeilly CM, Banes AJ, Benjamin M, Ralphs JR. Tendon cells in vivo form a three dimensional network of cell processes linked by gap junctions. J Anat. 1996;189:593-600.

[61] Bi Y, Ehirchiou D, Kilts TM, Inkson CA, Embree MC, Sonoyama W, et al. Identification of tendon stem/progenitor cells and the role of the extracellular matrix in their niche. Nat Med. 2007;13:1219-27.

[62] Almekinders LC, Weinhold PS, Maffulli N. Compression etiology in tendinopathy. Clin Sports Med. 2003;22:703-10.

[63] Bruns J, Kampen J, Kahrs J, Plitz W. Achilles tendon rupture: experimental results on spontaneous repair in a sheep-model. Knee Surg Sports Traumatol Arthrosc. 2000;8:364-9.

[64] Mehta S, Gimbel JA, Soslowsky LJ. Etiologic and pathogenetic factors for rotator cuff tendinopathy. Clin Sports Med. 2003;22:791-812.

[65] Wang JH-C, Iosifidis MI, Fu FH. Biomechanical basis for tendinopathy. Clin Orthop Relat Res. 2006;443:320-32.

[66] Selvanetti A, Cipolla M, Puddu G. Overuse tendon injuries: Basic science and classification. Oper Tech Sports Med. 1997;5:110-7.

[67] Bureau of Labor Statistics. Occupational Injuries and Illnesses: Counts, Rates, and Characteristics, 2005. Washington, D.C.: U.S. Department of Labor; 2006.

[68] Bonde JP, Mikkelsen S, Andersen JH, Fallentin N, Baelum J, Svendsen SW, et al. Prognosis of shoulder tendonitis in repetitive work: a follow up study in a cohort of Danish industrial and service workers. Occup Environ Med. 2003;60:E8.

[69] Baldwin ML, Butler RJ. Upper extremity disorders in the workplace: costs and outcomes beyond the first return to work. J Occup Rehabil. 2006;16:296-316.

[70] Silverstein B, Welp E, Nelson N, Kalat J. Claims incidence of work-related disorders of the upper extremities: Washington state, 1987 through 1995. Am J Public Health. 1998;88:1827-33.

[71] Andres BM, Murrell GAC. Treatment of tendinopathy: what works, what does not, and what is on the horizon. Clin Orthop Relat Res. 2008;466:1539-54.

[72] Carpenter JF, Thomopoulos S, Flanagan CL, DeBano CM, Soslowsky LJ. Rotator cuff defect healing: a biomechanical and histologic analysis in an animal model. Journal of Shoulder and Elb Surg. 1998;7:599-605.

[73] Xu Y, Murrell GAC. The basic science of tendinopathy. Clin Orthop Relat Res. 2008;466:1528-38.

[74] Maganaris CN, Narici MV, Almekinders LC, Maffulli N. Biomechanics and pathophysiology of overuse tendon injuries: Ideas on insertional tendinopathy. Sports Med. 2004;34:1005-17.

[75] Benjamin M, Evans EJ, Copp L. The histology of tendon attachments to bone in man. J Anat. 1986;149:89-100.

[76] Yang PJ, Temenoff JS. Engineering orthopedic tissue interfaces. Tissue Eng Part B Rev. 2009;15:127-41.

[77] Clark JM, Harryman DT. Tendons, ligaments, and capsule of the rotator cuff: Gross and microscopic anatomy. J Bone Joint Surg Am. 1992;74:713-25.

[78] Mochizuki T, Sugaya H, Uomizu M, Maeda K, Matsuki K, Sekiya I, et al. Humeral insertion of the supraspinatus and infraspinatus: New anatomical findings regarding the footprint of the rotator cuff. J Bone Joint Surg Am. 2008;90:962-9.

[79] Karas V, Wang VM, Dhawan A, Cole BJ. Biomechanical factors in rotator cuff pathology. Sports Med Arthrosc. 2011;19:202-6.

[80] Kim SY, Boynton EL, Ravichandiran K, Fung LY, Bleakney R, Agur AM. Three-dimensional study of the musculotendinous architecture of supraspinatus and its functional correlations. Clin Anat. 2007;20:648-55.

[81] Bey MJ, Song HK, Wehrli FW, Soslowsky LJ. Intratendinous strain fields of the intact supraspinatus tendon: the effect of glenohumeral joint position and tendon region. J Orthop Res. 2002;20:869-74.

[82] Kettunen JA, Kujala U, Sarna S, Kaprio J. Cumulative incidence of shoulder region tendon injuries in male former elite athletes. Int J Sports Med. 2011;32:451-4.

[83] Sein ML, Walton J, Linklater J, Appleyard R, Kirkbride B, Kuah D, et al. Shoulder pain in elite swimmers: Primarily due to swim-volume-induced supraspinatus tendinopathy. Brit J Sport Med. 2010;44:105-13.

[84] Lewis JS. Rotator cuff tendinopathy. Brit J Sport Med. 2009;43:236-41.

[85] Bank RA, TeKoppele JM, Oostingh G, Hazleman BL, Riley GP. Lysylhydroxylation and non-reducible crosslinking of human supraspinatus tendon collagen: changes with age and in chronic rotator cuff tendinitis. Annals of the Rheumatic Diseases. 1999;58:35-41.

[86] Balke M, Schmidt C, Dedy N, Banerjee M, Bouillon B, Liem D. Correlation of acromial morphology with impingement syndrome and rotator cuff tears. Acta Orthop. 2013;84:178-83.

[87] Neer CS. Anterior acromioplasty for the chronic impingement syndrome in the shoulder: A preliminary report. J Bone Joint Surg Am. 1972;54:41-50.

[88] Nicholson GP, Goodman DA, Flatow EL, Bigliani LU. The acromion: Morphologic condition and age-related changes. A study of 420 scapulas. Journal of shoulder and elbow surgery / American Shoulder and Elbow Surgeons [et al]. 1996;5:1-11.

[89] Burns WC, Whipple TL. Anatomic relationships in the shoulder impingement syndrome. Clin Orthop Relat Res. 1993:96-102.

[90] Nyffeler RW, Werner CML, Sukthankar A, Schmid MR, Gerber C. Association of a large lateral extension of the acromion with rotator cuff tears. J Bone Joint Surg Am. 2006;88:800-5.

[91] Walch G, Boileau P, Noel E, Donell ST. Impingement of the deep surface of the supraspinatus tendon on the posterosuperior glenoid rim: An arthroscopic study. J Shoulder Elbow Surg. 1992;1:238-45.

[92] Ellenbecker TS, Cools A. Rehabilitation of shoulder impingement syndrome and rotator cuff injuries: an evidence-based review. Brit J Sport Med. 2010;44:319-27.

[93] Fu FH, Harner CD, Klein AH. Shoulder Impingement Syndrome: A Critical Review. Clin Orthop Relat Res. 1991;269:162-73.

[94] Kim HM, Dahiya N, Teefey SA, Middleton WD, Stobbs G, Steger-May K, et al. Location and initiation of degenerative rotator cuff tears: an analysis of three hundred and sixty shoulders. J Bone Joint Surg Am. 2010;92:1088-96.

[95] Huang C-Y, Wang VM, Pawluk RJ, Bucchieri JS, Levine WN, Bigliani LU, et al. Inhomogeneous mechanical behavior of the human supraspinatus tendon under uniaxial loading. J Orthop Res. 2005;23:924-30.

[96] Longo UG, Franceschi F, Ruzzini L, Rabitti C, Morini S, Maffulli N, et al. Histopathology of the supraspinatus tendon in rotator cuff tears. Am J Sport Med. 2008;36:533-8.

[97] Järvinen M, Józsa L, Kannus P, Järvinen TL, Kvist M, Leadbetter W. Histopathological findings in chronic tendon disorders. Scand J Med Sci Sports. 1997;7:86-95.

[98] Kannus P, Józsa L. Histopathological changes preceding spontaneous rupture of a tendon: A controlled study of 891 patients. J Bone Joint Surg Am. 1991;73:1507-25.

[99] Archambault JM, Jelinsky SA, Lake SP, Hill AA, Glaser DL, Soslowsky LJ. Rat supraspinatus tendon expresses cartilage markers with overuse. J Orthop Res. 2007;25:617-24.

[100] Attia M, Scott A, Duchesnay A, Carpentier G, Soslowsky LJ, Huynh MB, et al. Alterations of overused supraspinatus tendon: A possible role of glycosaminoglycans and HARP/pleiotrophin in early tendon pathology. Journal of orthopaedic research : official publication of the Orthopaedic Research Society. 2011;30:61-71.

[101] Millar NL, Wei AQ, Molloy TJ, Bonar F, Murrell GAC. Heat shock protein and apoptosis in supraspinatus tendinopathy. Clinical orthopaedics and related research. 2008;466:1569-76.

[102] Szomor Z, Appleyard R, Murrell G. Overexpression of nitric oxide synthases in tendon overuse. J Orthop Res. 2005;24:80-6.

[103] Nobuhara K, Hata Y, Komai M. Surgical procedure and results of repair of massive tears of the rotator cuff. Clin Orthop Relat Res. 1994;304:54-9.

[104] Derwin KA, Baker AR, Spragg RK, Leigh DR, Iannotti JP. Commercial extracellular matrix scaffolds for rotator cuff tendon repair. Biomechanical, biochemical, and cellular properties. J Bone Joint Surg Am. 2006;88:2665-72.

[105] Derwin KA, Baker AR, Iannotti JP, McCarron JA. Preclinical models for translating regenerative medicine therapies for rotator cuff repair. Tissue Eng Part B Rev. 2010;16:21-30.

[106] Kobayashi M, Itoi E, Minagawa H, Miyakoshi N, Takahashi S, Tuoheti Y, et al. Expression of growth factors in the early phase of supraspinatus tendon healing in rabbits. J Shoulder Elb Surg. 2006;15:371-7.

[107] Takahashi T, Muneta T, Tsuji K, Sekiya I. BMP-7 inhibits cartilage degeneration through suppression of inflammation in rat zymosan-induced arthritis. Cell Tissue Res. 2011;344:321-32.

[108] Würgler-Hauri CC, Dourte L, Baradet TC. Temporal expression of 8 growth factors in tendon-to-bone healing in a rat supraspinatus model. J Shoulder Elb Surg. 2007;16:198S-203S.

[109] Chan BP, Fu S-C, Qin L, Lee KM, Rolf CG, Chan K-M. Effects of basic fibroblast growth factor (bFGF) on early stages of tendon healing: A rat patellar tendon model. Acta Orthop. 2000;71:513-8.

[110] Hildebrand KA, Woo SL, Smith DW, Allen CR, Deie M, Taylor BJ, et al. The effects of platelet-derived growth factor-BB on healing of the rabbit medial collateral ligament. An in vivo study. Am J Sports Med. 1998;26:549-54.

[111] Yoshikawa Y, Abrahamsson S-O. Dose-related cellular effects of platelet-derived growth factor-BB differ in various types of rabbit tendons in vitro. Acta Orthop. 2001;72:287-92.

[112] Soslowsky LJ, Carpenter JE, DeBano CM, Banerji I, Moalli MR. Development and use of an animal model for investigations on rotator cuff disease. J Shoulder Elbow Surg. 1996;5:383-92.

[113] Perry SM, McIlhenny SE, Hoffman MC, Soslowsky LJ. Inflammatory and angiogenic mRNA levels are altered in a supraspinatus tendon overuse animal model. J Shoulder Elbow Surg. 2005;14:79S-83S.

[114] Scott A, Cook JL, Hart DA, Walker DC, Duronio V, Khan KM. Tenocyte responses to mechanical loading in vivo: a role for local insulin-like growth factor 1 signaling in early tendinosis in rats. Arthritis Rheum. 2007;56:871-81.

[115] Attia M, Scott A, Duchesnay A, Carpentier G, Soslowsky LJ, Huynh MB, et al. Alterations of overused supraspinatus tendon: A possible role of glycosaminoglycans and HARP/pleiotrophin in early tendon pathology. J Orthop Res. 2011;30:61-71.

[116] Nagase H, Woessner J. Matrix metalloproteinases. J Biol Chem. 1999;274:21491-4.

[117] Nagase H, Visse R, Murphy G. Structure and function of matrix metalloproteinases and TIMPs. Cardiovasc Res. 2006;69:562-73.

[118] Pasternak B, Aspenberg P. Metalloproteinases and their inhibitors-diagnostic and therapeutic opportunities in orthopedics. Acta Orthop. 2009;80:693-703.

[119] Chakraborti S, Mandal M, Das S, Mandal A, Chakraborti T. Regulation of matrix metalloproteinases: an overview. Mol Cell Biochem. 2003;253:269-85.

[120] Chung L, Dinakarpandian D, Yoshida N, Lauer-Fields JL, Fields GB, Visse R, et al. Collagenase unwinds triple-helical collagen prior to peptide bond hydrolysis. EMBO J. 2004;23:3020-30.

[121] Aimes RT, Quigley JP. Matrix metalloproteinase-2 is an interstitial collagenase. Inhibitor-free enzyme catalyzes the cleavage of collagen fibrils and soluble native type I collagen generating the specific 3/4- and 1/4-length fragments. J Biol Chem. 1995;270:5872-6.

[122] Van Meurs J, Van Lent P, Stoop R, Holthuysen A, Singer I, Bayne E, et al. Cleavage of aggrecan at the Asn341-Phe342 site coincides with the initiation of collagen damage in murine antigen-induced arthritis: A pivotal role for stromelysin 1 in matrix metalloproteinase activity. Arthritis Rheum. 1999;42:2074-84.

[123] Riley GP, Curry V, DeGroot J, van El B, Verzijl N, Hazleman BL, et al. Matrix metalloproteinase activities and their relationship with collagen remodelling in tendon pathology. Matrix Biol. 2002;21:185-95.

[124] Riley GP, Harrall RL, Constant CR, Chard MD, Cawston TE, Hazleman BL. Tendon degeneration and chronic shoulder pain: changes in the collagen composition of the human rotator cuff tendons in rotator cuff tendinitis. Ann Rheum Dis. 1994;53:359-66.

[125] Ireland D, Harrall R, Curry V, Holloway G, Hackney R, Hazleman B, et al. Multiple changes in gene expression in chronic human Achilles tendinopathy. Matrix Biol. 2001;20:159-69.

[126] Lo IK, Marchuk LL, Hollinshead R, Hart DA, Frank CB. Matrix metalloproteinase and tissue inhibitor of matrix metalloproteinase mRNA levels are specifically altered in torn rotator cuff tendons. Am J Sports Med. 2004;32:1223-9.

[127] Büth H, Luigi Buttigieg P, Ostafe R, Rehders M, Dannenmann SR, Schaschke N, et al. Cathepsin B is essential for regeneration of scratch-wounded normal human epidermal keratinocytes. Eur J Cell Biol. 2007;86:747-61.

[128] Nakagawa TY, Rudensky AY. The role of lysosomal proteinases in MHC class II-mediated antigen processing and presentation. Immunol Rev. 1999;172:121-9.

[129] Zaidi M, Troen B, Moonga BS, Abe E. Cathepsin K, osteoclastic resorption, and osteoporosis therapy. J Bone Miner Res. 2001;16:1747-9.

[130] Creemers LB, Hoeben KA, Jansen DC, Buttle DJ, Beertsen W, Everts V. Participation of intracellular cysteine proteinases, in particular cathepsin B, in degradation of collagen in periosteal tissue explants. Matrix Biol. 1998;16:575-84.

[131] McGrath ME. The lysosomal cysteine proteases. Annu Rev Biophys Biomol Struct. 1999;28:181-204.

[132] Turk V, Turk B, Guncar G, Turk D, Kos J. Lysosomal cathepsins: Structure, role in antigen processing and presentation, and cancer. Adv Enzyme Regul. 2002;42:285-303.

[133] Jerala R. PH-induced Conformational Transitions of the Propeptide of Human Cathepsin L: A role for a molten globule state in zymogen activation. J Biol Chem. 1998;273:11498-504.

[134] Turk V, Bode W. The cystatins: protein inhibitors of cysteine proteinases. FEBS Lett. 1991;285:213-9.

[135] Kirschke H, Kembhavi AA, Bohley P, Barrett AJ. Action of rat liver cathepsin L on collagen and other substrates. Biochem J. 1982;201:367-72.

[136] Mason RW, Taylor MA, Etherington DJ. The purification and properties of cathepsin L from rabbit liver. Biochem J. 1984;217:209-17.

[137] Bühling F, Gerber A, Häckel C, Krüger S, Köhnlein T, Brömme D, et al. Expression of Cathepsin K in Lung Epithelial Cells. Am J Resp Cell Mol. 1999;20:612-9.

[138] Kafienah W, Brömme D, Buttle DJ, Croucher LJ, Hollander AP. Human cathepsin K cleaves native type I and II collagens at the N-terminal end of the triple helix. Biochem J. 1998;331 (Pt 3):727-32.

[139] Garnero P, Borel O, Byrjalsen I, Ferreras M, Drake FH, McQueney MS, et al. The collagenolytic activity of cathepsin K is unique among mammalian proteinases. J Biol Chem. 1998;273:32347-52.

[140] Thompson AD, Betz MW, Yoon DM, Fisher JP. Osteogenic differentiation of bone marrow stromal cells induced by coculture with chondrocytes encapsulated in three-dimensional matrices. Tissue Eng Part A. 2009;15:1181-90.

[141] Mo XT, Guo SC, Xie HQ, Deng L, Zhi W, Xiang Z, et al. Variations in the ratios of co-cultured mesenchymal stem cells and chondrocytes regulate the expression of cartilaginous and osseous phenotype in alginate constructs. Bone. 2009;45:42-51.

[142] Li X, Lee JP, Balian G, Greg Anderson D. Modulation of chondrocytic properties of fat-derived mesenchymal cells in co-cultures with nucleus pulposus. Connect Tissue Res. 2005;46:75-82.

[143] Varshney RR, Zhou R, Hao J, Yeo SS, Chooi WH, Fan J, et al. Chondrogenesis of synovium-derived mesenchymal stem cells in gene-transferred co-culture system. Biomaterials. 2010;31:6876-91.

[144] Yang HN, Park JS, Na K, Woo DG, Kwon YD, Park KH. The use of green fluorescence gene (GFP)-modified rabbit mesenchymal stem cells (rMSCs) co-cultured

with chondrocytes in hydrogel constructs to reveal the chondrogenesis of MSCs. Biomaterials. 2009;30:6374-85.

[145] Ball SG, Shuttleworth AC, Kielty CM. Direct cell contact influences bone marrow mesenchymal stem cell fate. Int J Biochem Cell Biol. 2004;36:714-27.

[146] Fischer J, Dickhut A, Rickert M, Richter W. Human articular chondrocytes secrete parathyroid hormone-related protein and inhibit hypertrophy of mesenchymal stem cells in coculture during chondrogenesis. Arthritis Rheum. 2010;62:2696-706.

[147] Chen S, Emery SE, Pei M. Coculture of synovium-derived stem cells and nucleus pulposus cells in serum-free defined medium with supplementation of transforming growth factor-beta1: a potential application of tissue-specific stem cells in disc regeneration. Spine (Phila Pa 1976). 2009;34:1272-80.

[148] Heino TJ, Hentunen TA, Vaananen HK. Conditioned medium from osteocytes stimulates the proliferation of bone marrow mesenchymal stem cells and their differentiation into osteoblasts. Exp Cell Res. 2004;294:458-68.

[149] Maxson S, Burg KJ. Conditioned media enhance osteogenic differentiation on poly(L-lactide-co-epsilon-caprolactone)/hydroxyapatite scaffolds and chondrogenic differentiation in alginate. J Biomater Sci Polym Ed. 2010;21:1441-58.

[150] Gerstenfeld LC, Barnes GL, Shea CM, Einhorn TA. Osteogenic differentiation is selectively promoted by morphogenetic signals from chondrocytes and synergized by a nutrient rich growth environment. Connect Tissue Res. 2003;44 Suppl 1:85-91.

[151] Ilmer M, Karow M, Geissler C, Jochum M, Neth P. Human osteoblast-derived factors induce early osteogenic markers in human mesenchymal stem cells. Tissue Eng Part A. 2009;15:2397-409.

[152] Wang Y, Volloch V, Pindrus MA, Blasioli DJ, Chen J, Kaplan DL. Murine osteoblasts regulate mesenchymal stem cells via WNT and cadherin pathways: mechanism depends on cell-cell contact mode. J Tissue Eng Regen Med. 2007;1:39-50.

[153] Civitelli R. Cell-cell communication in the osteoblast/osteocyte lineage. Arch Biochem Biophys. 2008;473:188-92.

[154] Loewenstein WR. Junctional intercellular communication: the cell-to-cell membrane channel. Physiol Rev. 1981;61:829-913.

[155] Schiller PC, Mehta PP, Roos BA, Howard GA. Hormonal regulation of intercellular communication: parathyroid hormone increases connexin 43 gene expression and gap-junctional communication in osteoblastic cells. Mol Endocrinol. 1992;6:1433-40.

[156] Civitelli R, Beyer EC, Warlow PM, Robertson AJ, Geist ST, Steinberg TH. Connexin43 mediates direct intercellular communication in human osteoblastic cell networks. J Clin Invest. 1993;91:1888-96.

[157] Zhou H, Mak W, Zheng Y, Dunstan CR, Seibel MJ. Osteoblasts directly control lineage commitment of mesenchymal progenitor cells through Wnt signaling. J Biol Chem. 2008;283:1936-45.

[158] Macias D, Ganan Y, Sampath TK, Piedra ME, Ros MA, Hurle JM. Role of BMP-2 and OP-1 (BMP-7) in programmed cell death and skeletogenesis during chick limb development. Development. 1997;124:1109-17.

[159] Urist MR. Bone: Formation by autoinduction. Science. 1965;150:893-9.

[160] Wozney JM. Overview of bone morphogenetic proteins. Spine. 2002;27:S2-S8.

[161] Kübler NR, Reuther JF, Faller G, Kirchner T, Ruppert R, Sebald W. Inductive properties of recombinant human BMP-2 produced in a bacterial expression system. Int J Oral Maxillofac Surg. 1998;27:305-9.

[162] Wang EA, Rosen V, D'Alessandro JS, Bauduy M, Cordes P, Harada T, et al. Recombinant human bone morphogenetic protein induces bone formation. Proc Natl Acad Sci USA. 1990;87:2220-4.

[163] Tsuji K, Bandyopadhyay A, Harfe BD, Cox K, Kakar S, Gerstenfeld L, et al. BMP2 activity, although dispensable for bone formation, is required for the initiation of fracture healing. Nat Genet. 2006;38:1424-9.

[164] Duprez D, Bell EJ, Richardson MK, Archer CW, Wolpert L, Brickell PM, et al. Overexpression of BMP-2 and BMP-4 alters the size and shape of developing skeletal elements in the chick limb. Mech Dev. 1996;57:145-57.

[165] Bostrom MP. Expression of bone morphogenetic proteins in fracture healing. Clin Orthop Relat Res. 1998:S116-23.

[166] Scheufler C, Sebald W, Hulsmeyer M. Crystal structure of human bone morphogenetic protein-2 at 2.7 A resolution. J Mol Biol. 1999;287:103-15.

[167] Gilde F, Maniti O, Guillot R, Mano JF, Logeart-Avramoglou D, Sailhan F, et al. Secondary structure of rhBMP-2 in a protective biopolymeric carrier material. Biomacromolecules. 2012;13:3620-6.

[168] Ruppert R, Hoffmann E, Sebald W. Human bone morphogenetic protein 2 contains a heparin-binding site which modifies its biological activity. Eur J Biochem. 1996;237:295-302.

[169] Koenig BB, Cook JS, Wolsing DH, Ting J, Tiesman JP, Correa PE, et al. Characterization and cloning of a receptor for BMP-2 and BMP-4 from NIH 3T3 cells. Mol Cell Biol. 1994;14:5961-74.

[170] Nishimura R, Kato Y, Chen D, Harris SE, Mundy GR, Yoneda T. Smad5 and DPC4 are key molecules in mediating BMP-2-induced osteoblastic differentiation of the pluripotent mesenchymal precursor cell line C2C12. J Biol Chem. 1998;273:1872-9.

[171] Groppe J, Greenwald J, Wiater E, Rodriguez-Leon J, Economides AN, Kwiatkowski W, et al. Structural basis of BMP signalling inhibition by the cystine knot protein Noggin. Nature. 2002;420:636-42.

[172] Burkus JK, Transfeldt EE, Kitchel SH, Watkins RG, Balderston RA. Clinical and Radiographic Outcomes of Anterior Lumbar Interbody Fusion Using Recombinant Human Bone Morphogenetic Protein-2. Spine. 2002;27:2396.

[173] McKay WF, Peckham SM, Badura JM. A comprehensive clinical review of recombinant human bone morphogenetic protein-2 (INFUSE® Bone Graft). Int Orthop. 2007;31:729-34.

[174] Zhao B, Katagiri T, Toyoda H, Takada T, Yanai T, Fukuda T, et al. Heparin potentiates the in vivo ectopic bone formation induced by bone morphogenetic protein-2. J Biol Chem. 2006;281:23246-53.

[175] Neovius E, Lemberger M, Docherty Skogh AC, Hilborn J, Engstrand T. Alveolar bone healing accompanied by severe swelling in cleft children treated with bone morphogenetic protein-2 delivered by hydrogel. J Plast Reconstr Aesthet Surg. 2013;66:37-42.

[176] Yu Y, Bliss JP, Bruce WJM, Walsh WR. Bone morphogenetic proteins and Smad expression in ovine tendon-bone healing. Arthroscopy. 2007;23:205-10.

[177] Scheufler C, Sebald W, Hülsmeyer M. Crystal structure of human bone morphogenetic protein-2 at 2.7 A resolution. J Mol Biol. 1999;287:103-15.

[178] Esko JD, Lindahl U. Molecular diversity of heparan sulfate. J Clin Invest. 2001;108:169-73.

[179] Mulloy B, Forster MJ, Jones C, Drake AF, Johnson EA, Davies DB. The effect of variation of substitution on the solution conformation of heparin: a spectroscopic and molecular modelling study. Carbohydr Res. 1994;255:1-26.

[180] Hirsh J, Anand SS, Halperin JL, Fuster V. Mechanism of action and pharmacology of unfractionated heparin. Arterioscler Thromb Vasc Biol. 2001;21:1094-6.

[181] Miller T, Goude MC, McDevitt TC, Temenoff JS. Molecular engineering of glycosaminoglycan chemistry for biomolecule delivery. Acta Biomater. 2013; Advance online publication.

[182] Casu B, Choay J, Ferro DR, Gatti G, Jacquinet JC, Petitou M, et al. Controversial glycosaminoglycan conformations. Nature. 1986;322:215-6.

[183] Ferro DR, Provasoli A, Ragazzi M, Torri G, Casu B, Gatti G, et al. Evidence for conformational equilibrium of the sulfated L-iduronate residue in heparin and in synthetic heparin mono- and oligo-saccharides: NMR and force-field studies. J Am Chem Soc. 1986;108:6773-8.

[184] Riesenfeld J, Roden L. Quantitative analysis of N-sulfated, N-acetylated, and unsubstituted glucosamine amino groups in heparin and related polysaccharides. Anal Biochem. 1990;188:383-9.

[185] Humphries DE, Wong GW, Friend DS, Gurish MF, Qiu WT, Huang C, et al. Heparin is essential for the storage of specific granule proteases in mast cells. Nature. 1999;400:769-72.

[186] Nelson RM, Cecconi O, Roberts WG, Aruffo A, Linhardt RJ, Bevilacqua MP. Heparin oligosaccharides bind L- and P-selectin and inhibit acute inflammation. Blood. 1993;82:3253-8.

[187] Sasisekharan R, Venkataraman G. Heparin and heparan sulfate: Biosynthesis, structure and function. Curr Opin Chem Biol. 2000;4:626-31.

[188] Zhang L, David G, Esko JD. Repetitive Ser-Gly sequences enhance heparan sulfate assembly in proteoglycans. J Biol Chem. 1995;270:27127-35.

[189] Tas J, Geenen LH. Microspectrophotometric detection of heparin in mast cells and basophilic granulocytes stained metachromatically with Toluidine Blue O. Histochem J. 1975;7:231-48.

[190] Rosenberg RD, Damus PS. The purification and mechanism of action of human antithrombin-heparin cofactor. J Biol Chem. 1973;248:6490-505.

[191] Choay J, Lormeau J-C, Petitou M, Sinaÿ P, Fareed J. Structural studies on a biologically active hexasaccharide obtained from heparin. Ann NY Acad Sci. 1981;370:644-9.

[192] Choay J, Petitou M, Lormeau JC, Sinaÿ P, Casu B, Gatti G. Structure-activity relationship in heparin: A synthetic pentasaccharide with high affinity for antithrombin III and eliciting high anti-factor Xa activity. Biochem Biophys Res Commun. 1983;116:492-9.

[193] Hricovíni M, Guerrini M, Bisio A, Torri G, Naggi A, Casu B. Active conformations of glycosaminoglycans. NMR determination of the conformation of

heparin sequences complexed with antithrombin and fibroblast growth factors in solution. Semin Thromb Hemost. 2002;28:325-34.

[194] Thunberg L, Bäckström G, Lindahl U. Further characterization of the antithrombin-binding sequence in heparin. Carbohydr Res. 1982;100:393-410.

[195] Brown KJ, Hendry IA, Parish CR. Acidic and basic fibroblast growth factor bind with differing affinity to the same heparan sulfate proteoglycan on BALB/c 3T3 cells: implications for potentiation of growth factor action by heparin. J Cell Biochem. 1995;58:6-14.

[196] DiGabriele AD, Lax I, Chen DI, Svahn CM, Jaye M, Schlessinger J, et al. Structure of a heparin-linked biologically active dimer of fibroblast growth factor. Nature. 1998;393:812-7.

[197] Faham S, Hileman RE, Fromm JR, Linhardt RJ, Rees DC. Heparin structure and interactions with basic fibroblast growth factor. Science. 1996;271:1116-20.

[198] Margalit H, Fischer N, Ben-Sasson SA. Comparative analysis of structurally defined heparin binding sequences reveals a distinct spatial distribution of basic residues. J Biol Chem. 1993;268:19228-31.

[199] Lundin L, Larsson H, Kreuger J, Kanda S, Lindahl U, Salmivirta M, et al. Selectively desulfated heparin inhibits fibroblast growth factor-induced mitogenicity and angiogenesis. J Biol Chem. 2000;275:24653-60.

[200] Ishihara M, Kariya Y, Kikuchi H, Minamisawa T, Yoshida K. Importance of 2-O-sulfate groups of uronate residues in heparin for activation of FGF-1 and FGF-2. J Biochem-Tokyo. 1997;121:345-9.

[201] Uniewicz KA, Ori A, Xu R, Ahmed Y, Wilkinson MC, Fernig DG, et al. Differential scanning fluorimetry measurement of protein stability changes upon binding to glycosaminoglycans: A screening test for binding specificity. Anal Chem. 2010;82:3796-802.

[202] Spivak-Kroizman T, Lemmon MA, Dikic I, Ladbury JE, Pinchasi D, Huang J, et al. Heparin-induced oligomerization of FGF molecules is responsible for FGF receptor dimerization, activation, and cell proliferation. Cell. 1994;79:1015-24.

[203] Harmer NJ, Robinson CJ, Adam LE, Ilag LL, Robinson CV, Gallagher JT, et al. Multimers of the fibroblast growth factor (FGF)-FGF receptor-saccharide complex are formed on long oligomers of heparin. Biochem J. 2006;393:741-8.

[204] Ornitz DM, Yayon A, Flanagan JG, Svahn CM, Levi E, Leder P. Heparin is required for cell-free binding of basic fibroblast growth factor to a soluble receptor and for mitogenesis in whole cells. Mol Cell Biol. 1992;12:240-7.

[205] Gospodarowicz D, Cheng J. Heparin protects basic and acidic FGF from inactivation. J Cell Physiol. 1986;128:475-84.

[206] Mueller SN, Thomas KA, Salvo JD, Levine EM. Stabilization by heparin of acidic fibroblast growth factor mitogenicity for human endothelial cells in vitro. J Cell Physiol. 1989;140:439-48.

[207] Tardieu M, Gamby C, Avramoglou T, Jozefonvicz J, Barritault D. Derivatized dextrans mimic heparin as stabilizers, potentiators, and protectors of acidic or basic FGF. J Cell Physiol. 1992;150:194-203.

[208] Sommer A, Rifkin DB. Interaction of heparin with human basic fibroblast growth factor: Protection of the angiogenic protein from proteolytic degradation by a glycosaminoglycan. J Cell Physiol. 1989;138:215-20.

[209] Higashiyama S, Abraham JA, Miller J, Fiddes JC, Klagsbrun M. A heparin-binding growth factor secreted by macrophage-like cells that is related to EGF. Science. 1991;251:936-9.

[210] Jiao X, Billings PC, O'Connell MP, Kaplan FS, Shore EM, Glaser DL. Heparan sulfate proteoglycans (HSPGs) modulate BMP2 osteogenic bioactivity in C2C12 cells. J Biol Chem. 2007;282:1080-6.

[211] Nairn AV, Kinoshita-Toyoda A, Toyoda H, Xie J, Harris K, Dalton S, et al. Glycomics of proteoglycan biosynthesis in murine embryonic stem cell differentiation. J Proteome Res. 2007;6:4374-87.

[212] Johnson CE, Crawford BE, Stavridis M, Ten Dam G, Wat AL, Rushton G, et al. Essential alterations of heparan sulfate during the differentiation of embryonic stem cells to Sox1-enhanced green fluorescent protein-expressing neural progenitor cells. Stem Cells. 2007;25:1913-23.

[213] Jackson RA, McDonald MM, Nurcombe V, Little DG, Cool SM. The use of heparan sulfate to augment fracture repair in a rat fracture model. J Orthop Res. 2006;24:636-44.

[214] Jackson RA, Murali S, van Wijnen AJ, Stein GS, Nurcombe V, Cool SM. Heparan sulfate regulates the anabolic activity of MC3T3-E1 preosteoblast cells by induction of Runx2. J Cell Physiol. 2007;210:38-50.

[215] Manton KJ, Leong DF, Cool SM, Nurcombe V. Disruption of heparan and chondroitin sulfate signaling enhances mesenchymal stem cell-derived osteogenic differentiation via bone morphogenetic protein signaling pathways. Stem Cells. 2007;25:2845-54.

[216] Haupt LM, Murali S, Mun FK, Teplyuk N, Mei LF, Stein GS, et al. The heparan sulfate proteoglycan (HSPG) glypican-3 mediates commitment of MC3T3-E1 cells toward osteogenesis. J Cell Physiol. 2009;220:780-91.

[217] Cool SM, Nurcombe V. Heparan sulfate regulation of progenitor cell fate. J Cell Biochem. 2006;99:1040-51.

[218] Mathews S, Mathew SA, Gupta PK, Bhonde R, Totey S. Glycosaminoglycans enhance osteoblast differentiation of bone marrow derived human mesenchymal stem cells. J Tissue Eng Regen Med. 2014;8:143-52.

[219] Yang L, Butcher M, Simon RR, Osip SL, Shaughnessy SG. The effect of heparin on osteoblast differentiation and activity in primary cultures of bovine aortic smooth muscle cells. Atherosclerosis. 2005;179:79-86.

[220] Bhandari M, Hirsh J, Weitz JI, Young E, Venner TJ, Shaughnessy SG. The effects of standard and low molecular weight heparin on bone nodule formation in vitro. Thromb Haemost. 1998;80:413-7.

[221] Boddohi S, Killingsworth CE, Kipper MJ. Polyelectrolyte multilayer assembly as a function of pH and ionic strength using the polysaccharides chitosan and heparin. Biomacromolecules. 2008;9:2021-8.

[222] Crouzier T, Ren K, Nicolas C, Roy C, Picart C. Layer-by-layer films as a biomimetic reservoir for rhBMP-2 delivery: controlled differentiation of myoblasts to osteoblasts. Small. 2009;5:598-608.

[223] Almodóvar J, Bacon S, Gogolski J, Kisiday JD, Kipper MJ. Polysaccharide-based polyelectrolyte multilayer surface coatings can enhance mesenchymal stem cell response to adsorbed growth factors. Biomacromolecules. 2010.

[224] Cooper CL, Dubin PL, Kayitmazer AB, Turksen S. Polyelectrolyte–protein complexes. Curr Opin Colloid Interface Sci. 2005;10:52-78.

[225] Chu H, Gao J, Chen C-W, Huard J, Wang Y. Injectable fibroblast growth factor-2 coacervate for persistent angiogenesis. Proc Natl Acad Sci USA. 2011;108:13444-9.

[226] Chu H, Johnson NR, Mason NS, Wang Y. A [polycation:heparin] complex releases growth factors with enhanced bioactivity. J Controlled Release. 2011;150:157-63.

[227] Sakiyama-Elbert SE, Hubbell JA. Development of fibrin derivatives for controlled release of heparin-binding growth factors. J Control Release. 2000;65:389-402.

[228] Manning CN, Kim HM, Sakiyama-Elbert S, Galatz LM, Havlioglu N, Thomopoulos S. Sustained delivery of transforming growth factor beta three enhances tendon-to-bone healing in a rat model. J Orthop Res. 2011;29:1099-105.

[229] Ifkovits JL, Burdick JA. Review: Photopolymerizable and degradable biomaterials for tissue engineering applications. Tissue Eng. 2007;13:2369-85.

[230] Lee KY, Mooney DJ. Hydrogels for tissue engineering. Chem Rev. 2001;101:1869-79.

[231] Baldwin AD, Robinson KG, Militar JL, Derby CD, Kiick KL, Akins J, Robert E. In situ crosslinkable heparin-containing poly(ethylene glycol) hydrogels for sustained anticoagulant release. J Biomed Mater Res A. 2012;100A:2106-18.

[232] Benoit DSW, Anseth KS. Heparin functionalized PEG gels that modulate protein adsorption for hMSC adhesion and differentiation. Acta Biomater. 2005;1:461-70.

[233] Cai S, Liu Y, Zheng Shu X, Prestwich GD. Injectable glycosaminoglycan hydrogels for controlled release of human basic fibroblast growth factor. Biomaterials. 2005;26:6054-67.

[234] Ishihara M, Shaklee PN, Yang Z, Liang W, Wei Z, Stack RJ, et al. Structural features in heparin which modulate specific biological activities mediated by basic fibroblast growth factor. Glycobiology. 1994;4:451-8.

[235] Kim M, Lee JY, Jones CN, Revzin A, Tae G. Heparin-based hydrogel as a matrix for encapsulation and cultivation of primary hepatocytes. Biomaterials. 2010;31:3596-603.

[236] Benhardt H, Cosgriff-Hernandez E. The Role of Mechanical Loading in Ligament Tissue Engineering. Tissue Eng Part B Rev. 2009;15:467-75.

[237] Zhou XZ, Leung VY, Dong QR, Cheung KM, Chan D, Lu WW. Mesenchymal stem cell-based repair of articular cartilage with polyglycolic acid-hydroxyapatite biphasic scaffold. Int J Artif Organs. 2008;31:480-9.

[238] Mauney JR, Volloch V, Kaplan DL. Role of adult mesenchymal stem cells in bone tissue engineering applications: current status and future prospects. Tissue Eng. 2005;11:787-802.

[239] Kolf CM, Cho E, Tuan RS. Mesenchymal stromal cells. Biology of adult mesenchymal stem cells: regulation of niche, self-renewal and differentiation. Arthritis Res Ther. 2007;9:204-14.

[240] Pittenger MF, Mackay AM, Beck SC, Jaiswal RK, Douglas R, Mosca JD, et al. Multilineage potential of adult human mesenchymal stem cells. Science. 1999;284:143-7.

[241] Hahn J-Y, Cho H-J, Kang H-J, Kim T-S, Kim M-H, Chung J-H, et al. Pre-treatment of mesenchymal stem cells with a combination of growth factors enhances gap junction formation, cytoprotective effect on cardiomyocytes, and therapeutic efficacy for myocardial infarction. J Am Coll Cardiol. 2008;51:933-43.

[242] Farrell E, Both SK, Odörfer KI, Koevoet W, Kops N, O'Brien FJ, et al. In-vivo generation of bone via endochondral ossification by in-vitro chondrogenic priming of adult human and rat mesenchymal stem cells. BMC Musculoskelet Disord. 2011;12:31-9.

[243] Castano-Izquierdo H, Alvarez-Barreto J, van den Dolder J, Jansen JA, Mikos AG, Sikavitsas VI. Pre-culture period of mesenchymal stem cells in osteogenic media influences their in vivo bone forming potential. J Biomed Mater Res A. 2007;82:129-38.

[244] Chung C, Burdick JA. Influence of three-dimensional hyaluronic acid microenvironments on mesenchymal stem cell chondrogenesis. Tissue Eng Part A. 2009;15:243-54.

[245] Wei A, Chung SA, Tao H, Brisby H, Lin Z, Shen B, et al. Differentiation of rodent bone marrow mesenchymal stem cells into intervertebral disc-like cells following coculture with rat disc tissue. Tissue Eng Part A. 2009;15:2581-95.

[246] Richardson SM, Walker RV, Parker S, Rhodes NP, Hunt JA, Freemont AJ, et al. Intervertebral disc cell-mediated mesenchymal stem cell differentiation. Stem Cells. 2006;24:707-16.

[247] Capila I, Linhardt RJ. Heparin-protein interactions. Angew Chem Int Ed Engl. 2002;41:391-412.

[248] Mitsi M, Forsten-Williams K, Gopalakrishnan M, Nugent MA. A catalytic role of heparin within the extracellular matrix. J Biol Chem. 2008;283:34796-807.

[249] Zhao B, Katagiri T, Toyoda H, Takada T, Yanai T, Fukuda T, et al. Heparin potentiates the in vivo ectopic bone formation induced by bone morphogenetic protein-2. J Biol Chem. 2006;281:23246-53.

[250] Dombrowski C, Song SJ, Chuan P, Lim X, Susanto E, Sawyer AA, et al. Heparan sulfate mediates the proliferation and differentiation of rat mesenchymal stem cells. Stem Cells Dev. 2009;18:661-70.

[251] Benoit DS, Durney AR, Anseth KS. The effect of heparin-functionalized PEG hydrogels on three-dimensional human mesenchymal stem cell osteogenic differentiation. Biomaterials. 2007;28:66-77.

[252] Choi WI, Kim M, Tae G, Kim YH. Sustained release of human growth hormone from heparin-based hydrogel. Biomacromolecules. 2008;9:1698-704.

[253] Tsurkan MV, Chwalek K, Levental KR, Freudenberg U, Werner C. Modular StarPEG-Heparin Gels with Bifunctional Peptide Linkers. Macromol Rapid Commun. 2010;31:1529-33.

[254] Tsurkan MV, Levental KR, Freudenberg U, Werner C. Enzymatically degradable heparin-polyethylene glycol gels with controlled mechanical properties. Chem Commun (Camb). 2010;46:1141-3.

[255] Cai S, Liu Y, Zheng Shu X, Prestwich GD. Injectable glycosaminoglycan hydrogels for controlled release of human basic fibroblast growth factor. Biomaterials. 2005;26:6054-67.

[256] Raimondi MT. Engineered tissue as a model to study cell and tissue function from a biophysical perspective. Curr Drug Discov Technol. 2006;3:245-68.

[257] Hahn MS, Taite LJ, Moon JJ, Rowland MC, Ruffino KA, West JL. Photolithographic patterning of polyethylene glycol hydrogels. Biomaterials. 2006;27:2519-24.

[258] Jo S, Shin H, Shung AK, John P. Fisher a, Mikos AG. Synthesis and Characterization of Oligo(poly(ethylene glycol) fumarate) Macromer. Macromolecules. 2001;34:2839-44.

[259] Shin H, Jo S, Mikos AG. Modulation of marrow stromal osteoblast adhesion on biomimetic oligo[poly(ethylene glycol) fumarate] hydrogels modified with Arg-Gly-Asp peptides and a poly(ethyleneglycol) spacer. J Biomed Mater Res. 2002;61:169-79.

[260] Park YD, Tirelli N, Hubbell JA. Photopolymerized hyaluronic acid-based hydrogels and interpenetrating networks. Biomaterials. 2003;24:893-900.

[261] Sekiya I, Larson BL, Smith JR, Pochampally R, Cui J-G, Prockop DJ. Expansion of human adult stem cells from bone marrow stroma: conditions that maximize the yields of early progenitors and evaluate their quality. Stem Cells. 2002;20:530-41.

[262] Chen WH, Lai MT, Wu AT, Wu CC, Gelovani JG, Lin CT, et al. In vitro stage-specific chondrogenesis of mesenchymal stem cells committed to chondrocytes. Arthritis Rheum. 2009;60:450-9.

[263] Temenoff JS, Park H, Jabbari E, Conway DE, Sheffield TL, Ambrose CG, et al. Thermally cross-linked oligo(poly(ethylene glycol) fumarate) hydrogels support osteogenic differentiation of encapsulated marrow stromal cells in vitro. Biomacromolecules. 2004;5:5-10.

[264] Henke M, Brandl F, Goepferich AM, Tessmar JK. Size-dependent release of fluorescent macromolecules and nanoparticles from radically cross-linked hydrogels. Eur J Pharm Biopharm. 2010;74:184-92.

[265] Temenoff JS, Athanasiou KA, LeBaron RG, Mikos AG. Effect of poly(ethylene glycol) molecular weight on tensile and swelling properties of oligo(poly(ethylene glycol) fumarate) hydrogels for cartilage tissue engineering. J Biomed Mater Res. 2002;59:429-37.

[266] Hammoudi TM, Lu H, Temenoff JS. Long-term spatially defined coculture within three-dimensional photopatterned hydrogels. Tissue Eng Part C Methods. 2010;16:1621-8.

[267] Hayami JW, Surrao DC, Waldman SD, Amsden BG. Design and characterization of a biodegradable composite scaffold for ligament tissue engineering. J Biomed Mater Res A. 2010;92:1407-20.

[268] Lei Y, Gojgini S, Lam J, Segura T. The spreading, migration and proliferation of mouse mesenchymal stem cells cultured inside hyaluronic acid hydrogels. Biomaterials. 2011;32:39-47.

[269] Varghese S, Hwang NS, Canver AC, Theprungsirikul P, Lin DW, Elisseeff J. Chondroitin sulfate based niches for chondrogenic differentiation of mesenchymal stem cells. Matrix Biol. 2008;27:12-21.

[270] Canal T, Peppas NA. Correlation between mesh size and equilibrium degree of swelling of polymeric networks. J Biomed Mater Res. 1989;23:1183-93.

[271] Park H, Guo X, Temenoff JS, Tabata Y, Caplan AI, Kasper FK, et al. Effect of Swelling Ratio of Injectable Hydrogel Composites on Chondrogenic Differentiation of Encapsulated Rabbit Marrow Mesenchymal Stem Cells In Vitro. Biomacromolecules. 2009;10:541-6.

[272] Rawadi G, Vayssière B, Dunn F, Baron R, Roman-Roman S. BMP-2 controls alkaline phosphatase expression and osteoblast mineralization by a Wnt autocrine loop. J Bone Miner Res. 2003;18:1842-53.

[273] Chen D, Zhao M, Mundy GR. Bone morphogenetic proteins. Growth Factors. 2004;22:233-41.

[274] Xiao G, Gopalakrishnan R, Jiang D, Reith E, Benson MD, Franceschi RT. Bone morphogenetic proteins, extracellular matrix, and mitogen-activated protein kinase signaling pathways are required for osteoblast-specific gene expression and differentiation in MC3T3-E1 cells. J Bone Miner Res. 2002;17:101-10.

[275] Lin H, Zhao Y, Sun W, Chen B, Zhang J, Zhao W, et al. The effect of crosslinking heparin to demineralized bone matrix on mechanical strength and specific binding to human bone morphogenetic protein-2. Biomaterials. 2008;29:1189-97.

[276] Thimm BW, Wust S, Hofmann S, Hagenmuller H, Muller R. Initial cell pre-cultivation can maximize ECM mineralization by human mesenchymal stem cells on silk fibroin scaffolds. Acta Biomater. 2011;7:2218-28.

[277] Nuttelman CR, Tripodi MC, Anseth KS. In vitro osteogenic differentiation of human mesenchymal stem cells photoencapsulated in PEG hydrogels. J Biomed Mater Res A. 2004;68:773-82.

[278] Bellows CG, Heersche JN, Aubin JE. Inorganic phosphate added exogenously or released from beta-glycerophosphate initiates mineralization of osteoid nodules in vitro. Bone Miner. 1992;17:15-29.

[279] Yao KL, Todescan R, Sodek J. Temporal changes in matrix protein synthesis and mRNA expression during mineralized tissue formation by adult rat bone marrow cells in culture. J Bone Miner Res. 1994;9:231-40.

[280] Chum ZZ, Woodruff MA, Cool SM, Hutmacher DW. Porcine bone marrow stromal cell differentiation on heparin-adsorbed poly(e-caprolactone)-tricalcium phosphate-collagen scaffolds. Acta Biomater. 2009;5:3305-15.

[281] Hausser HJ, Brenner RE. Low doses and high doses of heparin have different effects on osteoblast-like Saos-2 cells in vitro. J Cell Biochem. 2004;91:1062-73.

[282] Shibata Y, Abiko Y, Goto K, Moriya Y, Takiguchi H. Heparin stimulates the collagen synthesis in mineralized cultures of the osteoblast-like cell line, MC3T3-E1. Biochem Int. 1992;28:335-44.

[283] Moursi AM, Damsky CH, Lull J, Zimmerman D, Doty SB, Aota S, et al. Fibronectin regulates calvarial osteoblast differentiation. J Cell Sci. 1996;109 (Pt 6):1369-80.

[284] Gigli M, Consonni A, Ghiselli G, Rizzo V, Naggi A, Torri G. Heparin binding to human plasma low-density lipoproteins: dependence on heparin sulfation degree and chain length. Biochemistry. 1992;31:5996-6003.

[285] Lieleg O, Baumgärtel RM, Bausch AR. Selective filtering of particles by the extracellular matrix: an electrostatic bandpass. Biophys J. 2009;97:1569-77.

[286] Thorne RG, Lakkaraju A, Rodriguez-Boulan E, Nicholson C. In vivo diffusion of lactoferrin in brain extracellular space is regulated by interactions with heparan sulfate. Proc Natl Acad Sci USA. 2008;105:8416-21.

[287] Mauney JR, Kirker-Head C, Abrahamson L, Gronowicz G, Volloch V, Kaplan DL. Matrix-mediated retention of in vitro osteogenic differentiation potential and in vivo bone-forming capacity by human adult bone marrow-derived mesenchymal stem cells during ex vivo expansion. J Biomed Mater Res A. 2006;79:464-75.

[288] Kobayashi T, Lyons KM, McMahon AP, Kronenberg HM. BMP signaling stimulates cellular differentiation at multiple steps during cartilage development. Proc Natl Acad Sci U S A. 2005;102:18023-7.

[289] Kay R, Wong KS, Yu YL, Chan YW, Tsoi TH, Ahuja AT, et al. Low-molecular-weight heparin for the treatment of acute ischemic stroke. N Engl J Med. 1995;333:1588-94.

[290] Inoue Y, Nagasawa K. Selective N-desulfation of heparin with dimethyl sulfoxide containing water or methanol Carbohydr Res. 1976;46:87-95.

[291] Nakamura S, Ishihara M, Obara K, Masuoka K, Ishizuka T, Kanatani Y, et al. Controlled release of fibroblast growth factor-2 from an injectable 6-O-desulfated

heparin hydrogel and subsequent effect on in vivo vascularization. J Biomed Mater Res A. 2006;78:364-71.

[292] Westall FC, Rubin R, Gospodarowicz D. Brain-derived fibroblast growth factor: A study of its inactivation. Life Sciences. 1983;33:2425-9.

[293] Ghaderi D, Zhang M, Hurtado-Ziola N, Varki A. Production platforms for biotherapeutic glycoproteins: Occurrence, impact, and challenges of non-human sialylation. Biotechnol Genet Eng. 2012;28:147-76.

[294] Baneyx F. Recombinant protein expression in Escherichia coli. Curr Opin Biotechnol. 1999.

[295] Terpe K. Overview of bacterial expression systems for heterologous protein production: From molecular and biochemical fundamentals to commercial systems. Appl Microbiol Biotechnol. 2006;72:211-22.

[296] Nagasawa K, Inoue Y, Kamata T. Solvolytic desulfation of glycosaminoglycuronan sulfates with dimethyl sulfoxide containing water or methanol. Carbohydr Res. 1977;58:47-55.

[297] Kantor TG, Schubert M. A method for the desulfation of chondroitin sulfate. J Am Chem Soc. 1957;79:152-3.

[298] Farndale RW, Buttle DJ, Barrett AJ. Improved quantitation and discrimination of sulphated glycosaminoglycans by use of dimethylmethylene blue. Biochim Biophys Acta. 1986;883:173-7.

[299] Uniewicz KA, Ori A, Rudd TR, Guerrini M, Wilkinson MC, Fernig DG, et al. Following protein–glycosaminoglycan polysaccharide interactions with differential scanning fluorimetry. Methods in Molecular Biology. 2012;836:171-82.

[300] Niesen FH, Berglund H, Vedadi M. The use of differential scanning fluorimetry to detect ligand interactions that promote protein stability. Nat Protoc. 2007;2:2212-21.

[301] Baumann H, Scheen H, Huppertz B, Keller R. Novel regio- and stereoselective O-6-desulfation of the glucosamine moiety of heparin with N-methylpyrrolidinone–water or N,N-dimethylformamide–water mixtures. Carbohydr Res. 1998;308:381-8.

[302] Volkin DB, Tsai PK, Dabora JM, Gress JO. Physical stabilization of acidic fibroblast growth factor by polyanions. Arch Biochem Biophys. 1993;300:30-41.

[303] Krufka A, Guimond S, Rapraeger AC. Two Hierarchies of FGF-2 Signaling in Heparin: Mitogenic Stimulation and High-Affinity Binding/Receptor Transphosphorylation Biochemistry. 1996;35:11131-41.

[304] Thomopoulos S, Das R, Sakiyama-Elbert S, Silva MJ, Charlton N, Gelberman RH. bFGF and PDGF-BB for tendon repair: Controlled release and biologic activity by tendon fibroblasts in vitro. Ann Biomed Eng. 2010;38:225-34.

[305] Kaushik JK, Bhat R. Why is trehalose an exceptional protein stabilizer? An analysis of the thermal stability of proteins in the presence of the compatible osmolyte trehalose. J Biol Chem. 2003;278:26458-65.

[306] Takada T, Katagiri T, Ifuku M, Morimura N, Kobayashi M, Hasegawa K, et al. Sulfated polysaccharides enhance the biological activities of bone morphogenetic proteins. J Biol Chem. 2003;278:43229-35.

[307] Rudd TR, Uniewicz KA, Ori A, Guimond SE, Skidmore MA, Gaudesi D, et al. Comparable stabilisation, structural changes and activities can be induced in FGF by a variety of HS and non-GAG analogues: implications for sequence-activity relationships Org Biomol Chem. 2010;8:5390-7.

[308] Vedadi M, Niesen F, Allali-Hassani A, Federov O, Finerty P, Wasney G, et al. Chemical screening methods to identify ligands that promote protein stability, protein crystallization, and structure determination. Proc Natl Acad Sci USA. 2006;103:15835-40.

[309] Seto S, Temenoff J. Coculture Systems for Mesenchymal Stem Cells. In: Fisher J, Mikos A, Bronzino J, Peterson D, editors. Tissue Engineering: Principles and Practices. Boca Raton, FL: CRC Press; 2012. p. 21.1-.16.

[310] Barbero JL, Franco L, Montero F, Morán F. Structural studies on histones H1. Circular dichroism and difference spectroscopy of the histones H1 and their trypsin-resistant cores from calf thymus and from the fruit fly Ceratitis capitata. Biochemistry. 1980;19:4080-7.

[311] Clark DJ, Hill CS, Martin SR, Thomas JO. Alpha-helix in the carboxy-terminal domains of histones H1 and H5. EMBO J. 1988;7:69-75.

[312] Sher JS. Anatomy, biomechanics, and pathophysiology of rotator cuff disease. In: Iannotti JPaW, Gerald R, editor. Disorders of the Shoulder: Diagnosis and Management. Philadelphia: Lippincott, Williams, and Wilkins; 1999. p. 3-29.

[313] Soslowsky LJ, Thomopoulos S, Tun S, Flanagan CL, Keefer CC, Mostow J, et al. Neer award 1999 Overuse activity injures the supraspinatus tendon in an animal model: A histologic and biomechanical study. Journal of Shoulder and Elbow Surgery. 2000;9:79-84.

[314] Archambault JM, Jelinsky SA, Lake SP, Hill AA, Glaser DL, Soslowsky LJ. Rat supraspinatus tendon expresses cartilage markers with overuse. J Orthop Res. 2007;25:617-24.

[315] Gimbel JA, Van Kleunen JP, Mehta S, Perry SM, Williams GR, Soslowsky LJ. Supraspinatus tendon organizational and mechanical properties in a chronic rotator cuff tear animal model. Journal of biomechanics. 2004;37:739-49.

[316] Fu SC, Chan BP, Wang W, Pau HM, Chan KM, Rolf CG. Increased expression of matrix metalloproteinase 1 (MMP1) in 11 patients with patellar tendinosis. Acta orthopaedica Scandinavica. 2002;73:658-62.

[317] Lo IKY, Marchuk LL, Hollinshead R, Hart DA, Frank CB. Matrix metalloproteinase and tissue inhibitor of matrix metalloproteinase mRNA levels are specifically altered in torn rotator cuff tendons. The American journal of sports medicine. 2004;32:1223-9.

[318] Garnero P, Borel O, Byrjalsen I, Ferreras M, Drake FH, McQueney MS, et al. The collagenolytic activity of cathepsin K is unique among mammalian proteinases. J Biol Chem. 1998;273:32347-52.

[319] Deval C, Mordier S, Obled C, Bechet D, Combaret L, Attaix D, et al. Identification of cathepsin L as a differentially expressed message associated with skeletal muscle wasting. Biochemical Journal. 2001;360:143.

[320] Eeckhout Y, Vaes G. Further studies on the activation of procollagenase, the latent precursor of bone collagenase. Effects of lysosomal cathepsin B, plasmin and kallikrein, and spontaneous activation. The Biochemical journal. 1977;166:21-31.

[321] Goretzki L, Schmitt M, Mann K, Calvete J, Chucholowski N, Kramer M, et al. Effective activation of the proenzyme form of the urokinase-type plasminogen activator (pro-uPA) by the cysteine protease cathepsin L. FEBS letters. 1992;297:112-8.

[322] Cunnane G, FitzGerald O, Hummel KM, Gay RE, Gay S, Bresnihan B. Collagenase, cathepsin B and cathepsin L gene expression in the synovial membrane of patients with early inflammatory arthritis. Rheumatology (Oxford, England). 1999;38:34-42.

[323] Wilder CL, Park K-Y, Keegan PM, Platt MO. Manipulating substrate and pH in zymography protocols selectively distinguishes cathepsins K, L, S, and V activity in cells and tissues. Archives of biochemistry and biophysics. 2011:1-6.

[324] Li WA, Barry ZT, Cohen JD, Wilder CL, Deeds RJ, Keegan PM, et al. Detection of femtomole quantities of mature cathepsin K with zymography. Anal Biochem. 2010;401:91-8.

[325] Cook JL, Feller JA, Bonar SF, Khan KM. Abnormal tenocyte morphology is more prevalent than collagen disruption in asymptomatic athletes' patellar tendons. Journal of orthopaedic research : official publication of the Orthopaedic Research Society. 2004;22:334-8.

[326] Maffulli N, Longo UG, Franceschi F, rabitti C, Denaro V. Movin and Bonar scores assess the same characteristics of tendon histology. Clinical orthopaedics and related research. 2008;466:1605-11.

[327] Park KY, Li WA, Platt MO. Patient specific proteolytic activity of monocyte-derived macrophages and osteoclasts predicted with temporal kinase activation states during differentiation. Integr Biol (Camb). 2012;4:1459-69.

[328] Szomor ZL, Appleyard RC, Murrell GA. Overexpression of nitric oxide synthases in tendon overuse. J Orthop Res. 2006;24:80-6.

[329] Patterson-Kane JC, Wilson AM, Firth EC, Parry DA, Goodship AE. Exercise-related alterations in crimp morphology in the central regions of superficial digital flexor tendons from young thoroughbreds: a controlled study. Equine Vet J. 1998;30:61-4.

[330] Benjamin M, Toumi H, Ralphs JR, Bydder G, Best TM, Milz S. Where tendons and ligaments meet bone: attachment sites ('entheses') in relation to exercise and/or mechanical load. Journal of anatomy. 2006;208:471-90.

[331] Scott A, Cook JL, Hart DA, Walker DC, Duronio V, Khan KM. Tenocyte responses to mechanical loading in vivo: a role for local insulin-like growth factor 1 signaling in early tendinosis in rats. Arthritis and rheumatism. 2007;56:871-81.

[332] Gotoh M, Hamada K, Yamakawa H, Tomonaga A, Inoue A, Fukuda H. Significance of granulation tissue in torn supraspinatus insertions: An immunohistochemical study with antibodies against interleukin-1?, cathepsin D, and matrix metalloprotease-1. Journal of orthopaedic research : official publication of the Orthopaedic Research Society. 1997;15:33-9.

[333] Morko JP, Soderstrom M, Saamanen AM, Salminen HJ, Vuorio EI. Up regulation of cathepsin K expression in articular chondrocytes in a transgenic mouse model for osteoarthritis. Ann Rheum Dis. 2004;63:649-55.

[334] Morko J, Kiviranta R, Joronen K, Saamanen AM, Vuorio E, Salminen-Mankonen H. Spontaneous development of synovitis and cartilage degeneration in transgenic mice overexpressing cathepsin K. Arthritis Rheum. 2005;52:3713-7.

[335] Kozawa E, Nishida Y, Cheng XW, Urakawa H, Arai E, Futamura N, et al. Osteoarthritic change is delayed in a Ctsk-knockout mouse model of osteoarthritis. Arthritis Rheum. 2012;64:454-64.

[336] Bromme D, Lecaille F. Cathepsin K inhibitors for osteoporosis and potential off-target effects. Expert Opin Investig Drugs. 2009;18:585-600.

[337] Masarachia PJ, Pennypacker BL, Pickarski M, Scott KR, Wesolowski GA, Smith SY, et al. Odanacatib reduces bone turnover and increases bone mass in the lumbar spine of skeletally mature ovariectomized rhesus monkeys. J Bone Miner Res. 2012;27:509-23.

[338] Kannus P, Jozsa L. Histopathological changes preceding spontaneous rupture of a tendon. A controlled study of 891 patients. J Bone Joint Surg Am. 1991;73:1507-25.

[339] Burgess WH, Maciag T. The heparin-binding (fibroblast) growth factor family of proteins. Annu Rev Biochem. 1989;58:575-606.

[340] Roy S, Lai H, Zouaoui R, Duffner J, Zhou H, Jayaraman LP, et al. Bioactivity screening of partially desulfated low-molecular-weight heparins: a structure/activity relationship study. Glycobiology. 2011;21:1194-205.

[341] Patterson-Kane JC, Wilson AM, Firth EC, Parry DAD, Goodship AE. Exercise-related alterations in crimp morphology in the central regions of superficial digital flexor tendons from young Thoroughbreds: a controlled study. Equine Vet J. 1998;30:61-4.

[342] Park K-Y, Li WA, Platt MO. Patient specific proteolytic activity of monocyte-derived macrophages and osteoclasts predicted with temporal kinase activation states during differentiation. Integr Biol (Camb). 2012;12:1459-69.

[343] Deval C, Mordier S, Obled C, Bechet D, Combaret L, Attaix D, et al. Identification of cathepsin L as a differentially expressed message associated with skeletal muscle wasting. Biochem J. 2001;360:143-50.

[344] Cunnane G, FitzGerald O, Hummel KM, Gay RE, Gay S, Bresnihan B. Collagenase, cathepsin B and cathepsin L gene expression in the synovial membrane of patients with early inflammatory arthritis. Rheumatology 1999;38:34-42.

[345] Hou WS, Li Z, Gordon RE, Chan K, Klein MJ, Levy R, et al. Cathepsin K is a critical protease in synovial fibroblast-mediated collagen degradation. Am J Pathol. 2001;159:2167-77.

[346] Pap T, Müller-Ladner U, Gay RE, Gay S. Fibroblast biology: Role of synovial fibroblasts in the pathogenesis of rheumatoid arthritis. Arthritis Res. 2000;2:361-7.

[347] Reddy VY, Zhang QY, Weiss SJ. Pericellular mobilization of the tissue-destructive cysteine proteinases, cathepsins B, L, and S, by human monocyte-derived macrophages. Proc Natl Acad Sci USA. 1995;92:3849-53.

[348] Doi H, Nishida K, Yorimitsu M, Komiyama T, Kadota Y, Tetsunaga T, et al. Interleukin-4 downregulates the cyclic tensile stress-induced matrix metalloproteinases-13 and cathepsin B expression by rat normal chondrocytes. Acta Med Okayama. 2008;62:119-26.

[349] Lim JJ, Temenoff JS. The effect of desulfation of chondroitin sulfate on interactions with positively charged growth factors and upregulation of cartilaginous markers in encapsulated MSCs. Biomaterials. 2013;34:5007-18.

[350] Awad HA, Boivin GP, Dressler MR, Smith FNL, Young RG, Butler DL. Repair of patellar tendon injuries using a cell-collagen composite. J Orthop Res. 2003;21:420-31.

[351] Oliva F, Via AG, Maffulli N. Calcific tendinopathy of the rotator cuff tendons. Sports Med Arthrosc. 2011;19:237-43.

[352] Lovati AB, Corradetti B, Cremonesi F, Bizzaro D, Consiglio AL. Tenogenic differentiation of equine mesenchymal progenitor cells under indirect co-culture. Int J Artif Organs. 2012;35:996-1005.

[353] Schneider PRA, Buhrmann C, Mobasheri A, Matis U, Shakibaei M. Three-dimensional high-density co-culture with primary tenocytes induces tenogenic differentiation in mesenchymal stem cells. J Orthop Res. 2011;29:1351-60.

[354] Solorio LD, Fu AS, Hernández-Irizarry R, Alsberg E. Chondrogenic differentiation of human mesenchymal stem cell aggregates via controlled release of TGF-beta1 from incorporated polymer microspheres. J Biomed Mater Res A. 2010;92:1139-44.

[355] Chen F-M, Zhang M, Wu Z-F. Toward delivery of multiple growth factors in tissue engineering. Biomaterials. 2010;31:6279-308.

[356] Lee K, Silva EA, Mooney DJ. Growth factor delivery-based tissue engineering: general approaches and a review of recent developments. J R Soc Interface. 2011;8:153-70.

[357] Mao Z, Ma L, Zhou J, Gao C, Shen J. Bioactive thin film of acidic fibroblast growth factor fabricated by layer-by-layer assembly. Bioconjug Chem. 2005;16:1316-22.

[358] Crouzier T, Szarpak A, Boudou T, Auzély-Velty R, Picart C. Polysaccharide-blend multilayers containing hyaluronan and heparin as a delivery system for rhBMP-2. Small. 2010;6:651-62.

[359] Macdonald ML, Samuel RE, Shah NJ, Padera RF, Beben YM, Hammond PT. Tissue integration of growth factor-eluting layer-by-layer polyelectrolyte multilayer coated implants. Biomaterials. 2011;32:1446-53.

[360] Almeida PC, Nantes IL, Chagas JR, Rizzi CC, Faljoni-Alario A, Carmona E, et al. Cathepsin B activity regulation: Heparin-like glycosaminogylcans protect human cathepsin B from alkaline pH-induced inactivation. J Biol Chem. 2001;276:944-51.

[361] Almeida PC, Nantes IL, Rizzi CC, Júdice WA, Chagas JR, Juliano L, et al. Cysteine proteinase activity regulation: A possible role of heparin and heparin-like glycosaminoglycans. J Biol Chem. 1999;274:30433-8.

[362] Mach L, Mort JS, Glössl J. Maturation of human procathepsin B: Proenzyme activation and proteolytic processing of the precursor to the mature proteinase, in vitro, are primarily unimolecular processes. J Biol Chem. 1994;269:13030-5.

[363] Li Z, Yasuda Y, Li W, Bogyo M, Katz N, Gordon RE, et al. Regulation of collagenase activities of human cathepsins by glycosaminoglycans. J Biol Chem. 2004;279:5470-9.

[364] Shi GP, Sukhova GK, Grubb A, Ducharme A, Rhode LH, Lee RT, et al. Cystatin C deficiency in human atherosclerosis and aortic aneurysms. J Clin Invest. 1999;104:1191-7.

[365] Hashida S, Kominami E, Katunuma N. Inhibitions of cathepsin B and cathepsin L by E-64 in vivo.: Incorporation of [3H]E-64 into rat liver lysosomes in vivo. J Biochem. 1982;91:1373-80.

[366] El-Khoury GY, Brandser EA. MRI of tendon injuries. Iowa Orthop J. 1994;14:65-80.

[367] Ellman H. Diagnosis and Treatment of Incomplete Rotator Cuff Tears. Clin Orthop Relat Res. 1990;254:64-74.

[368] Chen J, Tung C-H, Mahmood U, Ntziachristos V, Gyurko R, Fishman MC, et al. In vivo imaging of proteolytic activity in atherosclerosis. Circulation. 2002;105:2766-71.

[369] Jaffer FA, Kim D-E, Quinti L, Tung C-H, Aikawa E, Pande AN, et al. Optical visualization of cathepsin K activity in atherosclerosis with a novel, protease-activatable fluorescence sensor. Circulation. 2007;115:2292-8.

[370] Burdick JA, Prestwich GD. Hyaluronic acid hydrogels for biomedical applications. Adv Mater. 2011;23:H41-56.

[371] Kim IL, Mauck RL, Burdick JA. Hydrogel design for cartilage tissue engineering: A case study with hyaluronic acid. Biomaterials. 2011;32:8771-82.

[372] Longaker MT, Chiu ES, Adzick NS, Stern M, Harrison MR, Stern R. Studies in fetal wound healing: A prolonged presence of hyaluronic acid characterizes fetal wound fluid. Ann Surg. 1991;213:292.

[373] Zou XH, Jiang YZ, Zhang GR, Jin HM, Hieu NTM, Ouyang HW. Specific interactions between human fibroblasts and particular chondroitin sulfate molecules for wound healing. Acta Biomater. 2009;5:1588-95.